Politecnico di Milano

School of Civil, Environmental and Land Management Engineering

Master of Science in Environmental and Land Planning Engineering - Land Protection and Natural Risks Prevention

A practical approach for simulating the effects of fires in deep tunnels considering the temperature induced damage

Supervisor: Prof. Donatella Sterpi

Master thesis of:
Arianna Mocchi
920662

Academic Year 2019-2020

Contents

List of Figures

List of Tables

Abstract

The aim of this work is to provide a simple and immediate tool that evaluates the interaction between the lining and the rock that constitute tunnels under different conditions. An analytical model is presented, which assumes that the tunnel is an axisymmetric cavity whose state of stress is generated during the excavation phase and successively altered due to the exposure to fire.
Firstly, the effects of the excavation phase are observed in terms of stress and convergence of the tunnel. To do this, the Convergence Confinement Method allows to determine the equilibrium condition between the rock mass and concrete ring and to establish the effects of their interaction and of installation of a certain type of lining. The promptness of the method is such that it becomes a practical effective tool, that can be easily implemented in the preliminary design phase.
Subsequently, the problem of fires in tunnel is analysed: these events are capable of inducing serious consequences on the structure, in particular due to the narrow spaces that facilitate the fast increase in temperatures and the spread of smoke.
The fire induced thermal variation in the lining and surrounding rock may be taken by empirical data or calculated by means of analytical or numerical models. In this work, a finite element analysis with *COMSOL Multiphysics* has been performed to evaluate the temperature variation induced by a standard fire for different time steps.
The effects of this thermal variation are analysed in terms of stresses and displacements. To this aim, a multi-layer model is implemented, based on the subdivision of the domains in many different layers. The results show that the consequences are not negligible, especially in terms of radial displacement and hoop stresses.
The present model allows to take into account the interaction between rock and lining and considers the non uniform effects of high temperatures on the support. In particular, concrete that is subjected to fire gradually loses compressive strength and stiffness, becoming a more ductile material.
In addition, the possibility of having spalling of the lining is evaluated. The results

show that, due to the high hoop stresses that are generated inside the material, parts of the intrados may detach.

Sommario

L'obiettivo del presente è lavoro è quello di fornire uno strumento semplice ed immediato che studi in diverse condizioni l'interazione tra l'anello di rivestimento e la roccia che costituiscono una galleria. Sono riportati dei modelli di tipo analitico che si basano sull'ipotesi di assialsimmetria del problema e che trattano due diverse condizioni: la fase di scavo e l'esposizione del tunnel a fuoco.
In primo luogo, si osservano gli effetti della fase di scavo in termini di stato di sforzo e convergenza della galleria. Per fare questo, il metodo della Curva Caratteristica (anche detto *Convergence Confinement Method*) permette di determinare l'equilibrio tra roccia e anello di calcestruzzo e di stabilire a priori quale sarà l'effetto dello scavo e dell'installazione di un determinato tipo di rivestimento. L'immediatezza del metodo è tale da diventare uno strumento efficace che può essere facilmente utilizzato in una prima fase di progettazione.
Successivamente si affronta il problema legato agli incendi in galleria: si tratta di una problematica frequente e in grado di creare gravi effetti sulla galleria stessa, in particolare a causa degli spazi ristretti che facilitano l'aumento delle temperature, la propagazione del fumo e tutti gli effetti che ne derivano. Tramite un'analisi agli elementi finiti sfruttando il software *COMSOL Multiphysics* si ricava la curva di temperatura indotta da un incendio standard per diversi step temporali e a diverse profondità. Nella fase di riscaldamento l'intradosso è caratterizzato da alti picchi di temperatura, successivamente si osserva una migrazione deli picchi verso gli strati più esterni, fino a raggiungere lo strato roccioso. Si considera nell'analisi anche la fase di raffreddamento.
Gli effetti di tale variazione termica sono analizzati in termini di sforzi e spostamenti. A tal fine si presenta un nuovo modello analitico in grado di valutare lo stato di sollecitazione e spostamento radiale al variare della temperatura e del tempo: il rivestimento arriva ad avere un consistente spostamento radiale ed è sede di un grande stato di sforzo, in particolare di tipo tangenziale.
Questo modello consente di tenere conto dell'interazione tra ammasso roccioso

e rivestimento e considera gli effetti delle alte temperature sul rivestimento. In particolare, il calcestruzzo sottoposto a fuoco perde resistenza a compressione e rigidezza, diventando così un materiale più duttile. Questa caratteristica gli permette di essere sottoposto a minor compressione.
Inoltre, si valuta la possibilità che si verifichi spalling nel rivestimento, ovvero che delle parti di materiale si stacchino all'intradosso a causa delle elevate pressioni a cui sono sottoposte.

Introduction

The safety of a tunnel is challenged when dealing with fire. Due to the high velocities that are frequently reached by vehicles and to the abundant quantities of fuel that are present, fires can develop easily. Moreover, it can take several hours to cease fire, since the small space available makes it difficult to control it. The spreading of smoke inside the tunnel increases the complexity for the operation and can also be the cause of many casualties.
As reported in Table 1, with an average of almost one case per year in the recent period, the fire in tunnels is actually a recurring problem. This is why it is important to describe the phenomenon by way of analytical or numerical models, with the objective of predicting what could happen and how to deal with it in order to limit the damages.

Date	Name	Country	Length	Duration	Max. Temperature
11 1996	Channel Tunnel	France-England	53850 m	7 hrs	1000°C
03 1999	Mont-Blanc Tunnel	France-Italy	11600 m	53 hrs	1000°C
05 1999	Tauern	Austria	8371 m	14 hrs	1200°C
07 2000	Rotsethhorn	Norway	1200 m	-	-
08 2001	Gleinalm	Austria	8300 m	37 min	-
10 2001	Gotthard	Switzerland	16300 m	24 hrs	1200°C
11 2003	Fløyfjell	Norway	3100 m	-	-
06 2005	Frejus	Italy-France	12895 m	6 hrs	1200°C

Table 1: *The most recent episodes of fire in tunnels. [Piarc, 2014]*

The maximum values of temperature that can be reached are far higher than the ones for an ordinary fire in a building. Moreover, a fire in tunnel may last some minutes but it may also need more than one day to be ceased.
The fire in Mont Blanc Tunnel (Figures 1 and 2) occurred on 24^{th} March 1999, caused by a truck which transported flour and margarine, that suddenly caught

Figure 1: *Effects of fire in Mont Blanc Tunnel, on March 1999. [Wallis, 2001]*

fire. Since smoke spread very quickly, it became very difficult for the firefighters to act: after 37 minutes only, smoke arrived at the entrance of the French side of the tunnel, which is 6 kilometers from the position of the truck.
Furthermore, the electric wiring was melted, so there was no more lighting of the tunnel and the lack of Oxygen made vehicles engines not able to work anymore. This disaster ended after 53 hours, leaving 39 casualties and 14 injured people.
The tunnel was reopened after three years.

Generally, tunnels subjected to fire do not collapse, however there are two main aspects to be considered: first, the lining subjected to high temperatures loses its strength and stiffness; second, the high temperature may induce a phenomenon of *spalling* of the lining's concrete: in some cases, this problem can involve several centimeters of lining, reaching values up to 25 centimeters.
Besides the lining, the surrounding rock experiences a remarkable change in its state of stress that should be properly taken into account when describing the problem.
Because of the recurrence of this phenomenon and of the serious damage that it may cause both in terms of social and economic loss, it is fundamental to have a practical and immediate tool that is able to describe the problem taking into account the various aspects that influence it.
In the present work, an analytical model is used to calculate the state of stress

Figure 2: *A shell of a truck after the fire. Mont Blanc, March 1999 [Wallis, 2001]*

that develops in the concrete lining and in the surrounding rock during and after a standard fire. The tunnel is assumed to be deep and circular, the concrete lining is constituted of ordinary concrete with linear elastic behaviour, while the rock is assumed to be elastic or perfectly-plastic. Due to the geometry of the problem, the model is axisymmetric and cylindrical coordinates are adopted.
The aim is to describe the effects of excavation on rock and the interaction between soil and lining as soon as it is installed. Then, the problem of fire in tunnels is analysed by calculating the thermal variation and the mechanical effects that alter the state of stress of both the lining and the rock. The model takes into account the decrease in the stiffness of concrete that is subjected to very high temperatures and the possibility of having spalling at the intrados.
Since the concrete ring is not uniformly heated by fire, the hypothesis of axial symmetry is a simplification of the model. Moreover, the hypothesis of elastic behaviour of concrete may represent a limit of the present model, since the effects of fire may be non-linear.
The State of the Art about the interaction between rock and concrete lining during the realization of the tunnel and about the effects of fire are reported in Chapter 1. Chapter 2 deals with the analytical solutions of the Convergence-Confinement

Method, which simulates the excavation process; followed by the description of the multi-layer cylinder model in Chapter 3. The final results of the model are reported in Chapter 4, together with a brief discussion on the practical meaning of the obtained results.

Chapter 1

State of the Art

1.1 Tunnel excavation

Rock excavation is being performed from the past for different purposes, such as to extract materials or to create transportation and communication paths and shelter spaces. Many applications and new techniques have improved throughout the years with the objective of assisting the design and the construction processes, in particular the modelling of the stress state variations induced by the excavation, and the consequent strain state.
However, there are still several aspects that need to be examined. For instance, a precise geological mapping of the rock mass is seldom available and this can result in inappropriate blasting that could cause instability.
Depending on the strength of the rock that is involved in the excavation process, suitable means of support or reinforcement are thus needed. When dealing with moderate or high strength, it is sufficient to adopt reinforcement measures such as bolts or cables. However, in the majority of cases a support is installed: shotcrete, concrete linings or steel sets, in particular when dealing with soft materials.
The support has the function of carrying the load of the surrounding rock and avoids the possibility of having an excessive convergence of the rock towards the centre of the tunnel. In fact, when the excavation face is approaching, the rock experiences inward radial displacement due to the stress release that involves an extended region ahead of the tunnel excavation face. The region that is influenced by the excavation of the tunnel starts at about half diameter ahead of the advancing face and covers about one and one half diameters behind the face (Figure 1.1).
The *Convergence Confinement Method* (CCM) has been conceived with the aim of establishing the pressure that will be sustained by the lining depending on its

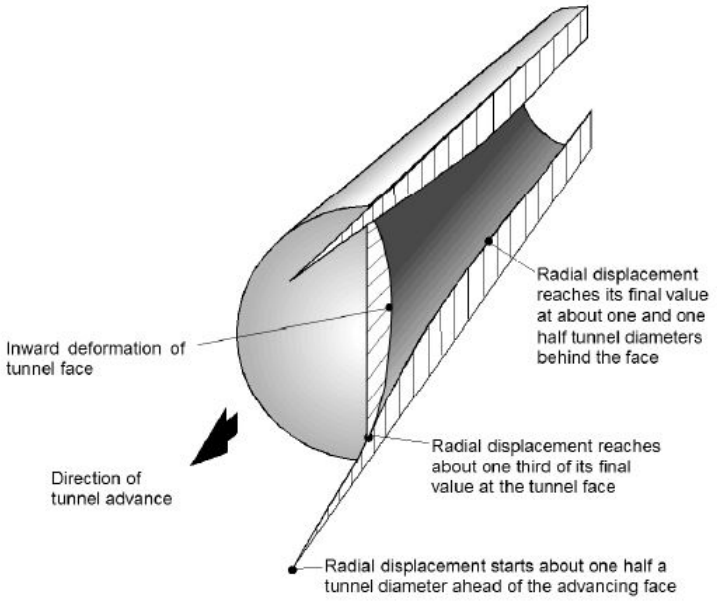

Figure 1.1: *Inward radial convergence during tunnel excavation [Hoek, 2000]*

mechanical characteristics and on the surrounding rock for a circular excavation of given diameter and at a given depth. Many solutions of this procedure have been discussed through the years, for various mechanical behaviours of the rock and mixtures of concrete. Amongst them, in [Carranza-Torres and Fairhurst, 2000] a practical application of the method is presented for rock that satisfies the Hoek-Brown failure criterion. In [Kolymbas, 2008] the same problem is solved by using the cohesive and non-cohesive Mohr-Coulomb criterion.
A comparison between the performances of good, average and poor quality rocks is presented in [Alejano et al., 2009].
Regarding the installation of the support, [Carranza-Torres et al., 2013] study the effects of a delayed installation: in the first step the analysis is mainly focused on the state of stress that develops in absence of lining, while in the second one the effects of its installation are evaluated.
The paper [Oreste, 2003b] has the objective of reading a more precise interpretation of the behaviour of the support by taking into account the variability with time of strength and stiffness of concrete or shotcrete, and thus the variability of the factor of safety against the lining's failure as well.
Although some simplifying assumptions are required, CCM has proved to be an effective procedure and this is why it will be used in the present work as well.

1.2 Fire in tunnels

1.2.1 Fire curves

A fire curve is a time-temperature curve that describes the evolution of the fire, depending on the origin and the space where it develops. Different design fire scenarios can be used to predict and evaluate the effects on fire and they can be either based on experimental data or calculated using deterministic methods.
In the case of tunnels, high temperatures can be reached very fast because of the restricted space available. The peak temperature is often reached within some minutes and after a plateau the temperatures start decreasing during the cooling phase. Both the heating and the cooling phases are relevant when dealing with tunnels, whereas in the case of building fire safety design the cooling phase is usually neglected.
Depending on the fire scenario, a specific design curve could be more appropriate than another, this is why the International Organisation of Standardisation proposes a methodology for the selection of design fire scenarios and design fires for any built environment including buildings, structures or transportation vehicles.
One of the most commonly used fire curve is the Standard fire curve ISO834 (Figure 1.2), which has been suggested by The European Standard [Eurocode2, 2005]. The temperature increases with time following a logarithmic law:

$$\theta_g = T_0 + 345 \cdot \log_{10}(8t + 1) \tag{1.1}$$

where T_0 [°C] is the initial temperature, t [min] refers to time and θ_g [°C] is the medium temperature attained.

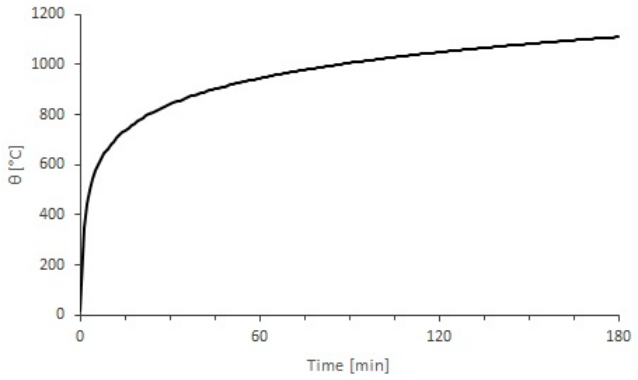

Figure 1.2: *Fire curve ISO834 with* $T_0 = 20°C$

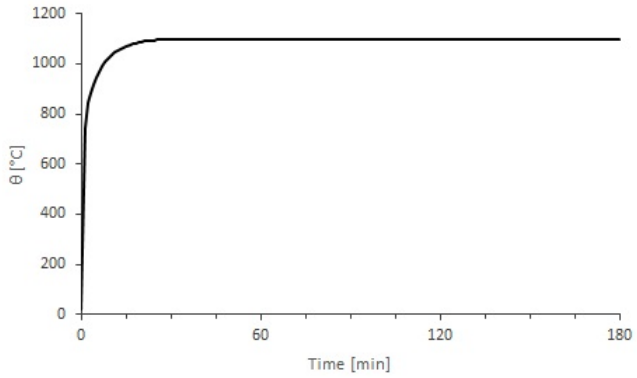

Figure 1.3: *Hydrocarbon Fire Curve with* $T_0 = 20°C$

ISO834 is a standard curve which has been created for cellulosic as burning materials and it is characterised by a slow variation of temperature: the peak value is reached after three hours.
For fires that develop in tunnels, combustion of liquids such as fuel or petroleum are recurrent and high temperatures can be reached very quickly: this is the reason why the Hydrocarbon Fire Curve (Figure 1.3) has been created as a valid alternative to ISO834. In this curve, due to the presence of Hydrocarbons, the maximum temperature 1100°C is reached after about 30 minutes. In this case, the time-temperature equation is:

$$\theta_g = T_0 + 1080 \cdot (1 - 0.325 \cdot e^{-0.167t} - 0.675 \cdot e^{-2.5t}) \tag{1.2}$$

The RWS curve (Figure 1.4) was developed by the Rijkswaterstaat, Ministry of

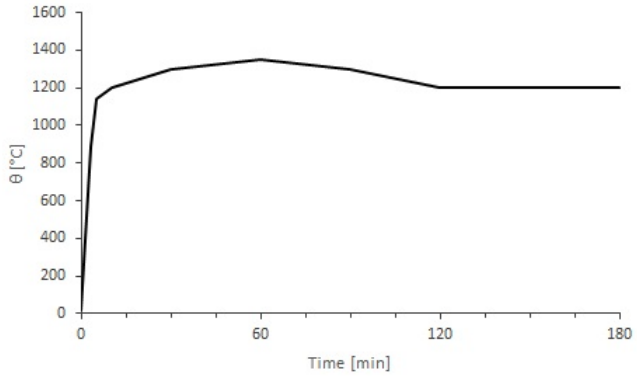

Figure 1.4: *RWS Fire Curve*

Transport in the Netherlands and it is representative of fire scenarios in enclosed

areas, such as in a tunnel. It is based on the assumption that in a worst case scenario, a 50 m^3 fuel, oil or petrol tanker fire with a fire load of 300MW could occur, lasting up to 120 minutes. The RWS curve was based on the results of testing carried out by TNO in the Netherlands in 1979. The correctness of the RWS fire curve as a design fire curve for road tunnels was reconfirmed in the Full Scale Tests in the Runehamar tunnel in Norway. [Promat-Tunnel]
The main problem about these fire curves is that none of them take into account the cooling phase, which is as much important as the heating one, as it will be shown later on.
Finally, the RABT Fire Curve was developed in Germany and presents two different curves, depending on the vehicles that are involved: cars or trains. Here only the case of road tunnels is be presented (Figure 1.5). The peak temperature is 1200° and it is reached within five minutes, it is constant for 25 minutes and then it decreases in the cooling phase until it reaches the initial value. Thus, this is the only fire curve that takes into account the cooling phase.
In Table 1.1 all the main characteristics of each curve are reported in order to be

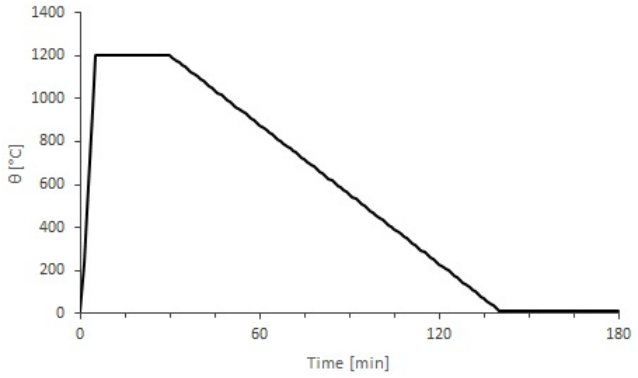

Figure 1.5: *RABT fire curve for cars.*

easily compared. In Figure (1.6) they are all represented in the same graph.

name	T_{max}**[°C]**	**time to reach** T_{max} **[min]**	**cooling phase**
ISO834	1200	180	no
Hydrocarbon	1100	30	no
RWS	1350	60	no
RABT-ZTV-cars	1200	5	yes

Table 1.1: *Main characteristics of standard fire curves*

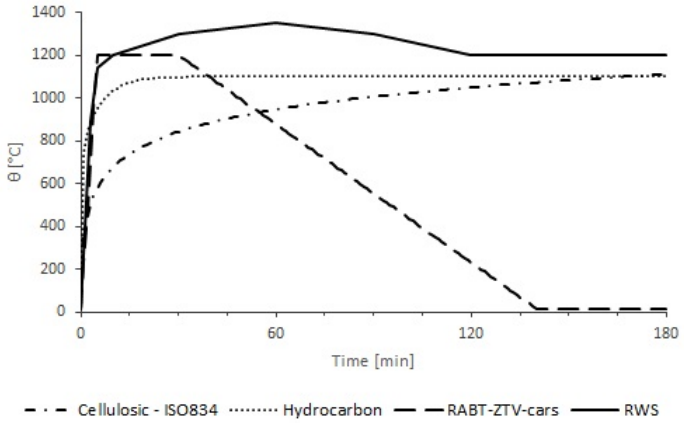

Figure 1.6: *Comparison between different fire curves*

In the article [Ingason, 2009] a different design fire curve in terms of heat release rate (HRR) and time is proposed. The HRR represents how fast energy is released and depends on geometry, type of fuels that are involved in the fire event and on the ventilation system (if present). The maximum heat release rate may be taken from a design table. For example, a design table can be found in World Road Association (PIARC) committee on road tunnels devoted to Fire and Smoke Control [PIARC, 1999] or in the National Fire Protection Association standard for road tunnels, [NFPA, 2008].
Besides the maximum HRR value, the curve is described by a fire growth rate, that is generally linear, quadratic or exponential. When dealing with tunnels, the cooling phase should be considered as well. Thus, to have a complete design curve, it is necessary to use different mathematical expressions for different time periods (i.e. the heating phase and the cooling one).
Ingason presents a new, single exponential design fire curve as function of two parameters: the maximum HRR and the total calorific value E_{tot}, plus the parameter n, which is an arbitrary value. The equation is:

$$\dot{Q}(t) = \dot{Q}_{max} nr(1 - e^{-kt})^{n-1} e^{-kt} \quad t \geqslant 0 \tag{1.3}$$

where $\dot{Q}(t)$ represents the heat release rate, $\dot{Q}_{max}$ is the maximum HRR, n is the retard index, r is the amplitude, k is the time width:

$$k = \frac{\dot{Q}_{max}}{E_{tot}} r \tag{1.4}$$

$$r = \left(1 - \frac{1}{n}\right)^{1-n} \tag{1.5}$$

Given these parameters, the time to reach the maximum HRR is defined as:

$$t_{max} = \frac{\ln n}{k} \tag{1.6}$$

It is difficult to associate n to a physical factor, but the article proposes empirical relations to set it as function of E_{max}, $\dot{Q}_{max}$ and t_{max}.
Since Equation (1.3) creates a design fire curve without keeping constant the maximum value (i.e. there is not a plateau in correpondence of the peak HRR), it is possible to get a new equation by summing two exponential. In this way, an exponential curve with a plateau-shaped maximum period is derived:

$$\dot{Q}(t) = \dot{Q}_{max}\left(n_1 r_1 (1 - e^{-k_1 t})^{n_1 - 1} e^{-k_1 t} + n_2 r_2 (1 - e^{-k_2 t})^{n_2 - 1} e^{-k_2 t}\right) \tag{1.7}$$

where:

$$n_2 = 7.1715 n_1^{0.60766} - 4.4009 \tag{1.8}$$

Depending on the value of n, several curves may be obtained, as shown in Figure (1.7). As the retard index n increases, the plateau is reached more slowly. The curves HRR-time are relevant when considering the possibility of having spalling during a fire event. In fact, this kind of damage depends on the velocity of heat release.

These design curves are fundamental to evaluate or predict all the thermal and non-thermal effects on the structure that is subjected to fire. Thus, when performing fire safety analysis, particular attention must be paid to choose the more realistic fire curve.

1.2.2 Thermal and mechanical models

After evaluating the kind of curve which best describes the fire event, the reaction of the structure is studied by considering its geometry and the properties of materials that both the concrete ring and the rock are composed of. The temperature variation inside the lining strictly depends on the insulation properties of concrete and on the characteristics of the tunnel, such as geometry and the presence of ventilation. It can be evaluated both by empirical data or by using programs that simulate the thermal transfer problem. Then, it is possible to estimate the state of stress that develops and consequently the strains and displacements.
In the case study of [Caner et al., 2005] a 300 mm thick unreinforced concrete lining is subjected to a fire. The compressive strength of concrete at 28 days is 28 MPa and moisture constitutes about 2% of its weight. Due to the presence of fire,

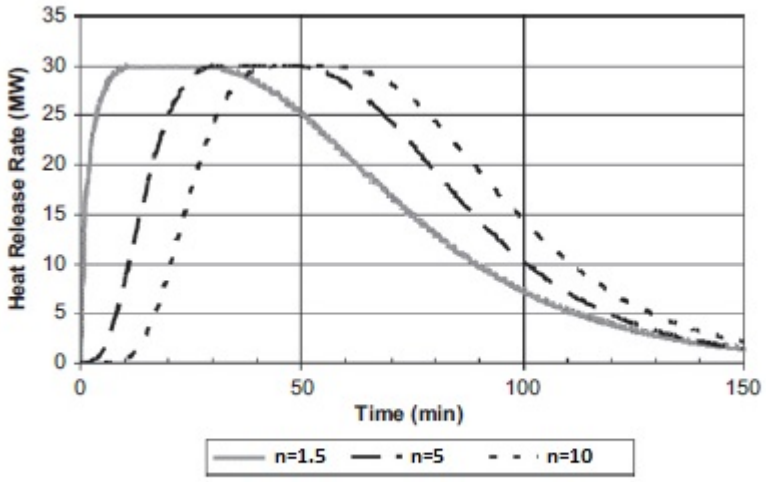

Figure 1.7: *Design fire curves for $\dot{Q}_{max}$=30 MW, E_{tot}=144 GJ and different retard indexes ($n_1 = 1.5$, $n_1 = 5$ and $n_1 = 10$*

)

the intrados of the lining reaches T=1100°C and it is supposed to maintain this temperature during the simulation (Hydrocarbon fire curve is used, Figure 1.3). A simulation is done using the program *RADTherm* to solve a transient heat transfer analysis, using the temperature-dependent thermal conductivity and specific heat values in ACI216R-89 [ACI, 2001]. Depending on the temperature attained on the concrete ring, the parameters of the material are changed manually.
Finally, the results of the heat transfer analysis two hours after the fire event are compared with the temperature profiles given by ACI 216R-89 for standard fires (Figure 1.8), demonstrating compliance with the experimental data.

The aim of [LoMonte et al., 2019] is to compare two different solutions of the problem of fire resistance: a cast-in-situ lining and a pre-cast segmental lining. The former is 0.9 m thick and is constituted by ordinary concrete ($f_{ck} = 28MPa$); the latter is less thick (0.32 meters) and is composed of seven segments made of polypropylene fibre concrete ($f_{ck} = 50MPa$). Both structures undergo thermal variation due to the presence of fire and the cooling phase is analysed as well. According to EN 1991-1-2 the heating phase is described by the Standard Curve ISO834 (Figure 1.2) followed by a linear cooling phase which lasts about 270 minutes. (Figure 1.9) The thermal problem and the consequent mechanical effects are

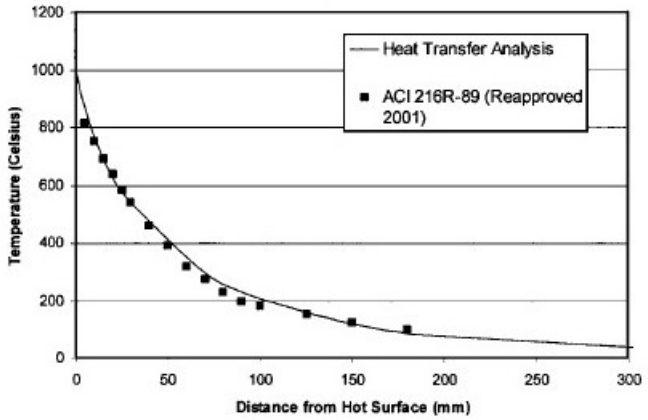

Figure 1.8: *Validation of heat transfer analysis in [Caner et al., 2005] using data from [ACI, 2001]. The data represent the temperature reached in the concrete lining two hours after the blasting of fire in the tunnel, depending on its radius r.*

modelled by means of Finite Element Modelling.

The temperature profile inside the concrete ring in both the solutions (Figure 1.10) shows that there are not many differences in the two cases. Moreover, the fire cooling phase must be properly taken into account when studying this kind of problems: in fact, the peak temperature inside the sheath is observed after the heating phase (Figure 1.11).

Looking at the results attained by [LoMonte et al., 2019] in Figure (1.10), it is shown that regardless of the geometry of the ring and of the mechanical characteristics that are considered, the concrete has relevant insulation properties. This is why the surrounding rock is subjected to a slight variation of temperature even when the thickness of the lining is very small. However, the mechanical model has to consider that the thermal expansion of the lining modifies the state of stress of the rock, too.

After developing the thermal model, a structural model is necessary to study the consequences of such a high temperature variation. Generally, current models are aimed at identifying the structural bearing capacity of the lining [Caner et al., 2005] or its factor of safety [Pichler et al., 2005]. These models should consider several aspects concerning fire in tunnels, in particular:

- *fire curve:* duration of the fire, temperature at the peak. It is possible to use experimental curves or analytical ones from literature.

- *mix design of concrete:* it can be constituted by different components that

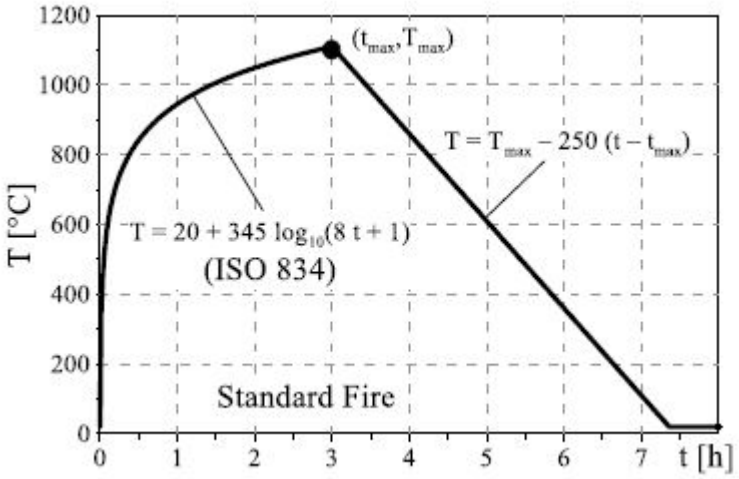

Figure 1.9: *Standard Fire curve according to EN 1991-1-2*

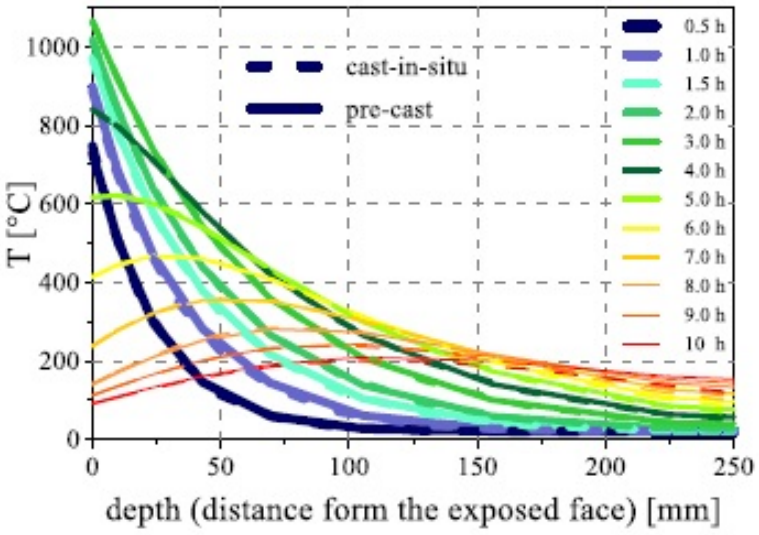

Figure 1.10: *Thermal profiles for different fire duration*

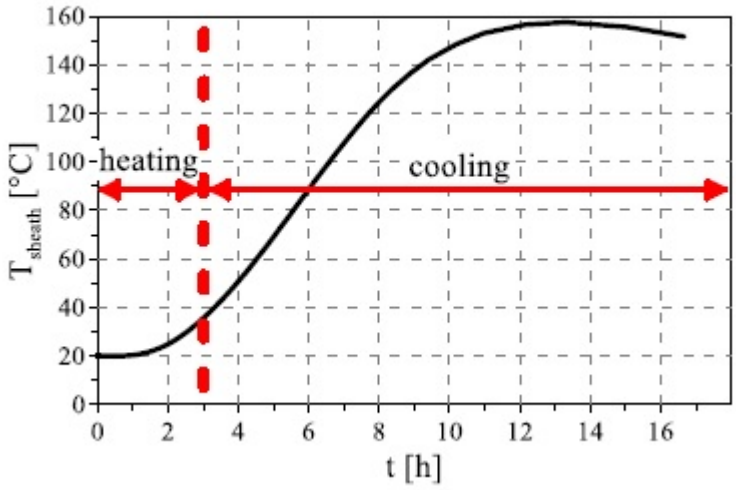

Figure 1.11: *Temperature inside the sheath during heating and cooling phases*

have distinct reactions in presence of fire.

- *effects of high temperature on concrete:* in presence of high temperatures, the mechanical properties describing the material deteriorate. Concrete experiences softening, due to physicochemical changes in the cement paste and in the aggregates and thermal incompatibility between the aggregates and the cement paste. [Larsson, 2006]
  Explosive spalling could also occur. When the temperature rises, the water inside the concrete tends to evaporate generating additional expansive pressure inside the concrete, which finally spalls.

- *interaction lining-soil:* it is generally modeled by assuming the soil as a set of elastic springs that react to radial or circumferential compression.

The literature agrees on the almost null probability of collapse of the tunnel, except from the cases of really long (i.e. in the order of days) exposure to high temperatures.

Regarding the structural behaviour of tunnels in presence of fire, [Bamonte et al., 2016] assess the performance of shotcrete using different mixes. The obtained results show that the shotcrete behaviour in compression is rather similar to that of ordinary concrete, while its thermal diffusivity is definitely lower at any temperature (150-800). The performance of shotcrete is compared with that by normal-strength concrete (NSC), considering a tunnel subjected to Standard Fire ISO834.

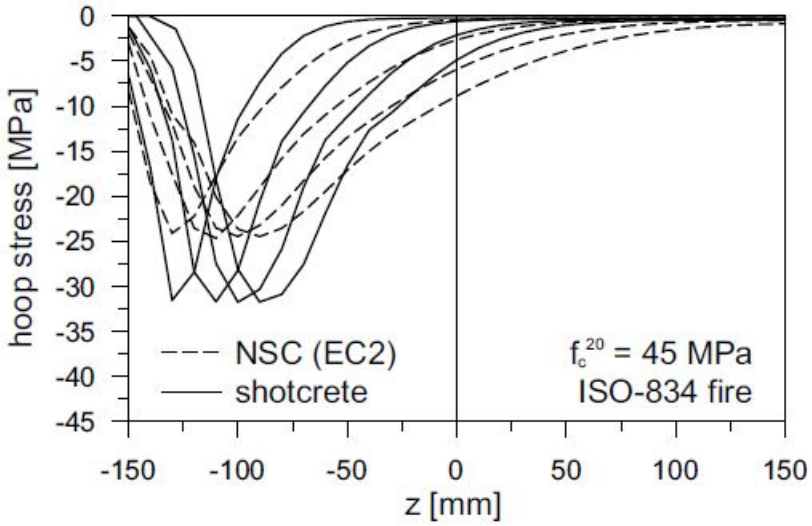

Figure 1.12: *Hoop stress migration along the radius of the lining, according to finite-element analysis. [Bamonte et al., 2016]*

The results show that the two materials behave similarly and that at the beginning the intrados of the lining is characterised by high values of compressive hoop stress because of thermal variation, while this trend tends to shift with time in the direction of the extrados (Figure 1.12).
The starting point of the present work is [Aliberti and Miglietta, 2014], where both analytical and finite element models are presented. The authors state that the presence of rock can be considered as a rigid constraint regardless the type of material and that it reacts to the expansion of the lining as a spring. Additionally, the simulations agree on confirming that the behaviour of concrete is in any case elastic.
The majority of studies that have treated this kind of problem are mainly focused on the behaviour of the concrete lining, while the surrounding ground is usually considered as an infinite elastic medium whose response is well represented by a set of elastic springs. However, a more precise approach would take into consideration the interaction between concrete and rock. Moreover, as the concrete spalls the lining becomes thinner and thinner, thus the possibility of thermal variation of the rock and the consequent change in its state of stress should be taken into consideration.

1.2.3 Effects of high temperatures on concrete

The exposure of concrete to fire can generate irreversible damage to the material. In particular, high temperatures can lead to:

- spalling of the lining: the stress state generated by high temperature in the concrete layers induce them to spall. This phenomenon depends on the maximum temperature that is reached and on heat release rate (HRR);
- degradation of the mechanical properties of concrete. Above temperatures of 550-600°C the material has lost enough strength so as not to be structurally useful [Khoury, 2000]. In particular, concrete looses its strength and its stiffness. This means that the Young's Modulus describing the stress-strain curves reduces with temperature.

Spalling

Spalling represents the most common failure that is produced by fire on concrete (Figure 1.13). The high temperatures that are reached during a fire make pore pressure rise due to the evaporating water, moreover the heated surface is compressed due to a thermal gradient in the cross section and cracks form because of the different thermal expansion between aggregate and cement paste. As alrready mentioned above, during a fire the material also loses its strength. When dealing with reinforced concrete, the difference in thermal expansion between concrete and steel rebars must be considered as well.
All these mechanisms may induce the spalling of concrete and are influenced by many factors: heating rate (about 20-100°C/min during fires [Aliberti and Miglietta, 2014]), permeability of the material, pore saturation level, presence of reinforcement, and level of applied loading [Khoury, 2000]. Spallling can be subdivided into five different categories, depending on the aforementioned mechanisms that involve the phenomenon:

- *violent spalling:* concrete pieces are popped off quickly due to pore pressure increase, thermal gradients and internal cracking. Pore pressure increase depends on heating rate, moisture content, permeability, porosity and the presence of polypropylene fibres [Promat-Tunnel]. Thermal gradient (Figure 1.15) is mainly influenced by heating rate, but it can also increase whenever the concrete ring is very large, or in presence of presteressing and lateral restraint.

- *progressive gradual spalling (sloughing off):* it is mainly influenced by the peak temperature, that determines the strength loss. Whenever concrete is heated from below and the peak temperature is very high, the material has not enough strength to carry its own weight, so some cracked pieces of concrete fall due to gravity.

- *corner spalling:* it is caused by the different deformation of concrete and reinforcement bars at high temperatures.

- *explosive spalling:* it is induced by the combination of pore pressure and thermal gradient. At the front of heat penetration, a "moisture clog" (area with high pore pressure) develops inside the concrete. Part of the moisture is pushed further into the colder part of the concrete due to the pressure gradient at the back of the clog. If the heated surface is under compression due to a thermal gradient the complete heated surface may be blown away with a loud bang. This type of spalling is especially likely to occur on structural members heated from more than one side, such as columns and beams. When moisture clogs are advancing into the concrete from all heated sides, at some point in time the moisture clogs will meet in the centre of the cross-section, giving a sudden rise in pore pressure which may cause large parts of the cross-section to explode. This type of spalling can also occur after a considerable duration of the fire if the concrete surface has been protected with an insulating layer.[Promat-Tunnel]

- *post-cooling spalling:* it occurs after the fire is over, after cooling down or maybe even during extinguishing, [Khoury, 2000]. This kind of spalling characterises concrete with calcareous aggregates: as soon as CaO rehydrates, it expands causing internal cracks and making concrete pieces fall.

In Figure 1.14 each type of spalling is described by the mechanisms that it involves.
As already mentioned, there are many factors that need to be evaluated in order to correctly interpret the problem. It is thus very difficult to consider all these aspects acting in a combined way when studying analytically the problem. Khoury suggests to use an abacus, which represents a first simplified attempt to distinguish the regions affected by spalling (Figure 1.16). In this abacus, moisture content and applied stress are considered.
However, since the phenomenon is generated by a combination of factors, it is still very difficult to identify a precise criterion which could establish whether there is spalling or not. This is the reason why the literature proposes some *spalling*

Figure 1.13: *Fire spalling on an external concrete wall [McNamee, 2013]*

	Pore pressure due to evaporation of moisture	Compression due to thermal gradient	Internal cracking due to different thermal expansion aggregate - cement paste	Cracking due to different thermal deformation concrete - steel	Strength loss due to chemical transitions
Violent Spalling	x	x	x		
Sloughing Off			x		x
Corner Spalling				x	
Explosive Spalling	x	x			
Post-Cooling Spalling			x		x

Figure 1.14: *Types of spalling and involved mechanisms. [Promat-Tunnel]*

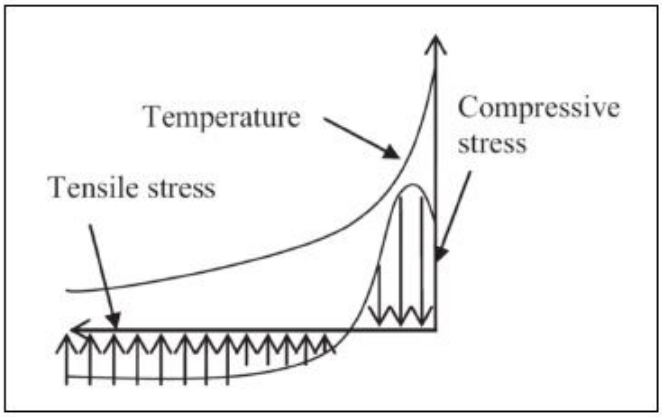

Figure 1.15: *Thermal stress induced by fire. The thermal conductivity of concrete is very low, thus the exposure to high temperatures makes the internal part of the lining compressed, while the cooler regions are characterised by tensile stresses. [Ma et al., 2015]*

scenarios, that is studying the effects of spalling on the structure by assuming different scenarios (i.e. different spalling depths), as in [Savov et al., 2005].
If the temperature has reached high values (in [Caner et al., 2005] when it goes beyond 300°C), concrete is too damaged and thus it must be substituted by new material as soon as the tunnel has cooled down enough. The new material should be similar to the previous one in order not to create weak zones along the tunnel.

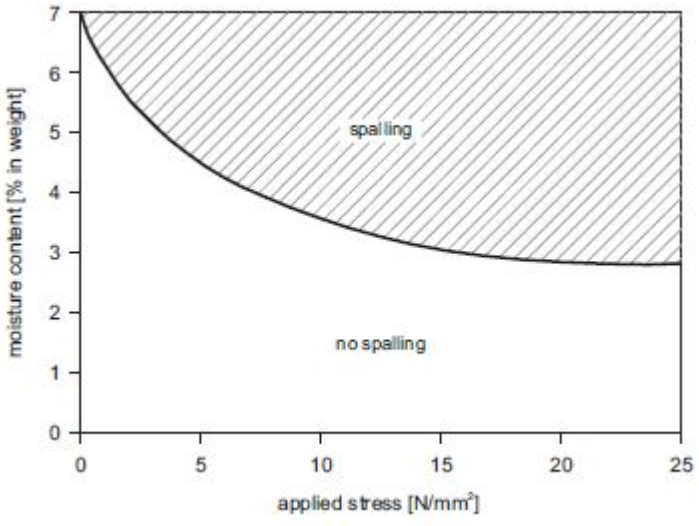

Figure 1.16: *Simple scheme that can be used to consider the possibility of having spalling, considering moisture content and applied stress [Khoury, 2000]*

Degradation of concrete properties

In [Eurocode2, 2005] the degradation of concrete with temperature θ is described by some parameters that depend on the type of aggregate which constitutes the material. Generally, concrete is described by its compressive strength, since it has almost null resistance to tension (this contribution is usually given by steel rebars). The parameters describing concrete samples are reported in the following table:

f_{ck}	peak strength of cylindrical sample of concrete at T_0
$f_{c,\theta}$	peak strength at temperature θ
$k_c(\Theta)$	reduction fator of peak strength with temperature. $(f_{c,\theta}/f_{ck})$
$\varepsilon_{c1,\Theta}$	compressive strain at peak stress at temperature θ
$\varepsilon_{cu1,\theta}$	ultimate compressive strain at temperature θ

Table 1.2: *Mechanical parameters describing concrete depending on temperature θ*

These parameters are used to build the stress-strain curves at each temperature (Figure 1.17). The peak is given by $(\varepsilon_{c1,\theta}, f_{c,\theta})$, and as soon as $\varepsilon \leqslant \varepsilon_{c1,\theta}$ the trend is non linear:

$$\sigma(\theta) = \frac{3\varepsilon f_{c,\theta}}{\varepsilon_{c1,\theta}\left[2 + \left(\frac{\varepsilon}{\varepsilon_{c1,\theta}}\right)^3\right]} \tag{1.9}$$

After the peak, it is possible to choose a linear or non-linear model. As temperature rises, the strength decreases, and the material becomes more ductile. This results in a shift of the peak towards the right (bigger values of strain) and downwards (decrease of strength). In Figure (1.18) the variation of parameters with θ is shown.

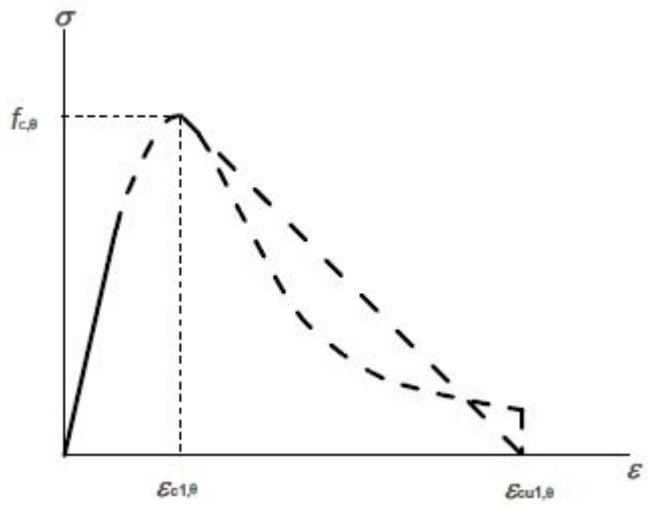

Figure 1.17: *Stress-strain relation according to [Eurocode2, 2005]*

Concrete	Siliceous aggregates			Calcareous aggregates		
temp. θ	$f_{c,\theta}$ / f_{ck}	$\varepsilon_{c1,\theta}$	$\varepsilon_{cu1,\theta}$	$f_{c,\theta}$ / f_{ck}	$\varepsilon_{c1,\theta}$	$\varepsilon_{cu1,\theta}$
[°C]	[-]	[-]	[-]	[-]	[-]	[-]
1	2	3	4	5	6	7
20	1,00	0,0025	0,0200	1,00	0,0025	0,0200
100	1,00	0,0040	0,0225	1,00	0,0040	0,0225
200	0,95	0,0055	0,0250	0,97	0,0055	0,0250
300	0,85	0,0070	0,0275	0,91	0,0070	0,0275
400	0,75	0,0100	0,0300	0,85	0,0100	0,0300
500	0,60	0,0150	0,0325	0,74	0,0150	0,0325
600	0,45	0,0250	0,0350	0,60	0,0250	0,0350
700	0,30	0,0250	0,0375	0,43	0,0250	0,0375
800	0,15	0,0250	0,0400	0,27	0,0250	0,0400
900	0,08	0,0250	0,0425	0,15	0,0250	0,0425
1000	0,04	0,0250	0,0450	0,06	0,0250	0,0450
1100	0,01	0,0250	0,0475	0,02	0,0250	0,0475
1200	0,00	-	-	0,00	-	-

Figure 1.18: *Values for the main parameters of the stress-strain relationships of normal weight concrete with siliceous or calcareous aggregates concrete at elevated temperatures. [Eurocode2, 2005]*

1.3 Thick-cylinder theory

To study analytically the stress-strains effects induced by fire on the lining the thick-cylinder theory can be used to model the problem. The rise in temperature due to fire is supposed to change with radius r, whereas there is no variation with coordinate θ: therefore, the problem is assumed axisymmetric.
The internal part of the hollow cylinder is subjected to high temperatures induced by the fire, while the external face is characterised by a low temperature variation thanks to the insulation properties of concrete. Thus, the temperature of the hollow cylinder decreases with the radius.
In order to study the mechanical effects on the structure induced by the variation of temperature, it is necessary to make a hypothesis on the temperature profile inside the lining and the rock, alternatively, to use empirical data. Then, by assuming linear elastic behaviour of the material, the thermal stresses, strains and displacements can be calculated.
The model of [Corradi Dell'Acqua, 2010] aims at investigating the effects of high temperatures on the lining. The temperature inside the cylinder varies according to a pre-established law. In this model, a logarithmic law and a polynomial one are considered. In the first case the temperature varies with a slightly increasing rate, while the polynomial temperature profile is characterised by a high rate for the first centimeters and a lower one in the external part of the cylinder.
Once the thermal profile has been established, by assuming linear elastic behaviour of concrete ring it is possible to calculate the stress state. The rock is considered as a set of elastic springs that reacts to the radial expansion of the concrete ring. The thermal variation induces the cylinder to expand in the outward direction, so that the surrounding soil is subjected to pressure generated by the expansion of concrete. On the other hand, the concrete ring is subjected to external pressure, which represents the contribution of the soil that reacts to the movement of the ring. This contribution can be calculated as the stiffness of the springs multiplied by the radial displacement of the ring. Thus, the soil represents a rigid constraint, which is not affected by temperature variation.
To have a better insight of the model, section 3.1 reports the equations and the results obtained for our specific case study.
Instead of assuming a continuous body, it is possible to discretize the support in sub-layers, each one characterised by its specific properties and thermal load. This idea was first presented in [Vedeld and Sollund, 2013] for a two-layer cylinder and later in [Vedeld and Sollund, 2014] the same authors have published a model for a

multi-layered cylinder. These models were published on the *International Journal of Pressure Vessels and Piping*, and they have been developed to analyse the behaviour of pressurized multi-layer pipelines used for the distribution of hot fluids. To solve the model, plane strain condition or generalized plane condition (i.e. axial strain is constant in each layer) are assumed.
Layer i is defined by its internal radius r_{i-1} and to its external radius r_i. Each layer is described by its Young Modulus E_i, Poisson's Ratio ν_i, thermal variation ΔT_i and coefficient of thermal dilation α_i. Then, the model requires as input data the external pressure p_{ext} at the external radius and the internal pressure p_{int} at the intrados (Figure 1.19).
The equations of the model are reported in section 3.2. Assuming a multi-layer model permits to discretize not only the concrete lining, but also the surrounding rock as part of a larger body. In this way, the rock is no more considered as an external constraint, but it is part of the geometry, that can be subjected to a temperature variation, too.
Moreover, the multi-layer model permits to take into account a not homogeneous body, where each layer is characterised by its own mechanical and thermal properties and may be associated to a discrete value of thermal variation instead of a value from an analytical profile of temperature. Assuming continuity of radial stress and displacement at the interface between layers, this model provides an important analytical tool to compute the stress and strain fields with distance r, that can be used for many applications.

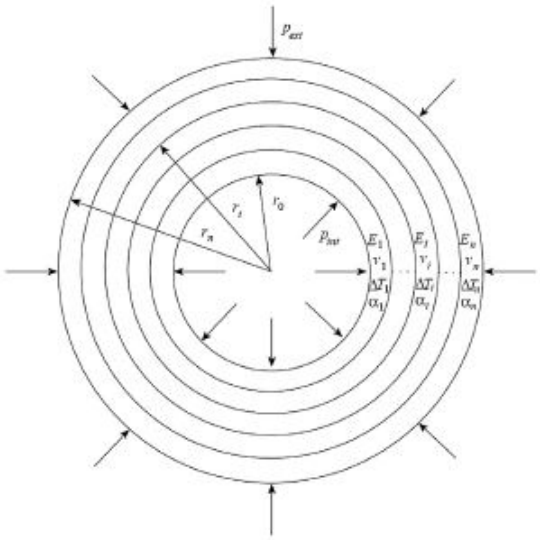

Figure 1.19: *Multi-layer cylinder. [Vedeld and Sollund, 2014]*

Chapter 2

The Convergence-Confinement Method

When performing a tunnel excavation, the initial state of stress of the rock is completely altered and it becomes necessary to study its variation in order to design the necessary support. As the face of the tunnel advances the surrounding rock experiences a reduction of stress and progressively tends to converge to the centre of the tunnel, until it reaches stability.
By using the Convergence-Confinement method it is possible to estimate the load which must be carried by a support that is installed behind the face of a tunnel. During excavation the rock close to the face is characterised by a particular condition which is described by the *face effect*. It means that the support which is installed just behind the face will not have to carry the entire load of the rock, since a part of it will be still carried by the ground mass ahead of the excavation face.
When the face is far enough from the support, the entire load of the rock must be supported by the concrete ring. The objective of the Convergence-Confinement Method is to evaluate the stress acting on the support from the time of its installation until the face effect has disappeared. Figure (2.1) shows a cylindrical tunnel of radius a where the support is installed at a distance L to the face. The rock in section A-A' represented in (2.1b) is characterised by an elastic region and depending on the stresses that develop in the rock there could be a plastic region as well. Looking at the figure, p_i represents the pressure of the support on the rock, while u_r is the radial displacement of the soil, which tends to converge to the centre of the tunnel. In (2.1c) the same cross-section is shown, but focused on the support. Its thickness is t_c and it is subjected to the pressure of rock, called p_s.

In order to correctly study the problem, some hypothesis must be set up:

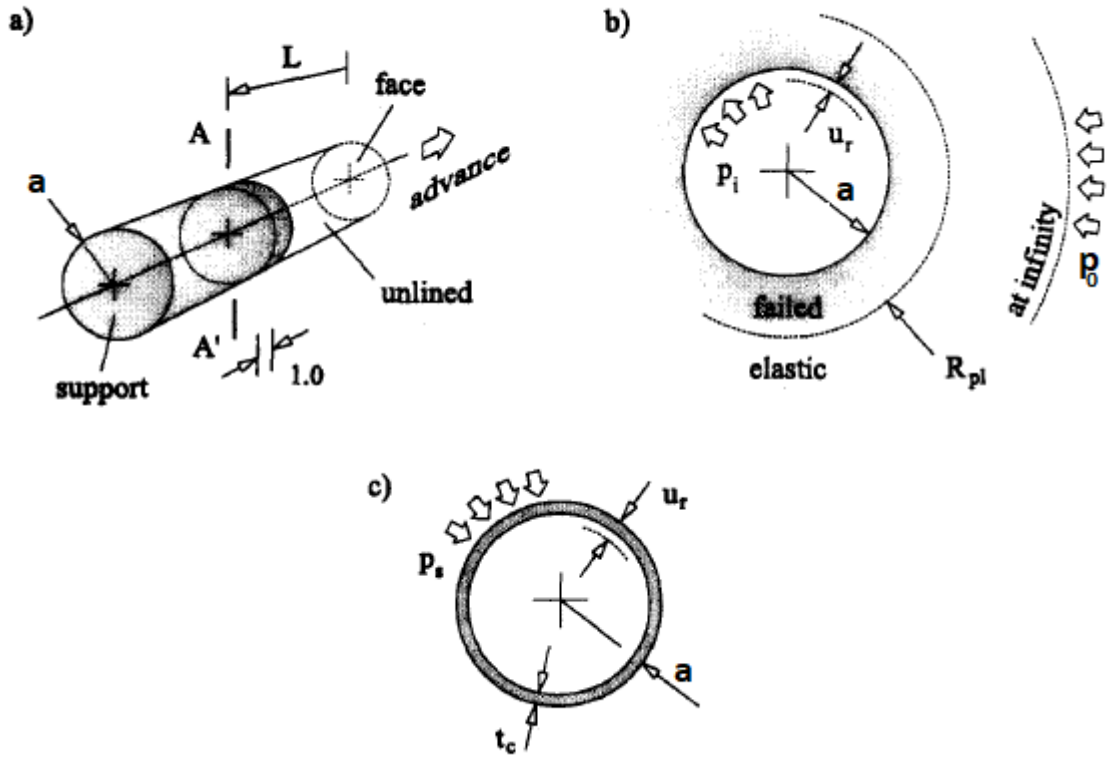

Figure 2.1: *a) Representation of the cylindrical tunnel of radius a, with installed support until section A-A' and face at distance L from the concrete ring b) Cross-section of the rock at A-A'c) Cross-section of the support at A-A'[Carranza-Torres and Fairhurst, 2000]*

- cylindrical coordinates (r, θ, z) are adopted;
- the tunnel is deep and circular, with constant radius a;
- the initial state of stress in the rock p_0 is isotropic and constant;
- the problem is axisymmetric and plain strain conditions are adopted ($\varepsilon_z = 0$);
- the medium is continuous, homogeneous and isotropic;
- the behaviour of the rock is elastic or perfectly-plastic;
- the behaviour of the concrete lining is elastic.

The state of stress of the rock in section A-A' changes during the excavation process. In particular, there are three main phases to be considered (Figure 2.2):

1. at time t=t_0, the support is installed. In this case, it will have to carry a null pressure, because the rock carries its load and it still has to converge. The stress release occurred for $t < t_0$ has induced a convergence before the construction of the support. The support will bear only pressures developing afterwards.

2. when $t_0 < t < t_D$ the support is more and more loaded and p_s increases while the excavation face advances.

3. at time $t = t_D$ the face of the tunnel is far enough from section A-A' and the rock has reached its final convergence u_r^D. The equilibrium between rock and lining is finally reached and the support has to carry the final loading p_s^D.

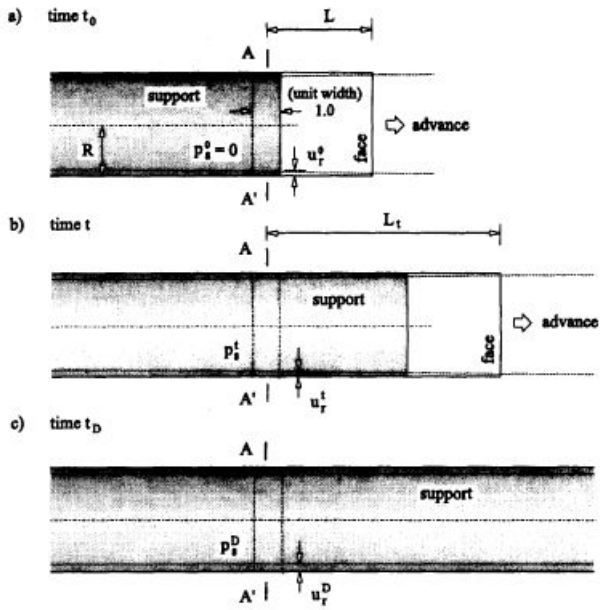

Figure 2.2: *Loading of the support at section A-A' related to the principal stages of excavation*

The procedure proposed by the Convergence-Confinement Method consists of representing graphically the behaviours of the rock and the support from the time of installation until equilibrium between the two is reached. This is realised by evaluating three curves:

- Longitudinal Deformation Profile (LDP), which shows the development of the

face effect along the tunnel in terms of rock convergence at different distances from the face;

- Ground Reaction Curve (GRC), which represents the behaviour of the rock during excavation in terms of radial convergence u_r and radial stress p at radius a;
- Lining Characteristic Curve (LCC), which is representative of the behaviour of the concrete support in terms of radial convergence u_r and radial stress p from the moment of its installation on.

The three curves are reported in Figure (2.3).

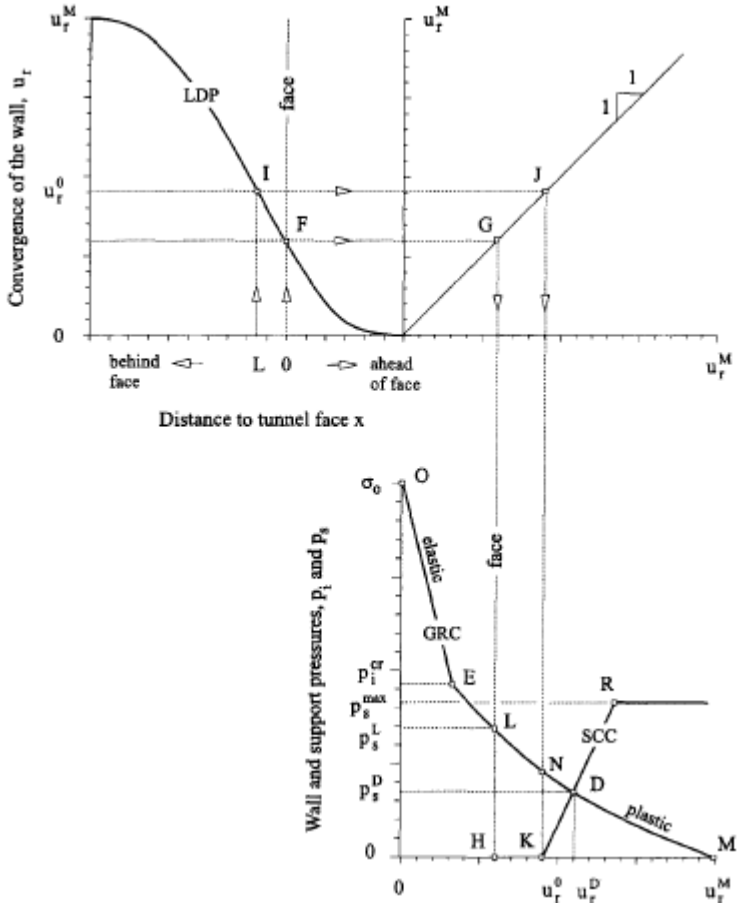

Figure 2.3: *Representation of LDP (Longitudinal Deformation Profile), GRC (Ground Reaction Curve) and LCC (Lining Characteristic Curve)*

The LDP shows clearly that the rock is influenced by the closeness of the exca-

vation face and consequently the convergence rate is low. Far behind the face, the convergence of the rock has reached the value u_r^M, which is the final value of displacement; while far ahead the convergence is null, since the rock is still undisturbed. Between these two boundary conditions, the rock moves towards the centre of the tunnel following the trend shown in the figure.
Looking at the LDP graph, point I and F are representative respectively of the support installation and of the face. Again, it is possible to notice that before installing the lining the rock has already moved towards the centre of the tunnel. The GRC can be subdivided into two parts: when the radial pressure is close to p_0 the rock has a linear elastic behaviour, but as σ_r decreases, a plastic region around the tunnel develops. Finally, the LCC is built assuming linear elastic behaviour of the concrete. Point K in the graph represents section A-A' shown in Figure (2.2), where the support is installed, and it corresponds with convergence u_0: it means that for $u < u_0$ the rock is free to converge, while from point K on the support interacts with the soil.
Point D represents the equilibrium between the two curves. Generally, when designing a tunnel it is important to fix a limit value of convergence for the support, then if the stiffness of concrete is known it is possible to calculate which is the minimum convergence u_0 and consequently to know when to install the support during excavation. Further details on the analytical origin of GRC and LCC are reported in the following sections.

2.1 Ground Reaction Curve

The Ground Reaction Curve represents the behaviour of the rock during the excavation phase. The initial state of stress of the rock is p_0, which is assumed to be constant and isotropic.
When the state of the rock is altered, it is necessary to study the problem referring to some basic assumptions: first of all, the equilibrium must be satisfied. Equation (2.1) guarantees that the state of stress is locally equilibrated in the medium. Its demonstration is reported in Appendix A.

$$\frac{\partial \sigma_r}{\partial r} + \frac{\sigma_r - \sigma_\theta}{r} = 0 \tag{2.1}$$

Secondarily, the compatibility requires the following relations between strains and displacements:

$$\varepsilon_r = \frac{\partial u_r}{\partial r} \tag{2.2}$$

$$\varepsilon_\theta = \frac{u_r}{r} \tag{2.3}$$

which can also be expressed using the following formula:

$$\frac{\varepsilon_r - \varepsilon_\theta}{r} = \frac{\partial \varepsilon_\theta}{\partial r} \tag{2.4}$$

Finally, the Hooke relations for linear elastic media:

$$\begin{cases} \varepsilon_r = \dfrac{\delta\sigma_r}{E} - \dfrac{\nu}{E}(\delta\sigma_\theta + \delta\sigma_z) \\ \varepsilon_\theta = \dfrac{\delta\sigma_\theta}{E} - \dfrac{\nu}{E}(\delta\sigma_r + \delta\sigma_z) \\ \varepsilon_z = \dfrac{\delta\sigma_z}{E} - \dfrac{\nu}{E}(\delta\sigma_\theta + \delta\sigma_r) \end{cases} \tag{2.5}$$

Since the problem is axisymmetric and plain strain conditions are adopted, $\varepsilon_z = 0$. Consequently, the stress along the axial coordinate is:

$$\delta\sigma_z = \nu(\delta\sigma_r + \delta\sigma_\theta) \tag{2.6}$$

On the basis of these relations it is possible to build the GRC. In the following paragraphs a brief analytical study of the curve is presented.

2.1.1 Elastic behaviour of the rock

When the stress variation induced by excavation is within a limited value, the rock behaviour is elastic (Figure 2.3). In this condition it can be demonstrated that:

$$\sigma_r + \sigma_\theta = c \tag{2.7}$$

as reported in Appendix B.
By imposing this hypothesis into the equilibrium equation (2.1), the following expression is obtained:

$$r\frac{\partial \sigma_r}{\partial r} = c - 2\sigma_r \tag{2.8}$$

Then, if the two members are integrated:

$$\int \frac{d\sigma_r}{c - 2\sigma_r} = \int \frac{1}{r} dr \tag{2.9}$$

The solution of the integral is:

$$c - 2\sigma_r = \frac{k}{r^2} \tag{2.10}$$

Once the expression of σ_r is obtained, it is possible to get the circumferential stress as well by introducing the hypothesis (2.7):

$$\begin{cases} \sigma_r = \dfrac{c}{2} - \dfrac{k}{2r^2} \\ \sigma_\theta = \dfrac{c}{2} + \dfrac{k}{2r^2} \end{cases} \tag{2.11}$$

In order to find the values of constants c and k, two boundary conditions are imposed:

$$\begin{cases} \sigma_r = p & \text{if } r = a \\ \sigma_r = p_0 & \text{if } r \to \infty \end{cases} \tag{2.12}$$

Finally, the state of stress in elastic rock is:

$$\begin{cases} \sigma_r = p_0 - \dfrac{(p_0 - p)}{r^2/a^2} \\ \sigma_\theta = p_0 + \dfrac{(p_0 - p)}{r^2/a^2} \\ \sigma_z = 2\nu p_0 \end{cases} \tag{2.13}$$

The stress variation induced by the excavation may be expressed as:

$$\begin{cases} \delta\sigma_r = \sigma_r - p_0 \\ \delta\sigma_\theta = \sigma_\theta - p_0 \end{cases} \tag{2.14}$$

By combining equations (2.13) and (2.14):

$$\begin{cases} \delta\sigma_r = -\dfrac{p_0 - p}{r^2/a^2} \\ \delta\sigma_\theta = \dfrac{p_0 - p}{r^2/a^2} \end{cases} \tag{2.15}$$

Once the stress path has been defined, the relation between the radial stress p and the elastic convergence of the tunnel u can be obtained by simple calculations. Hooke equations (2.5) for elastic media as function of the stress variation induced

by excavation may be rewritten as:

$$\begin{cases} \varepsilon_r = \dfrac{1+\nu}{E}\big[(1-\nu)\delta\sigma_r - \nu\delta\sigma_\theta\big] \\ \varepsilon_\theta = \dfrac{1+\nu}{E}\big[(1-\nu)\delta\sigma_\theta - \nu\delta\sigma_r\big] \\ \varepsilon_z = 0 \end{cases} \tag{2.16}$$

The equations of the stress variation (2.14) can be introduced in the Hooke equation for ε_θ:

$$\varepsilon_\theta = \frac{1+\nu}{E}\frac{(p_0 - p)}{r^2/a^2} \tag{2.17}$$

Compatibility between strains and displacements (Equation 2.4) is imposed, in order to calculate the radial convergence of the tunnel:

$$u(r) = \varepsilon_\theta \cdot r = \frac{1+\nu}{E}\frac{(p_0 - p)}{r}a^2 \tag{2.18}$$

This equation establishes that during the excavation of the tunnel the stresses reduce, while the tunnel experiences inward radial convergence. When considering $r = a$, i.e. at the tunnel radius, the elastic convergence as function of the excavation process is:

$$u = (p_0 - p)\frac{(1+\nu)}{E}a \tag{2.19}$$

When the behaviour of the rock is linear elastic the relationship between its convergence u and pressure p is linear. In particular, when $p = p_0$ there is no displacement, since the rock is at its undisturbed status, while the convergence reaches its maximum value u_{el} at $p = 0$, when the face effect has disappeared. Thus, the final convergence of the tunnel can be easily found by imposing $p = 0$:

$$u_{el} = p_0\frac{(1+\nu)}{E}a$$

The linear relationship between u and p is shown in Figure (2.4).

2.1.2 Elasto-plastic behaviour of the rock

As the excavation process proceeds, the radial stresses in the rock tend to decrease, while the hoop stresses increase. At some point, the behaviour of soil is no more elastic and a plastic region forms: in this zone the convergence u is no more

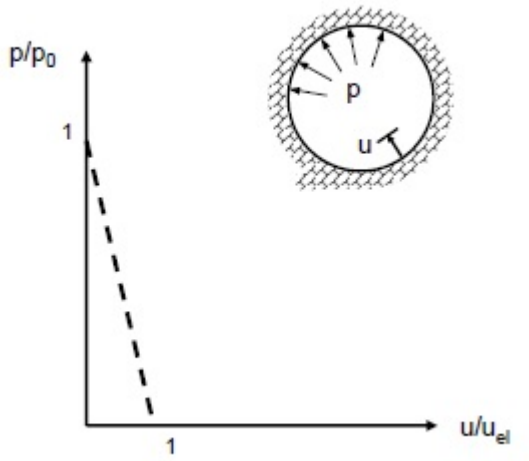

Figure 2.4: *GRC for elastic rock*

described by the elastic law that have been previously reported in Equation 2.19. The plastic region forms as soon as the stress components fulfill the Mohr Coulomb criterion. The associated flow rule is chosen and in order to find the expression for GRC, two additional mechanical parameters of the rock are required: the friction angle ϕ and coesion c. The function of plasticity is the envelope of the Mohr circles which represent failure states of stress. Figure (2.5) shows the Mohr Coulomb plastic function, assuming compression stresses as negative, while tension has positive sign.

The failure surface is defined as:

$$F(\sigma) = \sigma_r K_p - \sigma_\theta - 2c\sqrt{K_p} = 0 \tag{2.20}$$

where $K_p = \dfrac{1+\sin\phi}{1-\sin\phi}$.

When $F(\sigma) < 0$ the rock behaves elastically, while compliance with condition $F(\sigma) = 0$ guarantees the rock to have a plastic behaviour.
This criterion is typically used when dealing with soils or rocks. Alternatively, in the case of soils in undrained conditions, Tresca flow rule can be used.
The trends of the stresses that develop in the plastic region are not the same as the ones in the elastic zone. They can be found by combining the equilibrium (2.1) and the plasticity condition (2.20):

$$r\frac{\partial \sigma_r}{\partial r} = \sigma_r(K_p - 1) - 2c\sqrt{K_p} \tag{2.21}$$

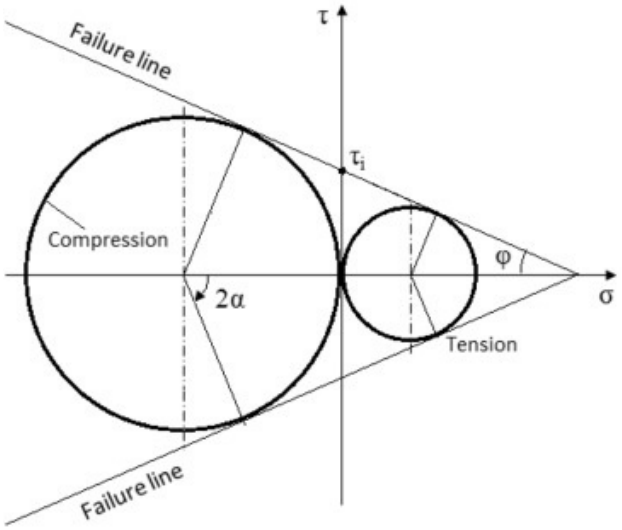

Figure 2.5: *Mohr-Coulomb plastic function*

which can be solved introducing the integral:

$$\frac{1}{K_p - 1} \int \frac{(K_p - 1)}{(K_p - 1)\sigma_r - 2c\sqrt{K_p}} d\sigma_r = \int \frac{1}{r} dr \tag{2.22}$$

The solution is:

$$\sigma_r = \frac{Dr^{K_p - 1} + 2c\sqrt{K_p}}{K_p - 1} \tag{2.23}$$

Constant D is evaluated assuming that on the boundary excavation surface ($r = a$) the radial stress $\sigma_r = p$:

$$p = \frac{Da^{K_p - 1} + 2c\sqrt{K_p}}{K_p - 1} \tag{2.24}$$

Finally, constant D is:

$$D = \frac{(K_p - 1)p - 2c\sqrt{K_p}}{a^{K_p - 1}} \tag{2.25}$$

The final expressions of plastic radial and tangential stresses are:

$$\begin{cases} \sigma_r = \left(\frac{r}{a}\right)^{K_p-1}(p-F)+F \\ \sigma_\theta = K_p\left(\frac{r}{a}\right)^{K_p-1}(p-F)+F \end{cases} \tag{2.26}$$

where $F = \dfrac{2c\sqrt{K_p}}{K_p-1}$.

For sake of simplicity, the trends of stresses as function of the radius r are reported in the following systems of equations:

$$\sigma_r = \begin{cases} \left(\frac{r}{a}\right)^{K_p-1}(p-F)+F & \text{if } a < r < r_{pl} \\ p_0 - \dfrac{p_0-p_{pl}}{\frac{r^2}{{r_{pl}}^2}} & \text{if } r > r_{pl} \end{cases} \tag{2.27}$$

$$\sigma_\theta = \begin{cases} K_p\left(\frac{r}{a}\right)^{K_p-1}(p-F)+F & \text{if } a < r < r_{pl} \\ p_0 + \dfrac{p_0-p_{pl}}{\frac{r^2}{{r_{pl}}^2}} & \text{if } r > r_{pl} \end{cases} \tag{2.28}$$

The interface between the elastic and the plastic regions coincides with the plastic radius r_{pl}, where the radial stress is p_{pl}. This value is easily obtained by imposing that the stress calculated in the elastic regime (2.13) fulfill the plasticity condition (2.20):

$$p_{pl} = 2\frac{p_0 + c\sqrt{K_p}}{K_p+1} \tag{2.29}$$

While the plastic radius can be calculated by imposing that the plastic radial stress σ_r for $r = r_{pl}$ is equal to p_{pl}:

$$2\frac{p_0 + c\sqrt{K_p}}{K_p+1} = \left(\frac{r_{pl}}{a}\right)^{K_p-1}(p-F)+F \tag{2.30}$$

The final expression of plastic radius is:

$$r_{pl} = a\left[2\frac{p_0 - F}{(p - F)(K_p + 1)}\right]^{\frac{1}{K_p - 1}} \tag{2.31}$$

In order to build the Ground Reaction Curve, the next step is to calculate the total inward convergence. It can be done using the flow rule for plastic materials, that in the associated case is:

$$\dot{\varepsilon} = \dot{\lambda}\frac{\partial F}{\partial \sigma} \tag{2.32}$$

and using the Mohr-Coulomb plasticity function (2.20). The expression of radial plastic convergence that is used in the present work comes from [Hoek, 2000]:

$$u_{pl} = a\frac{1+\nu}{E}\left[2(1-\nu)(p_0 - p_{pl})\left(\frac{r_{pl}}{a}\right)^2 - (1-2\nu)(p_0 - p)\right] \tag{2.33}$$

As soon as a plastic region forms in the rock, the total inward convergence increases: in fact, as shown in Figure (2.6), by following a linear trend the maximum convergence u_{el} would have been lower than the final value u_{ep}.

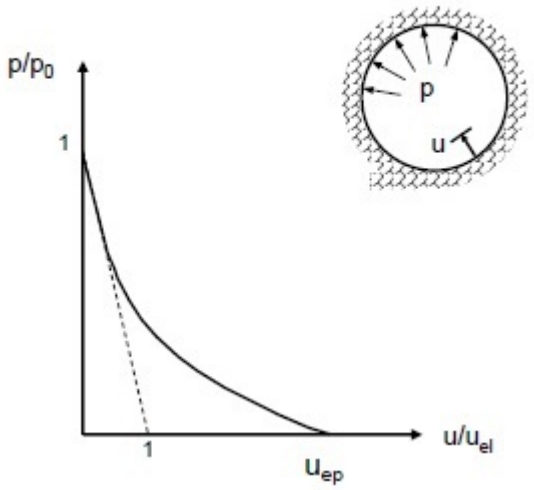

Figure 2.6: *Ground reaction curve for elasto-plastic behaviour*

2.2 Lining Characteristic Curve

The Lining Characteristic Curve represents the behaviour of the concrete ring which is subjected to the pressure of rock, by assuming that it behaves linearly and elastically. In order to correctly represent it, it is necessary to introduce some geometrical and mechanical parameters:

- Young's Modulus E_{con};
- Poisson coefficient ν_{con};
- stiffness of the support k_{con};
- thickness of the support t;

While E_{con}, ν_{con} and t are given, the stiffness must be calculated. In the present work, it is defined as:

$$k_{con} = \frac{E_{con}}{1+\nu_{con}} \frac{a^2-(a-t)^2}{a[(a-t)^2+a^2(1-2\nu_{con})]} \tag{2.34}$$

This formula has been obtained following the procedure of [Oreste, 2003a], that will be briefly presented in the following paragraphs.

The radial and the hoop stress may be expressed as functions of the strains from Hooke relations in (2.5):

$$\begin{cases} \sigma_r = \dfrac{E}{(1+\nu)(1-2\nu)}\big((1-\nu)\varepsilon_r + \nu\varepsilon_\theta\big) \\ \sigma_\theta = \dfrac{E}{(1+\nu)(1-2\nu)}\big((1-\nu)\varepsilon_\theta + \nu\varepsilon_r\big) \end{cases} \tag{2.35}$$

Then, equilibrium is imposed by Equation (2.1), obtaining:

$$\frac{1}{r}\frac{E}{(1+\nu)(1-2\nu)}\big((1-2\nu)\varepsilon_r-(1-2\nu)\varepsilon_\theta\big) = -\frac{\partial}{\partial r}\Big[\frac{E}{(1+\nu)(1-2\nu)}\big((1-\nu)\varepsilon_r+\nu\varepsilon_\theta\big)\Big] \tag{2.36}$$

Which then becomes:

$$(1-2\nu)\frac{\varepsilon_r-\varepsilon_\theta}{r} = -\frac{\partial}{\partial r}\Big((1-\nu)\varepsilon_r+\nu\varepsilon_\theta\Big) \tag{2.37}$$

It is then necessary to impose compatibility between strains and displacements, by substituting (2.4) and then introducing the expressions of strains in (2.2) and (2.3):

$$(1-2\nu)\frac{d}{dr}\left(\frac{u}{r}\right) = -\frac{d}{dr}\left((1-\nu)\frac{du}{dr} + \nu\frac{u}{r}\right) \tag{2.38}$$

The resulting equation is an ordinary differential one:

$$\frac{d^2u}{dr^2} + \frac{1}{r}\frac{du}{dr} - \frac{u}{r^2} = 0 \tag{2.39}$$

The solution of the differential equation is the following:

$$u = Ar + \frac{B}{r} \tag{2.40}$$

Where A and B are constants to be determined. This equation represents the radial displacement of a generic hollow cylinder, which may be subjected to thermal load or to pressure. By combining equations (2.2), (2.3) and (2.40):

$$\begin{cases} \varepsilon_r = A - \dfrac{B}{r^2} \\ \varepsilon_\theta = A + \dfrac{B}{r^2} \end{cases} \tag{2.41}$$

Hooke equations may be expressed as follows:

$$\begin{cases} \sigma_\theta = C\varepsilon_\theta + D\varepsilon_r \\ \sigma_r = C\varepsilon_r + D\varepsilon_\theta \end{cases} \tag{2.42}$$

where $C = \dfrac{E_{con}(1-\nu_{con})}{(1-2\nu_{con})(1+\nu_{con})}$ and $D = \dfrac{E_{con}\nu_{con}}{(1-2\nu_{con})(1+\nu_{con})}$.

It is then possible to express Hooke relations as functions of strains defined in (2.41):

$$\begin{cases} \sigma_\theta = C\left[A + \dfrac{B}{r^2}\right] + D\left[A - \dfrac{B}{r^2}\right] \\ \sigma_r = C\left[A - \dfrac{B}{r^2}\right] + D\left[A + \dfrac{B}{r^2}\right] \end{cases} \tag{2.43}$$

Finally, the problem can be solved by imposing two boundary conditions:

$$\begin{cases} u_a = (u - u_{in,con}) & \text{if r=a} \\ \sigma_r = 0 & \text{if r=a-t} \end{cases} \tag{2.44}$$

The first condition establishes that the convergence at the extrados of the support must be equal to the convergence of the rock from the instant of the support installation (thus excluding the displacement of the rock before the installation of the support); the second one imposes that there is no radial pressure acting on the intrados of the support. By inserting the first boundary condition in equation (2.40) the expression of constant B is:

$$B = a[(u - u_{in,con}) - Aa] \tag{2.45}$$

The second boundary condition is imposed by introducing it in (2.43):

$$C\left[A - \frac{B}{(a-t)^2}\right] + D\left[A + \frac{B}{(a-t)^2}\right] = 0 \tag{2.46}$$

Then, equation (2.45) is substituted in (2.46):

$$C\left[A - \frac{a[(u - u_{in,con}) - aA]}{(a-t)^2}\right] + D\left[A + \frac{a[(u - u_{in,con}) - aA]}{(a-t)^2}\right] = 0 \tag{2.47}$$

Finally, the expressions of constant A and constant B are:

$$\begin{cases} A = (u - u_{in,con})\dfrac{a(1-2\nu_{con})}{(a-t)^2 + a^2(1-2\nu_{con})} \\ B = (u - u_{in,con})\dfrac{a(a-t)^2}{(a-t)^2 + a^2(1-2\nu_{con})} \end{cases} \tag{2.48}$$

Constants A and B can be substituted in equations (2.43), in order to find the correct expression of the radial stress.

$$\sigma_r = (u - u_{in,con})\frac{E_{con}a[r^2 - (a-t)^2]}{(1+\nu_{con})[(a-t)^2 + a^2(1-s\nu_{con})]r^2} \tag{2.49}$$

Equations (2.48) can be rewritten as:

$$\begin{cases} A = \dfrac{p}{k_{con}} \dfrac{a(1-2\nu_{con})}{(a-t)^2 + a^2(1-2\nu_{con})} \\ B = \dfrac{p}{k_{con}} \dfrac{a(a-t)^2}{(a-t)^2 + a^2(1-2\nu_{con})} \end{cases} \tag{2.50}$$

The expressions for constants A and B can be substituted in equations (2.2) and (2.3), in order to calculate σ_θ in correspondence of the intrados (i.e. for $r = a - t$):

$$\sigma_\theta = \frac{p}{k_{con}} \frac{2E_{con}a}{(1+\nu_{con})[(a-t)^2 + a^2(1-2\nu_{con}]} \tag{2.51}$$

Writing Equation (2.49) with reference to radius $r = a$, where a radial stress $\sigma_r = p$ is applied:

$$\begin{aligned} p &= (u - u_{in,con}) \frac{E_{con}[a^2 - (a-t)^2]}{(1+\nu_{con})[(a-t)^2 + a^2(1-s\nu_{con})]a} \\ &= (u - u_{in,con}) k_{con} \end{aligned} \tag{2.52}$$

allows to introduce the stiffness of the lining as the constant ratio between the radial stress and the convergence, as in Equation (2.34).
The final step to correctly represent the LCC is the calculation of p_{max}, which is the maximum value of pressure that can be carried by the lining before its yielding. It is calculated following the procedure of [Oreste, 2003a], assuming that $\sigma_{\theta,max} = f_{ck}$, i.e. that the maximum circumferential stress is equal to the uniaxial compression strength of concrete.
Substituting the expression of k_{con} and imposing $\sigma_{\theta,max} = f_{ck}$, the final value for p_{max} is:

$$p_{max} = \frac{f_{ck}}{2} \left[1 - \frac{(a-t)^2}{a^2} \right] \tag{2.53}$$

2.3 Interpretation of the results

The Convergence-Confinement Method allows to describe the effects of excavation by analysing the behaviour of the lining and the rock mass simultaneously. The analytical equations in section 2.1 and section 2.2 are a simple way to determine

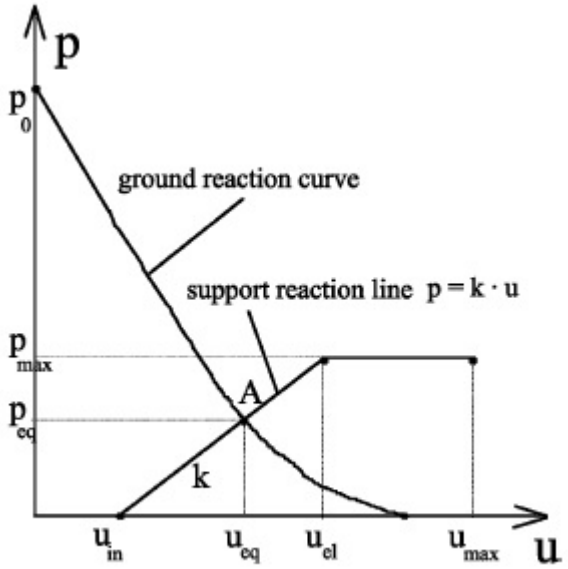

Figure 2.7: *The convergence–confinement method. Key: p: internal tunnel pressure; u: radial displacement of the wall (positive towards the tunnel axis); p_0: in situ hydrostatic stress; p_{eq}: pressure acting on the support structure; p_{max}: pressure that induces the plastic failure of the structure (support capacity); k: support stiffness $[force/length^3]$; u_{in} displacement of the wall before support installation; u_{eq}: displacement at equilibrium; u_{el}: displacement of the wall on reaching the elastic limit in the support; u_{max}: displacement of the wall on collapse of the support; and A: equilibrium point of the tunnel-support system.[Oreste, 2003a]*

the stress state that develops both in the lining and in the rock while performing tunnel excavation. The intersection between the GRC and the LCC represents the equilibrium point and gives information about the final convergence of the tunnel and the radial stress that characterises both domains (Figure 2.7).
The final convergence towards the centre of the tunnel is represented by point A in the figure, but the rock and the lining are characterised by different values of displacement: in fact, the lining is usually installed some instants after the excavation, when the rock has already converged of u_{in}. Thus, the convergence of the lining is equal to $u_{eq} - u_{in}$.

In the case of deep tunnels the undisturbed rock is initially subjected to quite high values of pressure, this is why it is suggested to let the pressure decrease naturally, without installing the lining for the first instants after excavation. This means that the initial convergence for deep tunnels $u_{in,deep}$ is higher than the initial convergence for shallow tunnels $u_{in,shallow}$. Moreover, in deep tunnels it is

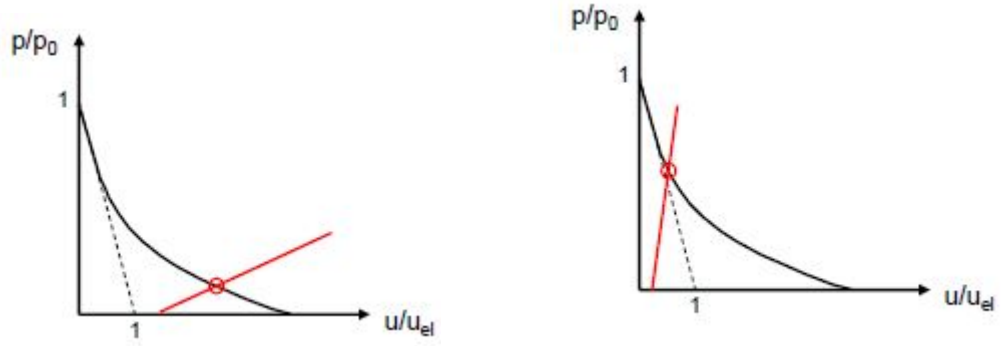

(a) Deep tunnels

(b) Shallow tunnels

Figure 2.8: *Different LCCs for the realization of deep and shallow tunnels.*

preferable to use a type of lining which is constituted of a not too rigid concrete (Figure 2.8a). In this way, the radial pressure can greatly reduce, at the cost of having a high value of convergence.

2.4 Case study

In this section the Convergence-Confinement Method is applied to a *reference tunnel*. The same problem is considered in this section, to study the excavation effects and in Sections 3 and 4, to study the fire induced effects. The main geometrical and mechanical characteristics of the rock and the concrete support are reported respectively in Table 2.1 and Table 2.2.

radius	a	m	4
depth	H	m	300
weight	γ	kN/m^3	25
Young modulus	E	kPa	$1 \cdot 10^6$
Poisson's ratio	ν	/	0.25
friction angle	ϕ	°	30
cohesion	c	kPa	200

Table 2.1: *Geometrical and mechanical parameters of the rock surrounding the tunnel at T=20°*

The undisturbed rock (far enough from the tunnel) is characterised by a compressive isotropic state of stress $p_0 = -7500\, kPa$. For the given geometry, it is

thickness	t_c	m	0.3
Young Modulus	E_{con}	kPa	$1.8 \cdot 10^7$
Poisson's ratio	ν_{con}	/	0.3
uniaxial compression strength	f_{ck}	kPa	31000

Table 2.2: *Geometrical and mechanical parameters of the concrete ring at T=20°C*

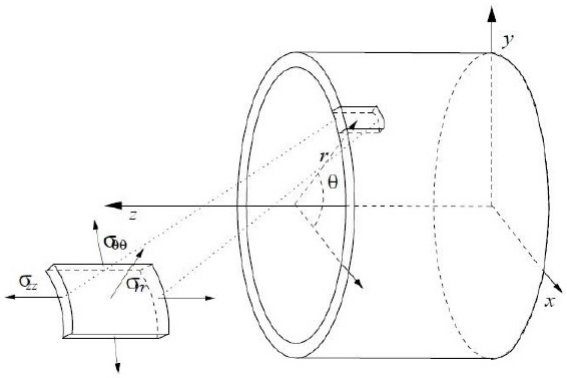

Figure 2.9: *Cylindrical coordinates are adopted in the model. Tensile stresses are positive.*

convenient to adopt a cylindrical system of coordinates (Figure 2.9) where z is the axis of the tunnel, r is its radius and θ is the angle between the r-axis and the position vector. Since the tunnel is assumed to be very long, the problems will be solved in plane strain conditions.
When dealing with deep tunnels, the undisturbed condition is generally characterised by high values of p_0 and it is suggested to let the free convergence of the tunnel develop, so that the support structure will be required to carry a not excessive load p. Considering the LCC (Figure 2.8) this means that point A is located towards the right part of the curve.
To correctly design the structure, the first step is to set the maximum convergence of the concrete lining: in this case, $u_{max} = 0.1\,m$.
Given the characteristics of the materials, the stiffness k_{con} may be calculated by using Eq. (2.34), resulting in $k_{con} = 398\,MPa/m$. The initial convergence, which is the value of radial displacement of the rock before installing the lining, is calculated as:

$$u_{in} = u_{max} - \frac{p}{k_{con}} = 0.0987m \tag{2.54}$$

where p indicates the radial pressure at the equilibrium (i.e. point A in Figure 2.7), which is equal to $506.85\,kPa$. Thus, the installation of the lining is done after a substantial displacement of the rock (Figure 2.10). The yielding of the LCC can

be calculated using Eq. (2.53), resulting at $p = -2237.81\, kPa$.

In these conditions, a plastic region forms from the intrados $r = 4\, m$ until

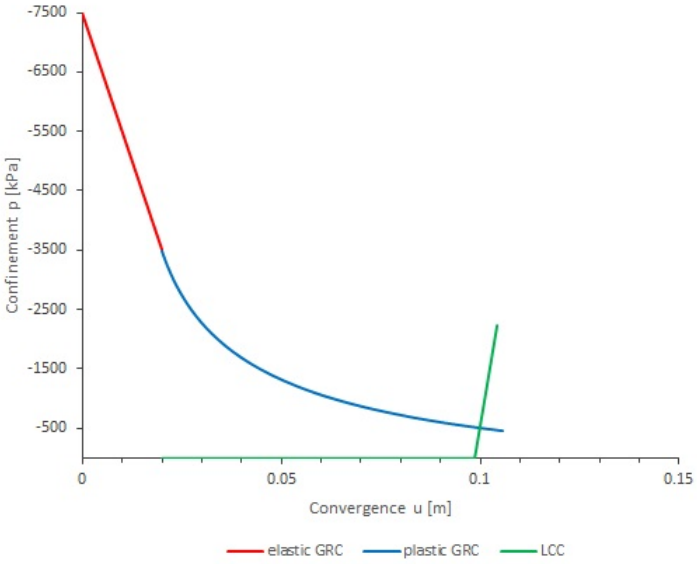

Figure 2.10: *Representation of the Ground Reaction Curve and Lining Characteristic Curve and determination of the equilibrium point (u,p) which guarantees a maximum convergence of 0.1 meter.*

$r = r_{pl} = 7.91\, m$.

In the present work the associated Mohr-Coulomb plasticity function has been chosen. The solution presented in Appendix C for non-associated behaviour could be used as an alternative to the present model.

Figure 2.11 shows the state of stress inside the rock, both in the plastic and elastic zones. Due to the process of excavation, the rock mass is no more characterised by high compressive stresses, but it experiences a stress release. Both the radial and the hoop stresses increase while approaching the elastic zone.

The plastic radius marks the passage to the elastic zone, and continuity of stresses is guaranteed. In this region, the radial stress increases and the circumferential decreases, but they both tend to p_0, which is the undisturbed isotropic state of stress.

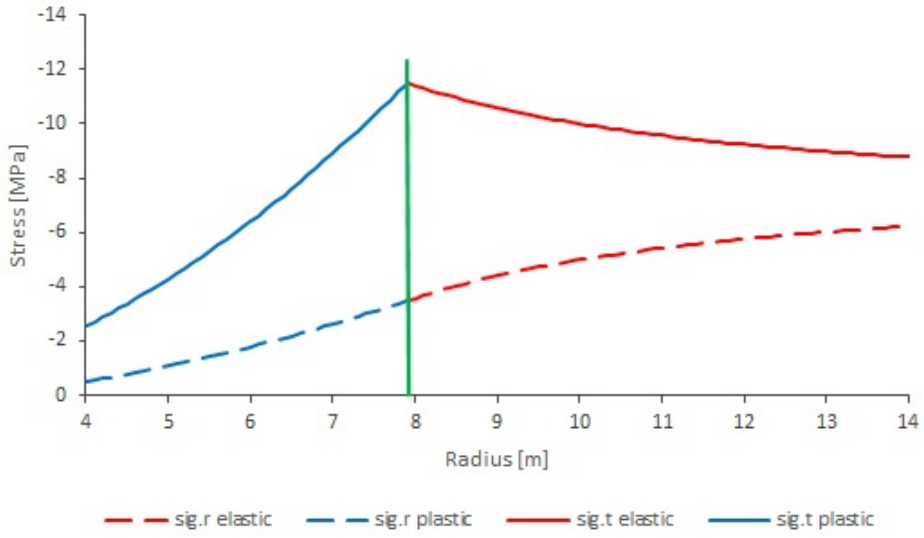

Figure 2.11: *State of stress with p=-506.85 kPa, u=0.1m and* p_0*=-7500 kPa*

Chapter 3

Fires in tunnel: analytical models

As soon as the fire ignites, the lining is subjected to a considerable variation of temperature that induces its radial expansion towards the rock. At the same time, the concrete ring provides thermal insulation so that the rock does not experience a substantial rise in temperature. However, the initial state of stress is modified by the presence of fire and consequently the equilibrium between rock and support is perturbed, resulting in a new mechanical interaction problem to be solved.
In particular, due to the radial expansion of the support, the rock is subjected to an additional radial compressive stress, which could lead to a stress path back to the elastic region, as suggested in [Amberg, 2011]. In this paper a tunnel is re-compressed after excavation. The additional contribution in radial compression may be due to different factors, especially if a rigid lining is placed. It generally occurs because of swelling or creep, but it may also be caused by external factors, such as an increasing of the support pressure as the collapse of an adjacent tunnel section or the excavation of a new tunnel near an existing one.
In this case, the additional pressure is given by the expansion of the lining. The representation of the state of stress of the ground in the Mohr-Coulomb graph shows that the Mohr circle is no more tangent to the failure envelope and thus the behaviour of the rock is elastic once again (Figure 3.1).
Due to this assumption, the models that have been conceived to solve the problem of fire in tunnels are based on a stress path back to the elastic field.
To investigate the fire induced effects on the lining, the thick-cylinder theory is adopted, considering a hollow cylinder that is subjected to thermal variation and also constrained by the presence of the surrounding rock. In this section two analytical models are presented: all the geometrical and mechanical data that are considered refer to the case study in section (2.4).

The first model describes the behaviour of a hollow cylinder subjected to thermal load or to internal and external pressure [Corradi Dell'Acqua, 2010]. In the Master Thesis of [Aliberti and Miglietta, 2014] the two authors have used it to describe the effects of thermal and mechanical load on the concrete ring. It represents a first attempt to solve the problems related to the presence of fire. The support is considered as a single, homogeneous ring, while the soil is composed of a set of elastic springs that react to the expansion of the concrete lining subjected to fire (i.e. Winkler's Theory). It is possible to make this assumption since the problem is axisymmetric, thus the springs react only in the radial direction.
As a second approach, the multi-layer model of [Vedeld and Sollund, 2014] presented in section 1.3 will be discussed. This model is used as a starting point of the present work, with the objective of setting up an analytical tool which considers the interaction between the rock and the concrete lining in presence of thermal variation. In fact, the support is constituted of several layers, each one described by its own properties and, above all, each one is associated with a different thermal variation, which depends on the thermal conductivity of the material.
Moreover, this model allows to take into account the damage induced by fire on the support, specifically on its mechanical properties. This leads to an additional change in the stress state of the lining.
In this model, after evaluating the state of stress, it will be proved that the rock returns to the elastic field, while the lining reaches a plastic condition and experiences degradation.

3.1 Axysimmetric cylinder in plain strain condition

This model is based on the approach described by [Corradi Dell'Acqua, 2010]. The support of the tunnel is represented by a cylinder of internal radius a and external radius b, subjected to an internal pressure p, an external one q and to a variation of temperature $\Delta T(r)$ uniformly distributed at the intrados. In order to solve the problem, these hypotheses must be satisfied:

1. linear elastic behaviour of the soil;
2. very deep tunnel ($t << H$, where H is the vertical distance from the centre of the tunnel to the ground surface);
3. horizontal-to-vertical stress ratio $K_0 = 1$, which means that $\sigma'_V = \sigma'_H$. This assumption refers to an ideal deep tunnel and the problem becomes axisymmetric;

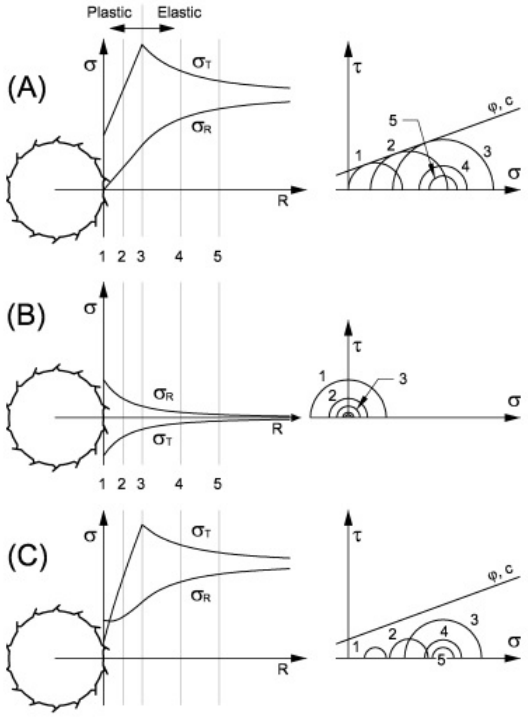

Figure 3.1: *A. State of stress of the tunnel after excavation; B. effect of an internal radial pressure; C. subsequent increasing of the radial pressure. [Amberg, 2011]*

4. the temperature does not depend on the anomaly θ

Figure (3.2) shows a simple scheme of the problem. The objective is to find the

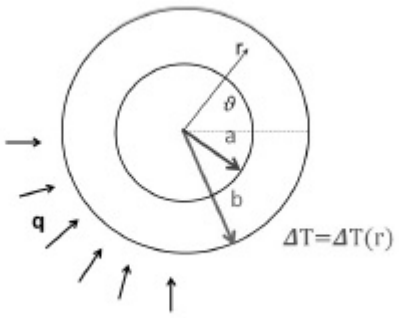

Figure 3.2: *External pressure acting on the lining and variation of temperature* ΔT

state of stress in the concrete ring, which is influenced by both the variation of temperature and by the presence of the surrounding rock. In fact, when subjected to high temperatures, the support tends to expand radially, causing the reaction of the rock. Thus, the external pressure q represents the pressure of rock, which influences the state of stress in the concrete ring by giving an additional contribution called σ_q. Since the problem is elastic, the superposition principle allows to sum it to the thermal effect, so that:

$$\sigma = \sigma_q + \sigma_{\Delta T} \tag{3.1}$$

In this model the geostatic pressure is neglected, since the objective is to evaluate the effect of fire. However, it could be easily added to the state of stress as a constant.
The first step is to evaluate the stiffness of the elastic soil: this is done adopting the beam theory of Winkler foundation, so considering the soil to be constituted of many springs of constant k_r. It is simply calculated as:

$$k_r = \frac{p}{u_r(a)} \tag{3.2}$$

considering that the rock is a very thick cylinder of internal radius a and external radius $b \to \infty$ that is subjected to internal pressure p (see Figure 3.3). It is sufficient to apply a fictitious p and calculate the subsequent radial displacement to find the stiffness. Given the characteristics of the tunnel in section 2.4, the stiffness of the rock is $k_r = 0.198\ N/mm^3$.

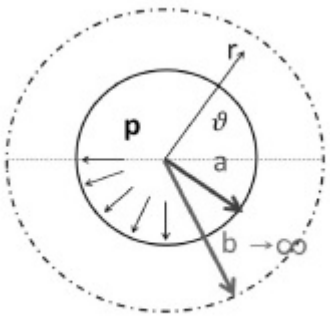

Figure 3.3: *Rock system subjected to internal pressure p induced by the expansion of the concrete lining*

Secondly, the temperature variation in the concrete ring must be set: $\Delta T(a)$ at the intrados and $\Delta T(b)$ at the extrados. The effect of temperature can be found by imposing linear elastic constitutive laws (2.16) and simply adding a term related to the variation of temperature:

$$\begin{cases} \varepsilon_r = \dfrac{1+\nu}{E}[(1-\nu)\sigma_r - \nu\sigma_\theta + (1-\nu)\Theta] \\ \varepsilon_\theta = \dfrac{1+\nu}{E}[(1-\nu)\sigma_\theta - \nu\sigma_r + (1-\nu)\Theta] \end{cases} \tag{3.3}$$

where $\Theta(r) = \dfrac{E}{1-\nu} \cdot \alpha \cdot \Delta T(r)$.

The thermally induced stress inside the lining along the radius is represented by function Θ and several distinct trends can be chosen to represent the response of a certain material to temperature variations. Here, two different choices are compared:

- polynomial quadratic distribution:

$$\Theta(r) = \Theta_b - \frac{\Theta_b - \Theta_a}{(b/a-1)^2} \cdot (b/a - r/a)^2 \tag{3.4}$$

- logarithmic distribution:

$$\Theta(r) = \Theta_a - (\Theta_a - \Theta_b) \cdot \frac{\ln(r/a)}{\ln(b/a)} \tag{3.5}$$

Where Θ_a and Θ_b are the values of Θ in correspondence of the internal and external radius. Considering the tunnel in Paragraph (2.4) and imposing $\Delta T(a)$ =900°C and $\Delta T(b)$ =50°C, the two curves are shown in Figure (3.4).

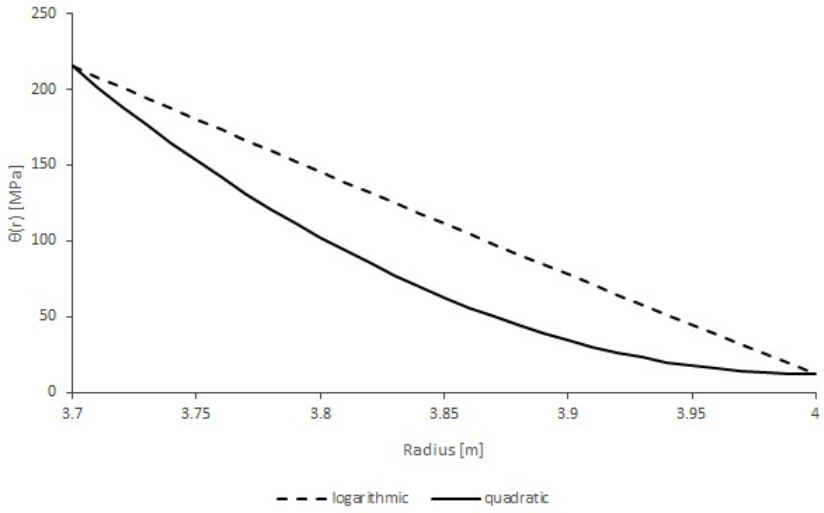

Figure 3.4: *Polynomial and Logarithmic distributions of* $\Theta(r)$ *in the concrete ring*

Once the temperature variation in the concrete ring has been set, the mechanical problem can be easily solved using the following equations:

- radial stress:

$$\sigma_r = -p\frac{a^2}{r^2} - \frac{1}{r^2}\int_a^r r\Theta(r)dr + K\left(1 - \frac{a^2}{r^2}\right) \tag{3.6}$$

- hoop stress:

$$\sigma_\theta = p\frac{a^2}{r^2} + \frac{1}{r^2}\int_a^r r\Theta(r)dr - \Theta(r) + K\left(1 + \frac{a^2}{r^2}\right) \tag{3.7}$$

- radial displacement:

$$s_r(r) = a\frac{1+\nu}{E}\left[\frac{a}{r}\left(p + \frac{1}{a^2}\int_a^r r\Theta(r)dr + K\right) + \frac{r}{a}K(1-2\nu)\right] \tag{3.8}$$

where

$$K = \frac{1}{b^2 - r^2}\left[-qb^2 + pa^2 + \int_a^b r\Theta(r)dr\right]$$

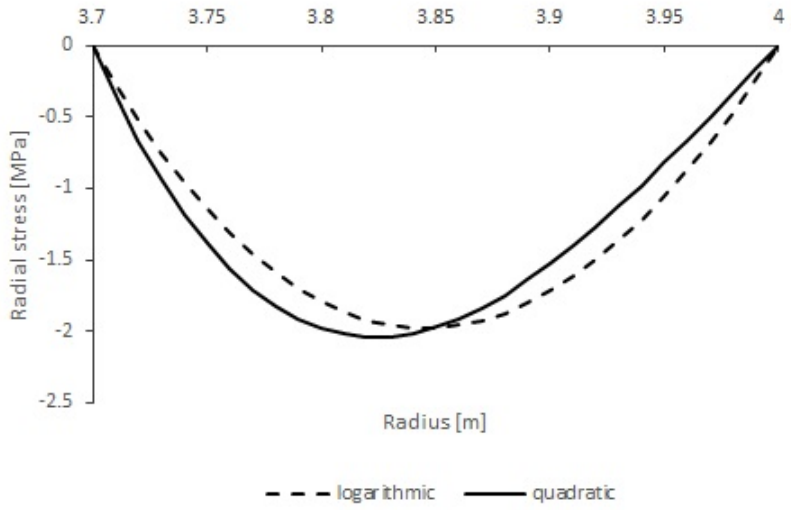

Figure 3.5: *Radial stress σ_r [MPa] due to temperature variation ΔT*

In the first step only the effects of the temperature variation are shown (Figures 3.5, 3.6 and 3.7). The results of the two models are in agreement about the state of stress that is generated inside the concrete ring.

The radial stress is null at the intrados and at the extrados of the concrete ring, while it reaches its maximum value of compression (i.e. negative value) in correspondence of the medium thickness. Regarding circumferential stress, the internal part of the support is compressed, while the external one is characterised by tensile stress.
The support tends to expand radially, reaching the maximum value of displacement of about 17 mm for the quadratic model and about 10 mm for the logarithmic one.

After evaluating the state of stress caused by high temperatures, the pressure q exerted by the soil on the lining is calculated. The two values of radial displacement (one for each temperature distribution) are used to calculate the two values of additional pressure (Table 3.1).

	logarithmic	quadratic
q[MPa]	1.93	3.37

Table 3.1: *External pressure q acting on the extrados b of the concrete ring*

The effect of the external pressure results in an increase in compressive radial

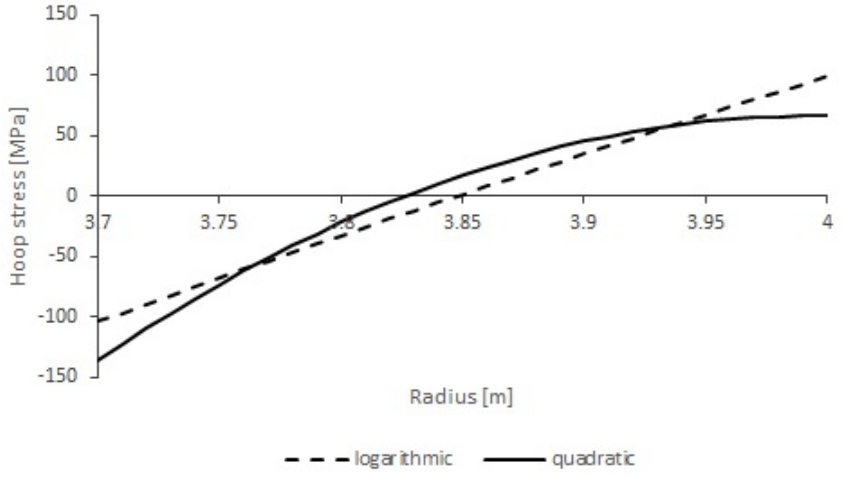

Figure 3.6: *Circumferential stress σ_θ [MPa] due to temperature variation ΔT*

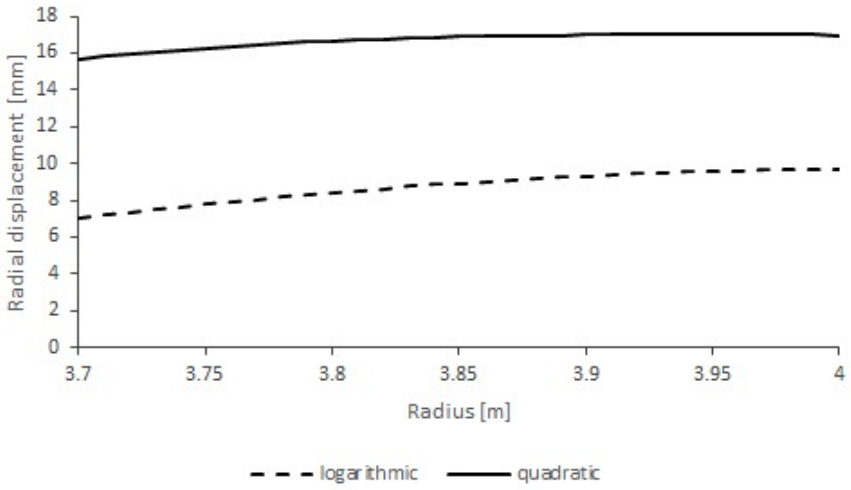

Figure 3.7: *Radial displacement induced by the variation of temperature. Negative values indicate displacement towards the centre of the tunnel, while positive ones represent movement in the direction of the extrados.*

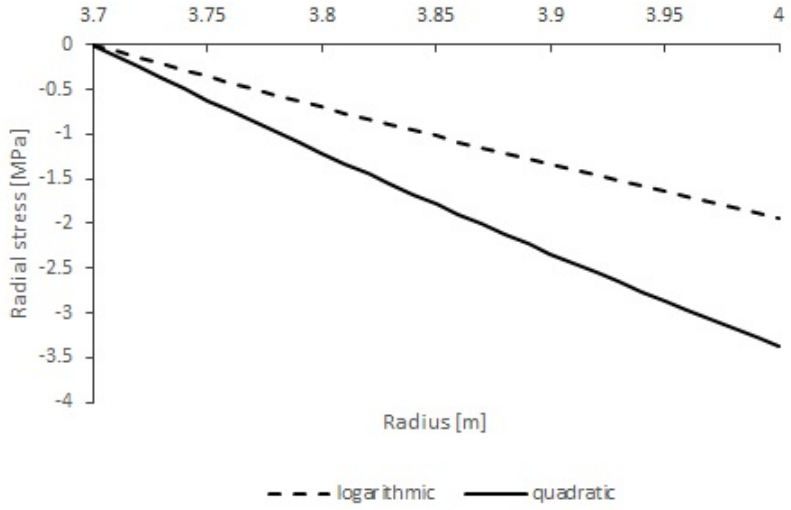

Figure 3.8: *Radial stress in the concrete lining generated by external pressure q*

stress, especially at $r = b$ (Figure 3.8) where σ_r is equal in modulus to the values of q reported in Table (3.1). Moreover, the loading by the soil gives an additional contribution to hoop stresses in terms of compression that remains almost constant along the radius of the concrete ring (Figure 3.9). As one could expect, the radial displacement generated by the surrounding rock has negative values, which means that the additional pressure makes the lining move towards the centre of the tunnel (Figure 3.10).

The superposition principle allows the sum of the two contributions, as already seen in equation (3.1), although the interaction effect would require an iterative procedure on the value of displacement u_r. The final state of stress is shown in Figures (3.11) and (3.12), while the final radial displacement of the lining are displayed in Figure (3.13). The results show that the circumferential stresses in the external part of the lining has lower tensile stresses if the pressure of soil is taken into account. The internal 20 cm of lining are compressed, while the remaining 10 cm are still characterised by tensile hoop stress.The radial stress grows as well in compression (i.e. negative values), reaching the maximum value in correspondence of the extrados.

For the sake of simplicity, the results have been reported in the same graph, by using both the quadratic and the logarithmic model. The contribution of the initial state of stress $p*$ due to the excavation process is also taken into account in the analysis by summing it to the temperature induced stress state. It represents

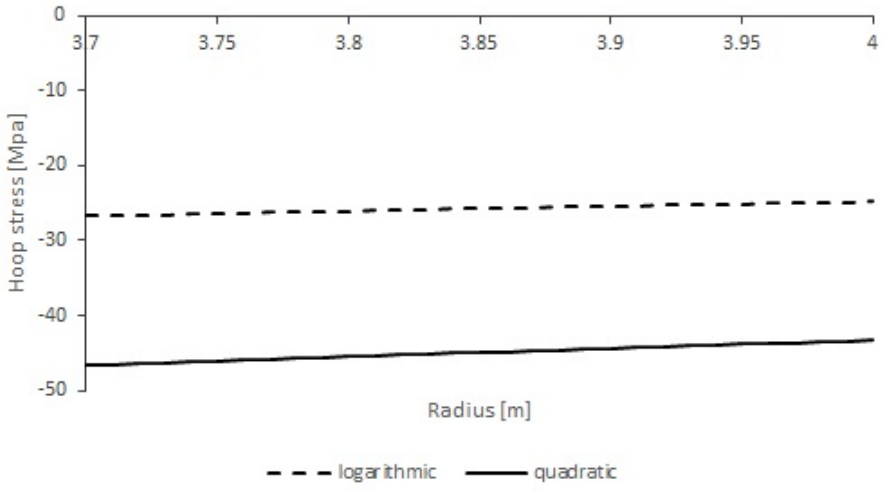

Figure 3.9: *Circumferential stress in the concrete lining generated by external pressure q*

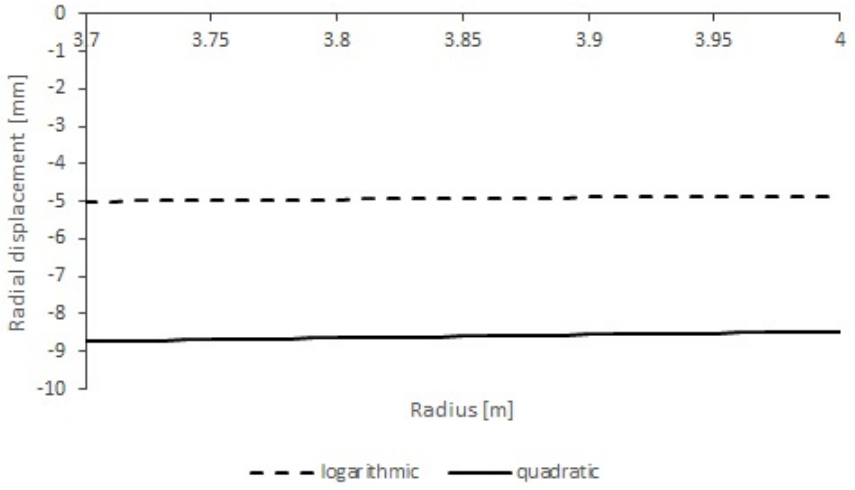

Figure 3.10: *Radial displacement of the lining induced by the pressure of the external rock q. Negative values indicate movement towards the centre of the tunnel.*

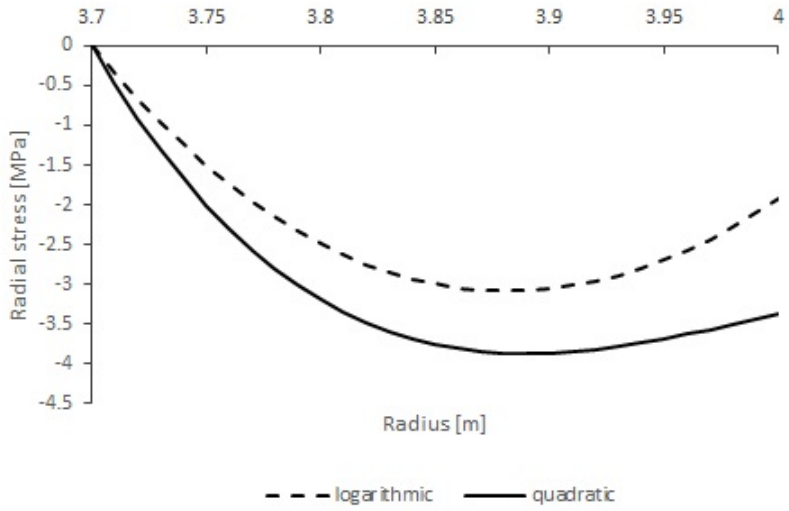

Figure 3.11: *Radial Stresses in the concrete lining induced by ΔT and by the external pressure q.*

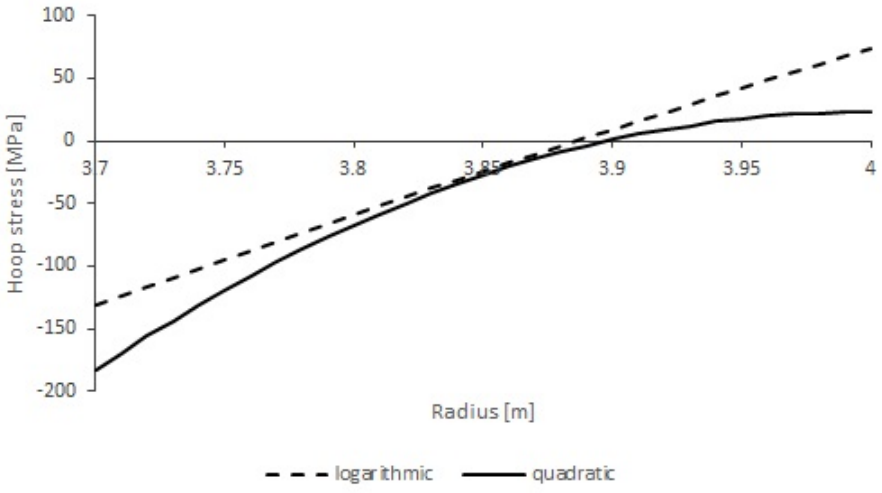

Figure 3.12: *Hoop Stresses in the concrete lining induced by ΔT and by the external pressure q.*

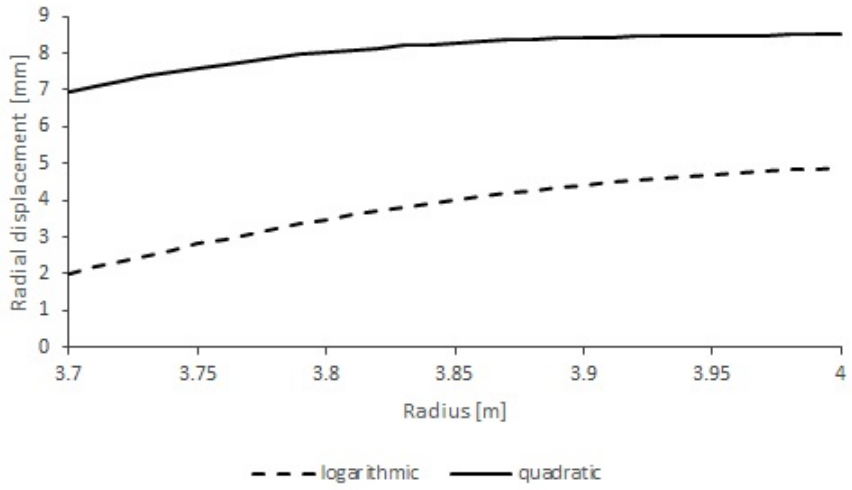

Figure 3.13: *Final radial displacement of the lining. Positive values indicate movement in the direction of the rock.*

the starting point of the analysis, when the extrados of the support is substantially compressed (Figures 3.14, 3.15 and 3.16). However, it may be noticed that the geostatic stress state is not as relevant as the fire induced one, in fact it only gives a small contribution in compression.
The quadratic model is more severe than the logarithmic one: the final values both of radial and circumferential stresses are higher than in the other model. It can also be demonstrated by looking at the final values of radial displacement at the intrados. This model represent a first attempt to solve the mechanical problem that is induced by fire. However, even though it leads to realistic values, it is still

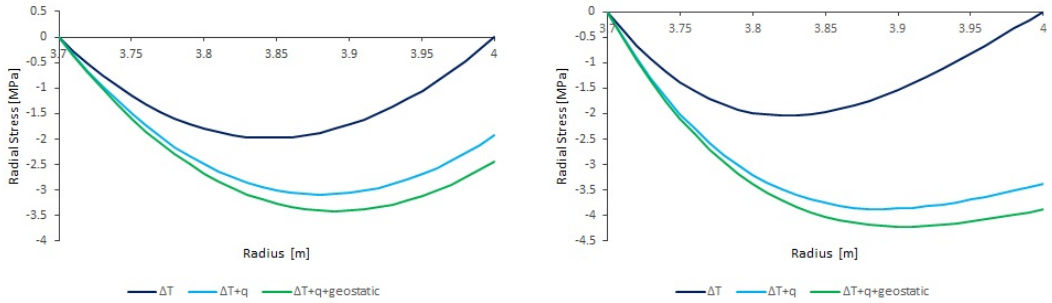

(a) *Logarithmic model* ***(b)*** *Quadratic model*

Figure 3.14: *Radial stress 1) caused by a variation of temperature; 2) considering ΔT and the pressure of soil; 3) final state of stress (considering the geostatic pressure $p*$ as well)*

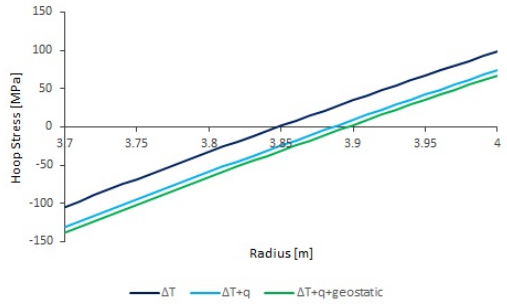

(a) *Logarithmic model*

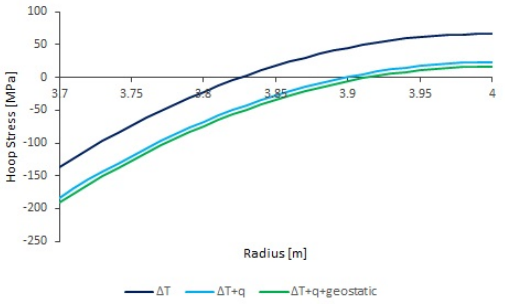

(b) *Quadratic model*

Figure 3.15: *Circumferential stress 1) caused by a variation of temperature; 2) considering ΔT and the pressure of soil; 3) final state of stress (considering the geostatic pressure $p*$ as well)*

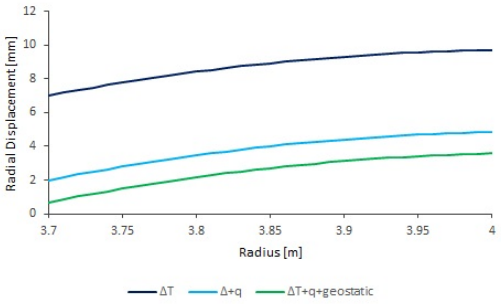

(a) *Logarithmic model*

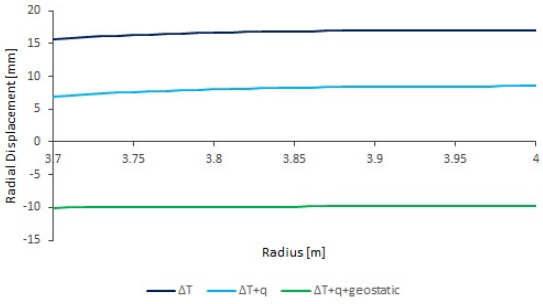

(b) *Quadratic model*

Figure 3.16: *Radial displacement 1) caused by a variation of temperature; 2) considering ΔT and the pressure of soil; 3) final state of stress (considering the geostatic pressure $p*$ as well)*

an approximation of the case of study. In particular:

1. the system is considered homogeneous, while the lining system may consist of layers of different mechanical and thermal properties.

2. the variation of temperature is theoretical and there is no possibility to use experimental data, unless an analytical curve is created by interpolation.

3. the interaction between rock and lining is not considered, since the two systems are analysed separately. In fact, the solution would require an iterative procedure since the pressure q exerted by the rock depends on the magnitude of the radial expansion $u_r(b)$ of the lining, and at the same time the radial expansion depends on the pressure exerted by the rock.

3.2 Multi-layer cylinder model

3.2.1 Hypotheses and analytical description

The Convergence Confinement Method allows to analyse the behaviour of the rock and the support simultaneously, considering the problem as interaction. As soon as the temperatures rise due to fire the lining tends to expand, but the presence of the rock limits this movement. At the same time, the state of stress of the rock is perturbed by the expansion of the lining. This is why it is important to solve the fire problem by considering interaction between the two domains.
In this section a new model is presented: it was first developed by Vedeld and Sollund in [Vedeld and Sollund, 2014] with the objective of evaluating the state of stress that is produced inside multi-layer pipes where hot fluids are flowing. Thanks to the similarity in geometry the model can be used to solve the problem of fire inside tunnels. The cylinder can be subdivided into many layers that discretize the concrete ring and the rock, each one characterised by its own geometrical, mechanical and thermal properties.
To be more precise, each layer i is delimited by its internal and external radius r_{i-1} and r_i and is characterised by thermal variation ΔT_i, thermal expansion coefficient α_i, Poisson's ratio ν_i and Young Modulus E_i. The interaction between each layer is described by the contact pressure q_i which is transmitted by layer i to $i+1$ and viceversa. It represents the interface pressure, that is equal to p_0 for $r = r_0$ and to p_{ext} for $r = r_n$.
The main hypotheses of the model are:

1. The materials in the cylinder layers are assumed to be linearly elastic, homogeneous and isotropic.
2. Initial stresses and strains are disregarded (geostatic pressure is not considered, since there is equilibrium between rock and support before the fire starts).
3. Small displacements are assumed. Changes in geometry due to any loading are disregarded.
4. Each layer is subjected to a uniform temperature.
5. Perpendicularity of sections to the cylinder axis is maintained after deformation. If a section is plane and perpendicular to the axis, it remains so.
6. It is assumed that material gaps or overlapping cannot be generated in the cross-section.

The problem is in generalized plane strain conditions, so it is assumed that constant deformations occur along the axis of the tunnel z. As a consequence, all the layers are characterised by the same value of axial strain $\varepsilon_z = constant$. It is possible to estimate this value by making some assumptions: first of all, the cylinder is restrained at $z = 0$, while it can move axially at the other end, at $z = L$. As shown in Figure (3.17) in the reference point RP an axial spring of stiffness K is positioned and an axial load N is applied. Equilibrium in the axial direction is guaranteed by adding a term that represents the axial stress integrated over the cross-section of each layer, as shown in the following formula:

$$\sum_{i=1}^{n}(\sigma_{z,i}A_i) = -K \cdot u_z(L) + N \tag{3.9}$$

where the cross-sectional Area of each layer is $A_i = \pi t_i(2r_i - t_i)$ and t_i is the thickness of the i-th layer. Regarding the axial displacement u_z, since strains in this directions are constant in each layer i, it is possible to claim that:

$$\frac{du_z}{dz} = C \Rightarrow u_z = C_z\frac{z}{L} \tag{3.10}$$

where C_z indicates the axial displacement in $z = L$, while for $z = 0$ no displacement is established. Moreover, due to the axial symmetry of the problem, there is no hoop displacement in all layers.
The analytical solution is based again on the equilibrium relation (2.1), on Hooke

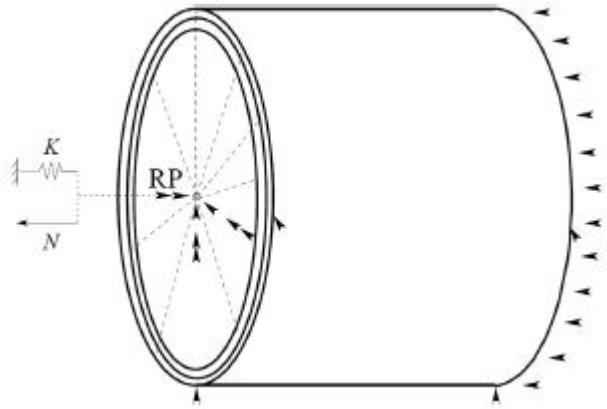

Figure 3.17: *Axial Load N and spring at the reference point for $z = L$. Translational constraints in $z = 0$ (single arrows) and rotational constraints indicated by double arrows.*

equations for elastic media (2.5) and on compatibility between strains and displacements (2.4). The temperature variation causes an additional contribution to the state of stress and thus a thermal term is added to Hooke equations:

$$\begin{bmatrix} \sigma_{r,i} \\ \sigma_{\theta,i} \\ \sigma_{z,i} \end{bmatrix} = \hat{E}_i \begin{bmatrix} 1-\nu_i & \nu_i & \nu_i \\ \nu_i & 1-\nu_i & \nu_i \\ \nu_i & \nu_i & 1-\nu_i \end{bmatrix} \begin{bmatrix} \dfrac{du_{r,i}}{dr} - \alpha_i \Delta T_i \\ \dfrac{u_{r,i}}{r} - \alpha_i \Delta T_i \\ \dfrac{du_z}{dz} - \alpha_i \Delta T_i \end{bmatrix} \tag{3.11}$$

where:

$$\hat{E}_i = \frac{E_i}{(1-2\nu_i)(1+\nu_i)} \tag{3.12}$$

The Equation for radial convergence (2.40) can be expressed as:

$$u_{r,i} = \lambda_i \frac{A_i}{r} + \beta_i C_i r \tag{3.13}$$

where:

$$\lambda_i = -\frac{1}{\hat{E}_i(1-2\nu_i)}, \quad \beta_i = \frac{1}{\hat{E}_i}$$

The displacement field is thus described by:

$$\begin{cases} u_{r,i} = \lambda_i \dfrac{A_i}{r} + \beta_i C_i r \\ u_{\theta,i} = 0 \\ u_{z,i} = u_z = C_z \dfrac{z}{L} = \varepsilon_z z \end{cases} \tag{3.14}$$

Combining Eq. (3.11) and Eq. (3.13), the state of stress can be expressed as:

$$\begin{bmatrix} \sigma_{r,i} \\ \sigma_{\theta,i} \\ \sigma_{z,i} \end{bmatrix} = \begin{bmatrix} \dfrac{A_i}{r^2} + C_i - \mu_i \\ -\dfrac{A_i}{r^2} + C_i - \mu_i \\ 2\nu_i C_i + \hat{E}_i(1-\nu_i)\varepsilon_z - \varphi_i \end{bmatrix} \tag{3.15}$$

where:

$$\varphi_i = \hat{E}_i \alpha_i \Delta T_i (1+\nu_i), \quad \varepsilon_z = \frac{C_z}{L}, \quad \mu_i = \varphi_i - \hat{E}_i \nu_i \varepsilon_z$$

In order to solve the problem, the only unknowns are coefficients A_i, C_i and the axial strain ε_z.

The first step is to impose the continuity of radial stresses and displacement at the interface between layers:

$$\begin{cases} \sigma_{r,i}(r_i) = \sigma_{r,i+1}(r_i) \\ u_{r,i}(r_i) = u_{r,i+1}(r_i) \end{cases} \tag{3.16}$$

These boundary conditions are applied to the expressions of radial displacement and radial stresses, obtaining the following equations:

$$\begin{cases} \dfrac{A_i}{r_i^2} + C_i - \hat{E}_i \alpha_i \Delta T_i (1+\nu_i) = \dfrac{A_{i+1}}{r_i^2} + C_{i+1} - \hat{E}_{i+1} \alpha_{i+1} \Delta T_{i+1} (1+\nu_{i+1}) \\ \lambda_i \dfrac{A_i}{r_i} + \beta_i C_i r_i = \lambda_{i+1} \dfrac{A_{i+1}}{r_i} + \beta_{i+1} C_{i+1} r_i \end{cases} \tag{3.17}$$

Then, it is possible to evaluate the expressions for coefficients A_{i+1} and C_{i+1} as functions of A_i and C_i:

$$A_{i+1} = A_i \left(\frac{\lambda_i - \beta_{i+1}}{\lambda_{i+1} - \beta_{i+1}} \right) + C_i r_i^2 \left(\frac{\beta_i - \beta_{i+1}}{\lambda_{i+1} - \beta_{i+1}} \right) - \frac{\beta_{i+1} r_i^2 (\varphi_{i+1} - \varphi_i)}{\lambda_{i+1} - \beta_{i+1}} \tag{3.18}$$

$$C_{i+1} = \frac{A_i}{r_i^2}\left(\frac{\lambda_{i+1}-\lambda_i}{\lambda_{i+1}-\beta_{i+1}}\right) + C_i\left(\frac{\lambda_{i+1}-\beta_i}{\lambda_{i+1}-\beta_{i+1}}\right) + (\varphi_{i+1}-\varphi_i)\left(\frac{\lambda_{i+1}}{\lambda_{i+1}-\beta_{i+1}}\right) \quad (3.19)$$

In the next step, it is necessary to impose that the radial stress at radius r_i equals the contact pressure q_i, by taking into account that the boundary surfaces are subjected to known values q_0 and q_n. In this way the state of stress can be related to the internal and external loads acting on the cylinder.

$$\sigma_{r,i}(r_{i-1}) = -q_{i-1} \Rightarrow \frac{A_i}{r_{i-1}^2} + C_i - \varphi_i = -q_{i-1} \quad (3.20)$$

$$\sigma_{r,i+1}(r_{i+1}) = -q_{i+1} \Rightarrow \frac{A_{i+1}}{r_{i+1}^2} + C_{i+1} - \varphi_{i+1} = -q_{i+1} \quad (3.21)$$

By combining Eq.(3.18) and (3.19) with the above expressions, coefficients A_i and C_i can be expressed as function of the contact pressure:

$$\frac{A_i}{r_i^2} = \gamma_i \frac{T_i q_{i-1} - q_{i+1}(\lambda_{i+1}-\beta_{i+1}) - \varphi_i(\beta_{i+1}\gamma_{i+1}-\lambda_{i+1}) - T_i\varphi_i - \varphi_{i+1}\beta_{i+1}(1-\gamma_{i+1})}{S_i - T_i} \quad (3.22)$$

$$C_i = \frac{-S_i q_{i-1} + q_{i+1}(\lambda_{i+1}-\beta_{i+1}) + \varphi_i(\beta_{i+1}\gamma_{i+1}-\lambda_{i+1}) + S_i\varphi_i + \varphi_{i+1}\beta_{i+1}(1-\gamma_{i+1})}{S_i - T_i} \quad (3.23)$$

where:

$$S_i = (\lambda_i - \beta_{i+1})\gamma_{i+1}\gamma_i + (\lambda_{i+1}-\lambda_i)\gamma_i$$
$$T_i = \lambda_{i+1} - \beta_i + (\beta_i - \beta_{i+1})\gamma_{i+1}$$
$$\gamma_{i+1} = \frac{r_i^2}{r_{i+1}^2}$$

Considering Equation (3.21) in the generic form for index i, it becomes:

$$\sigma_{r,i}(r_i) = -q_i \Rightarrow \frac{A_i}{r_i^2} + C_i - \varphi_i = -q_i \quad (3.24)$$

Then, coefficients A_i and C_i can be inserted into the equation to get the expression for q_{i+1}.

$$q_{i+1} = \frac{(S_i - \gamma_i T_i)q_{i-1} - (S_i - T_i)q_i + (1-\gamma_{i+1})(1-\gamma_i)(\varphi_i\beta_i - \varphi_{i+1}\beta_{i+1})}{(1-\gamma_i)(\lambda_{i+1}-\beta_{i+1})} \quad (3.25)$$

Finally,the expressions of the two coefficients can be simplified by combining the above expression with Eq. (3.22) and Eq. (3.23):

$$\frac{A_i}{r_i^2} = \frac{\gamma_i(q_i - q_{i-1})}{1-\gamma_i} \tag{3.26}$$

$$C_i = \frac{\gamma_i(q_{i-1} - q_i)}{1-\gamma_i} + \varphi_i \tag{3.27}$$

The last step consists in determining q_i at each radius depending only on the external and internal pressures, which are the only known contact pressures. In the model these terms are obtained using the following recurrence relation:

$$q_i = \frac{a_i}{a_n} q_n + \left(c_i - \frac{c_n}{a_n} a_i\right) q_0 + \left(d_i - \frac{d_n}{a_n} a_i\right) q_0 \varepsilon_z \tag{3.28}$$

where:

$$a_0 = 0, \quad a_1 = 1, \quad c_0 = 1, \quad c_1 = 0, \quad d_0 = d_1 = 0 \tag{3.29}$$

and:

$$a_{i+1} = \frac{(S_i - \gamma_i T_i)a_{i-1} - (S_i - T_i)a_i}{(1-\gamma_i)(\lambda_{i+1} - \beta_{i+1})} \tag{3.30}$$

$$c_{i+1} = \frac{(S_i - \gamma_i T_i)c_{i-1} - (S_i - T_i)c_i}{(1-\gamma_i)(\lambda_{i+1} - \beta_{i+1})} + \frac{(1-\gamma_{i+1})(\varphi_i\beta_i - \varphi_{i+1}\beta_{i+1})}{q_0(\lambda_{i+1} - \beta_{i+1})} \tag{3.31}$$

$$d_{i+1} = \frac{(S_i - \gamma_i T_i)d_{i-1} - (S_i - T_i)d_i}{(1-\gamma_i)(\lambda_{i+1} - \beta_{i+1})} + \frac{(1-\gamma_{i+1})(\nu_i - \nu_{i+1})}{q_0(\lambda_{i+1} - \beta_{i+1})} \tag{3.32}$$

These formulas have been demonstrated by mathematical induction in [Vedeld and Sollund, 2014], and they can be easily implemented in.
The expression of the contact pressure q_i (Eq. 3.28) can be subdivided into two main terms: one related to the contribution of external and internal pressures and of the thermal loading, the other to the axial deformation:

$$q_i = q_i^0 + \zeta_i \varepsilon_z \tag{3.33}$$

where:

$$\zeta_i = \left(d_i - \frac{d_n}{a_n}a_i\right)q_0 \tag{3.34}$$

$$q_i^0 = \frac{a_i}{a_n}q_n + \left(c_i - \frac{c_n}{a_n}a_i\right)q_0 \tag{3.35}$$

The axial deformation can be calculated starting from the equilibrium equation 3.9 which in the present study becomes:

$$\sum_{i=1}^{n} = \sigma_{z,i}\pi(r_i^2 - r_{i-1}^2) = N - KL\varepsilon_z \tag{3.36}$$

By inserting the equation of axial stress reported in Eq.(3.15), the equilibrium can be expressed by:

$$\pi\sum_{i=1}^{n} r_i^2(1-\gamma_i)\Bigg\{2\nu_i\frac{1}{1-\gamma_i}(\gamma_i q_{i-1}^0 - q_i^0) - (1-2\nu_i)\varphi_i + \\ + \left[E_i + 2\nu_i\frac{1}{1-\gamma_i}(\gamma_i\zeta_{i-1} - \zeta_i)\right]\varepsilon_z\Bigg\} = N - KL\varepsilon_z \tag{3.37}$$

Finally, the constant axial strain can be calculated as:

$$\varepsilon_z = \frac{N + \pi\sum_{i=1}^{n} r_i^2[(1-2\nu_i)(1-\gamma_i)\varphi_i - 2\nu_i(\gamma_i q_{i-1}^0 - q_i^0)]}{KL + \pi\sum_{i=1}^{n} r_i^2[E_i(1-\gamma_i) + 2\nu_i(\gamma_i\zeta_{i-1} - \zeta_i)]} \tag{3.38}$$

The external pressure p_n is null since r_n is far enough and the conditions of the rock are undisturbed.

Concerning the internal pressure p_0, the literature suggests that in close environments such as passive houses there is a substantial increase in pressure due to the rise in temperature generated by fire. In [Bekish, 2018] it is claimed that in certain conditions it is even impossible to open the door because of the high overpressures that have been generated. In [Janardhan and Hostikka, 2017] a fire pool is positioned in an apartment, reaching T=300°C. The values of overpressure from numerical analysis and experimental data range between 100 and 1650 Pa, strongly depending on leakage and also on ventilation systems in the house.

In the case of deep tunnels the rise in pressure does not attain considerable values since there are openings, however the variation of temperature may induce a small increase in internal pressure due to the presence of gases at high temperatures. In this model it is imposed $p_0 = 0.5\,kPa$. In any case, there is a low sensitivity of the results with respect to limited values of internal pressure.

3.2.2 Numerical implementation

In order to solve the thermo-mechanical problem, the multi-layer model may be easily implemented using an electronic spreadsheet, where both the concrete lining and the surrounding rock are discretized in layers.
The choice of the thickness of each layer mainly depends on the thermal gradient that develops: the concrete lining should be subdivided into many thin layers, because it is characterised by high gradients of temperature. On the other hand, the rock may be subdivided into thin layers in its internal region, where it is subjected to high gradients, while in its external part it may be subdivided into thicker layers.
After setting up the problem, using an electronic spreadsheet the fire induced stress state in each layer can be calculated by following the analytical procedure explained in Paragraph 3.2.1. It may be used not only in plain strain conditions, but also in generalized plain stress conditions.
This kind of model permits to consider the interaction between the lining and the rock. They are simply modelled as adjacent layers and their interface is characterised by continuity in radial stresses and displacements.
The numerical implementation of the method requires that each instant is evaluated separately, since the temperature profile characterises a specific time instant. To refine the analysis, more spreadsheets should be used to discretize the analysis in time.
Even though it is based on some simplifying assumptions, this model can be easily implemented and gives realistic results very fast. This is why it represents a very good alternative to finite element models, which require much more time to be solved. The immediacy and simplicity of the method make it a very useful tool to be used for a preliminary design of a tunnel and to evaluate its fire performance.

3.2.3 Validation of multi-layer model

The multi-layer model provides the possibility to study the response to fire of a not homogeneous medium. This means that damage caused by fire on the mechanical properties of concrete may be taken into account by imposing different mechanical and thermal parameters in each layer. However, if the system is considered homogeneous, the solution of the model should reproduce that of the analytical model proposed in section 3.1, where the concrete ring is described by a single, homogeneous layer, except for the approximation introduced by the discretization, that should be negligible if sufficiently refined.

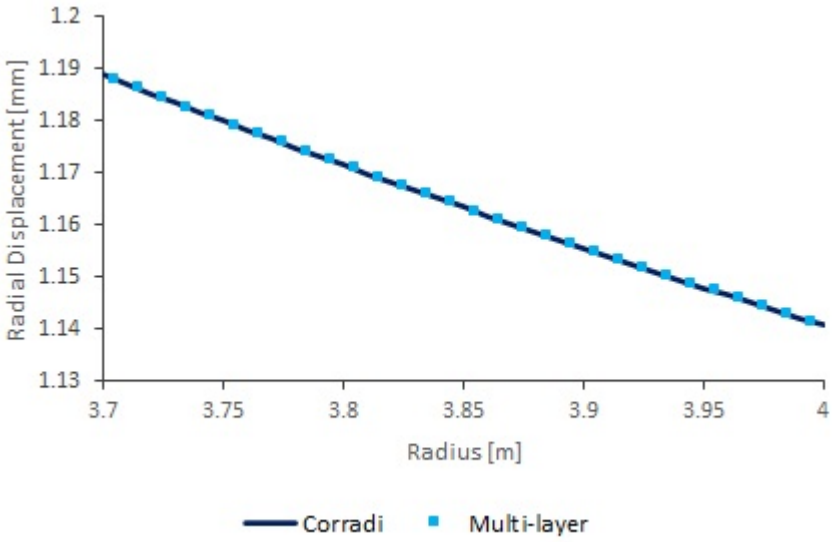

Figure 3.18: *Validation of the multi-layer model. Radial displacement of the concrete ring when subjected to* $p_{int} = 1000\,kPa$ *and* $p_{ext} = 500\,kPa$

In this section, the multi-layer model is validated using as a reference the analytical model of [Corradi Dell'Acqua, 2010]. To this aim, the same logarithmic distribution of temperature is imposed in the two analyses, while the geometry and the material properties are those of section 2.4. The accuracy of the model is checked in two different cases:

- the concrete ring is subjected to internal and external pressures only;
- the concrete ring is heated in a non-uniform way, following a logarithmic distribution of temperature.

In the first case, the support is subjected to an internal pressure of 1000 kPa and an external pressure of 500 kPa. The effects of such loads are reported in Figures 3.18, 3.19, 3.20 and 3.21.

The hollow cylinder expands radially because of the high internal pressure, reaching the maximum displacement in correspondence of the intrados, of about 1.19 mm. The radial stress is characterised by a linear variation between the two boundary conditions (i.e. p_{int} and p_{ext}) and the concrete ring is radially compressed. Hoop stresses are positive, so the material tends to expand in the circumferential direction due to the contribution by the internal pressure in the radial direction. Finally, the stress state in the axial direction is constant.
The results of the two models are in agreement on the response of the system when

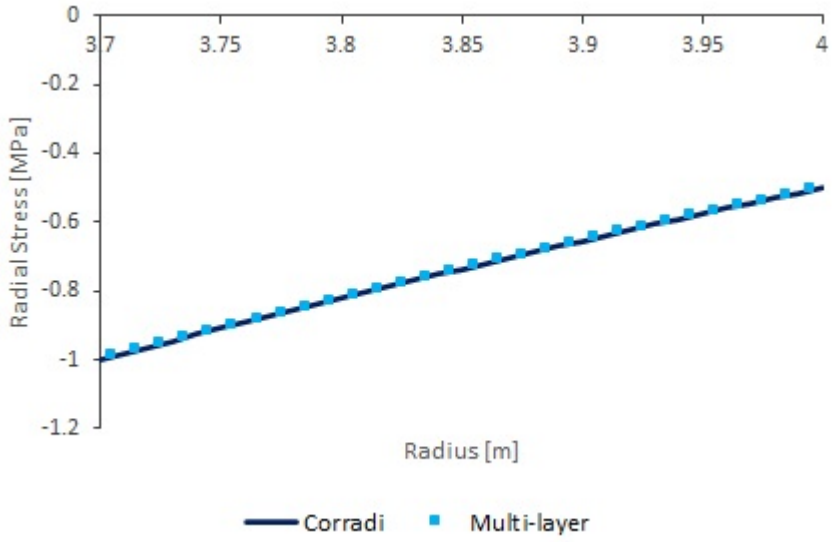

Figure 3.19: *Validation of the multi-layer model. Radial stress in the concrete ring when subjected to* $p_{int} = 1000\,kPa$ *and* $p_{ext} = 500\,kPa$

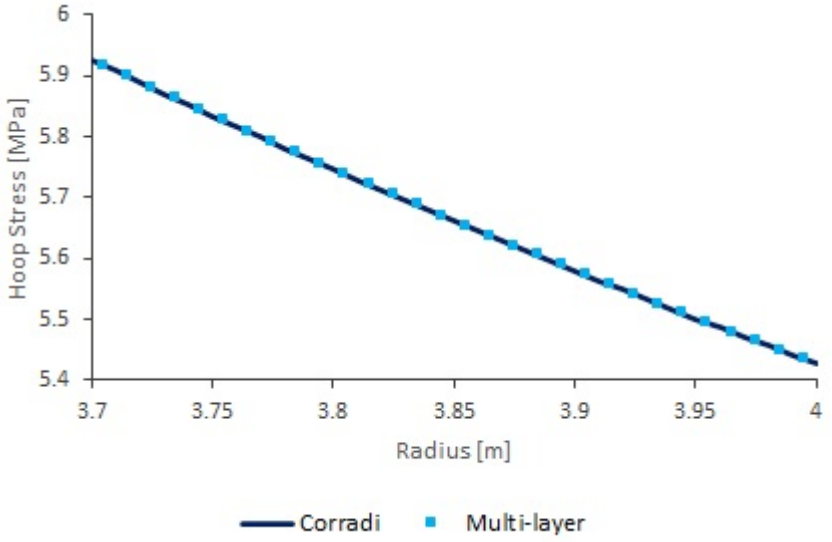

Figure 3.20: *Validation of the multi-layer model. Hoop stress in the concrete ring when subjected to* $p_{int} = 1000\,kPa$ *and* $p_{ext} = 500\,kPa$

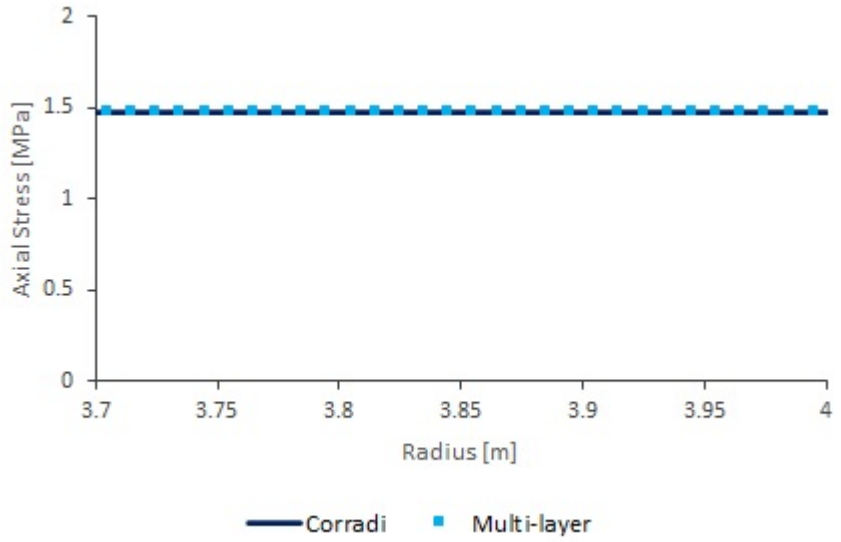

Figure 3.21: *Validation of the multi-layer model. Axial stress in the concrete ring when subjected to* $p_{int} = 1000\,kPa$ *and* $p_{ext} = 500\,kPa$

subjected to pressure, thus the multi-layer model is validated.
In the second case, considering the initial temperature of the lining of 20°C, the support is assumed to be non-uniformly heated, following a logarithmic function for the temperature. The hollow cylinder is heated at the intrados, where it raches a temperature of 1000°C. Due to the high thermal insulation of concrete, the extrados is characterised by a thermal variation of 180°C, reaching 200°C.
The stress state calculated using the two models is reported in Figures 3.22, 3.23, 3.24 and 3.25.

In this case, the results of the models agree except from a slight difference in the radial stresses, where a difference of 7% is found at the position of maximum stress (r=3.45 m). For σ_θ, σ_z and u_r the maximum discrepancies between the continuous and the discretized model are respectively 1.7%, 0.54% and 0.03%. It is worth remarking that the stress state is mainly governed by the circumferential stresses values, since they are two orders of magnitude bigger than those in the radial direction.
Concerning convergence, the graph shows that a rise in temperature could cause a substantial displacement of the lining, reaching values up to 2.75 cm.
If the concrete lining is subjected to both pressure and thermal load, the stress state may be simply calculated by imposing the superposition principle, i.e. by summing the two contributions of temperature and pressure.

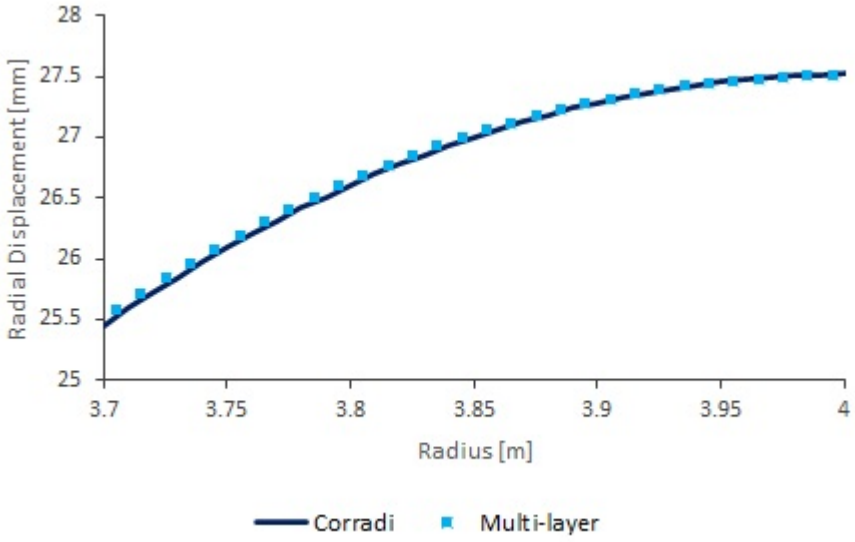

Figure 3.22: *Validation of the multi-layer model. Radial displacement of the concrete ring when subjected to thermal load.*

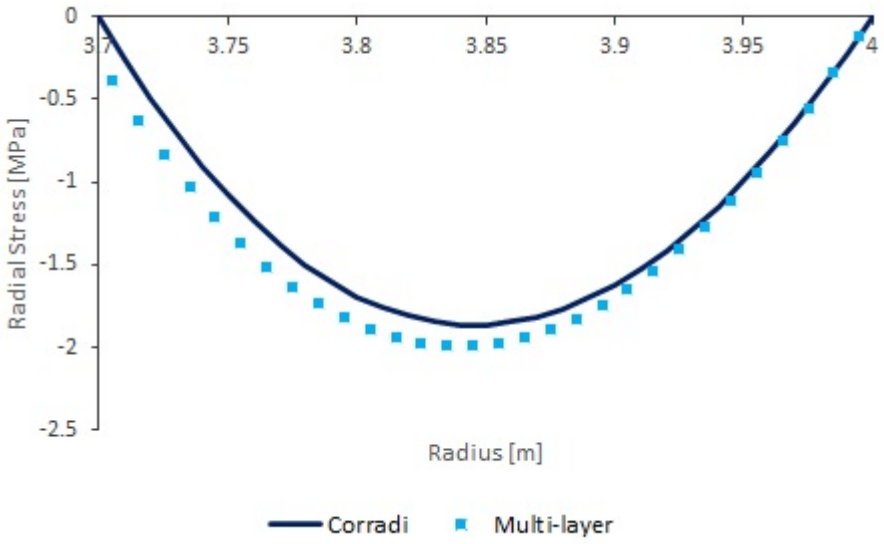

Figure 3.23: *Validation of the multi-layer model. Radial stress in the concrete ring when subjected to thermal load.*

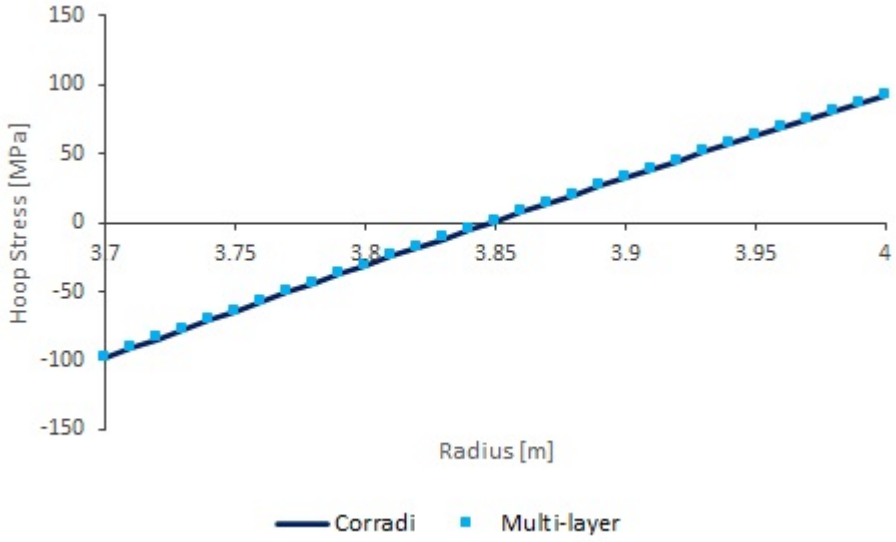

Figure 3.24: *Validation of the multi-layer model. Hoop stress in the concrete ring when subjected to thermal load.*

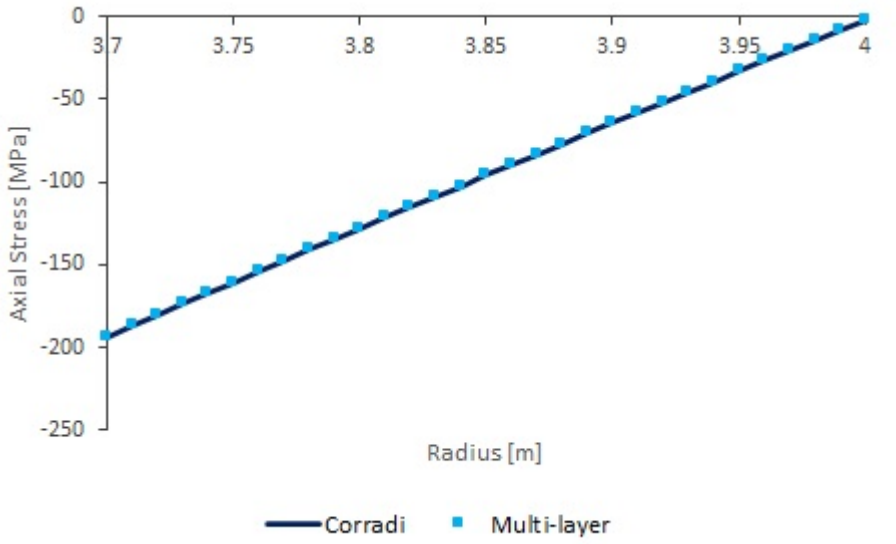

Figure 3.25: *Validation of the multi-layer model. Axial stress in the concrete ring when subjected to thermal load.*

3.3 Degradation of concrete

3.3.1 Strength and stiffness

Since the concrete lining is subjected to very high temperatures, the effects of fire on the material cannot be neglected. Thus, it is necessary to find a way to consider degradation when calculating the state of stress in the multi-layer model.
The Standards suggests to take into account these effects by choosing different stress-strain curves describing the material, each one characterised by its peak strength and strain as functions of temperature.
However, in the present work a slight different procedure is adopted: since each layer of the model is described by its Young's Modulus, the aim is to get an expression of E depending on temperature θ, so that each layer can be assigned with a temperature-dependent Young's Modulus. This can be accomplished starting from the data that are reported in the normative (Table 1.18): these values can be interpolated using non linear equations. Coefficient $k_{c\theta}$ represents the ratio between the strength at the initial conditions and the strength at temperature θ and can be interpolated with a cubic function:

$$k_{c\theta} = 1.77 \cdot 10^{-9} \cdot \theta^3 - 2.958 \cdot 10^{-6} \cdot \theta^2 + 0.0002 \cdot \theta + 1.0048 \tag{3.39}$$

The curve is reported in Figure (3.26). It well fits the tabulated values with a maximum discrepancy of 18.6% (800°C), even though there is a small discrepancy in correspondence of 1200°C. This discrepancy is trivial, since this value of temperature is not frequently reached.
The graph shows that at about 550°C the peak strength is half the initial value, whereas from 1000°C on the concrete loses almost all its strength.
Coefficient $k_{c\theta}$ will be then multiplied by the concrete compressive strength f_{ck} in order to get the maximum stress at temperature θ.
The literature suggests to adopt a compressive strength value at initial conditions ranging between 25 and 35 MPa: [Caner et al., 2005] uses $f_{ck} = 28$ MPa at 28 days, the same value is adopted in [LoMonte et al., 2019], while [Savov et al., 2005] chooses a compressive strength of 30 MPa in its case study. In this work, the concrete is associated with an initial compressive strength f_{ck} of 31 MPa.
Coefficient $\varepsilon_{c1,\theta}$ (Figure 3.27) is the value of strain in correspondence of the peak strength. It grows up to 600°C following an exponential trend, then it remains

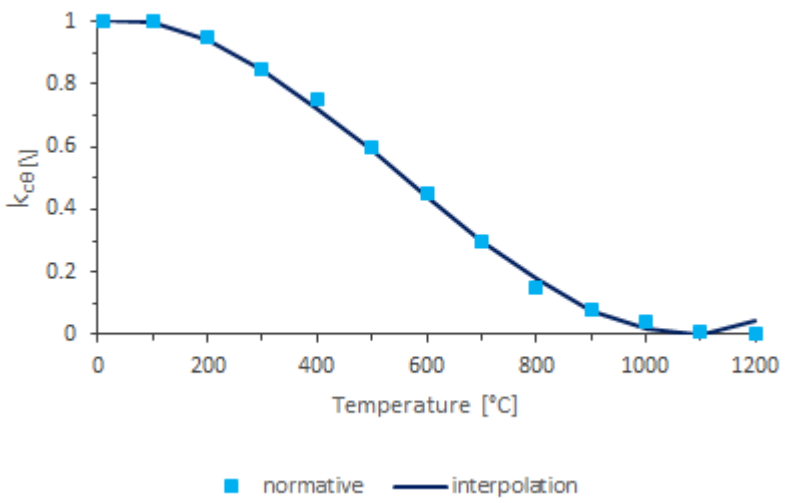

Figure 3.26: *Decrease of characteristic strength of concrete with temperature. Interpolation of $k_{c\theta}$ values taken from [Eurocode2, 2005]*

stable at 0.025:

$$\varepsilon_{c1,\theta} = \begin{cases} 0.0025 \cdot \exp^{0.0037 \cdot \theta} & for\ \theta < 600 \\ 0.025 & for\ \theta \geq 600 \end{cases} \tag{3.40}$$

The peak deformation grows for temperatures that are lower than 600°C, revealing a growing ductility of the material with temperature. Above this threshold, the strain remains constant: thus, the material is expected to reach its peak strength keeping the same value of deformation.
The ultimate compressive strain $\varepsilon_{cu1,\theta}$ (Figure 3.28) follows a linear trend:

$$\varepsilon_{cu1,\theta} = 2.5 \cdot 10^{-5} \cdot \theta + 0.0199 \tag{3.41}$$

Once these data have been interpolated, it is possible to build the stress-strain curves at any temperature (Figure 3.29). To this aim, the non-linear trend suggested by [Eurocode2, 2005] has been chosen for the pre-peak values (Eq. 1.9), while a linear trend is adopted for the post-peak.
For values of θ up to 600°C the peak migrates in rightward direction, revealing an increase in ductility of the material and thus a decrease of the Young's Modulus with temperature. The peak stress diminishes as well and for very high values of temperature the concrete loses the majority of its strength.

The Young's Modulus is defined as the tangent at each point of the curve for a specific temperature. However, in this work a simplified approach is assumed: for

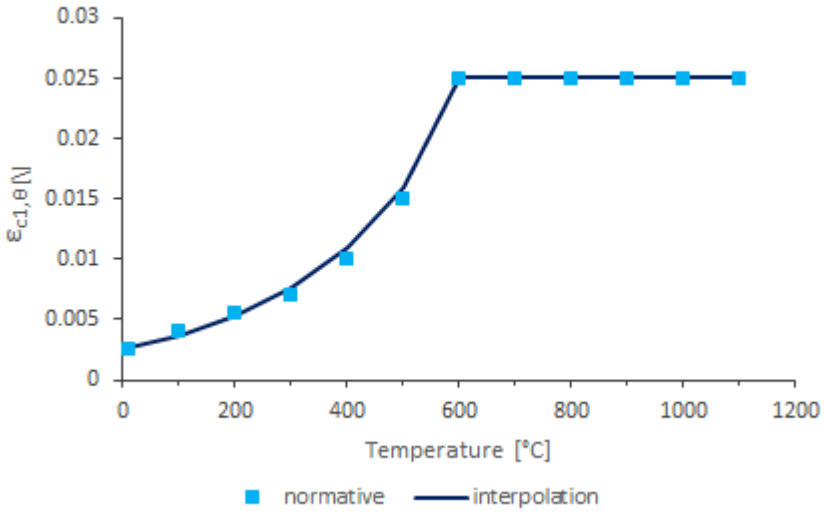

Figure 3.27: *Deformation at peak strength for concrete at different temperatures. Interpolation of data taken by [Eurocode2, 2005]*

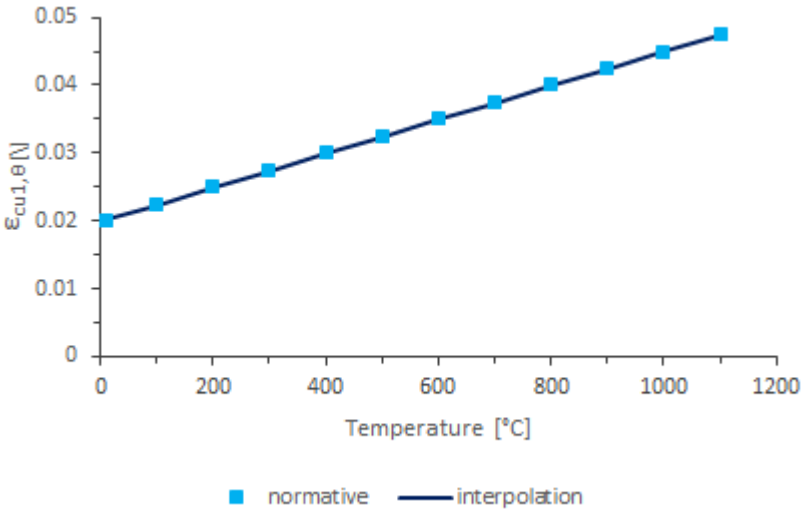

Figure 3.28: *Ultimate compressive deformation of concrete. Interpolation of data taken by [Eurocode2, 2005]*

.

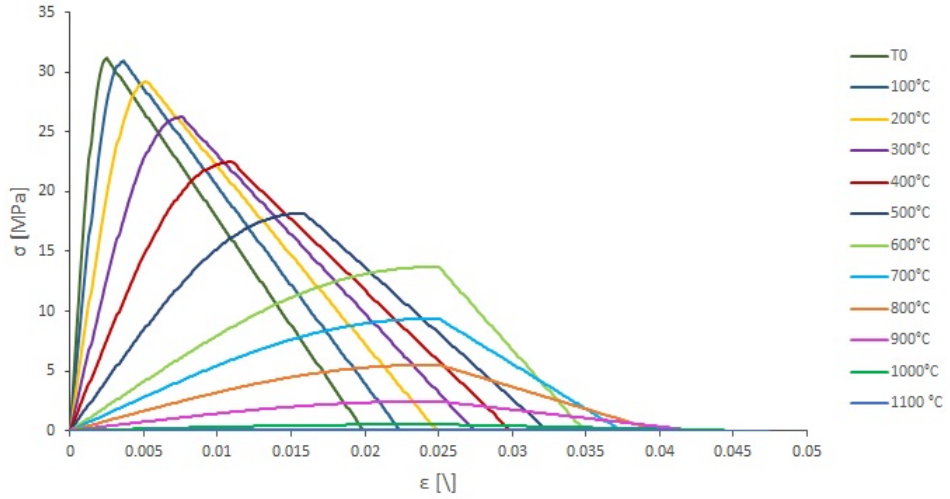

Figure 3.29: *Stress-strain curves at different temperatures.*

the pre-peak curve, the secant value of stiffness is considered:

$$E(\theta) = \frac{f_{c\theta,0.5}}{\varepsilon_{c1\theta,0.5}} \tag{3.42}$$

The values of E of each stress-strain curve can be interpolated using a decreasing function, in this case an exponential decay is adopted:

$$E = -2.519 \cdot 10^{-5} \cdot \theta^3 + 0.0662 \cdot \theta^2 - 58.528 \cdot \theta + 17811 \tag{3.43}$$

This function (Figure 3.30) well approximates the stiffness reduction of concrete, considering the maximum difference from the secant values of about 733 MPa in correspondence of 500°C. This error is due to the fact that the peak strain values (Figure 3.27) are described by a piecewise function.
This equation allows one to associate each layer of the support with a temperature-dependant Young's Modulus. The inner layers, which are subjected to a very high rise in temperature, experience a strong decrease in stiffness and strength, while the external layers of the lining are characterised by a value of E very close to the initial one (i.e. 18 GPa).

The reduction of stiffness with temperature has been investigated in the literature too, revealing very different behaviours depending on the type of aggregate that constitutes the sample. A review of experimental data can be found in [Rilem Technical Committee, 2004].

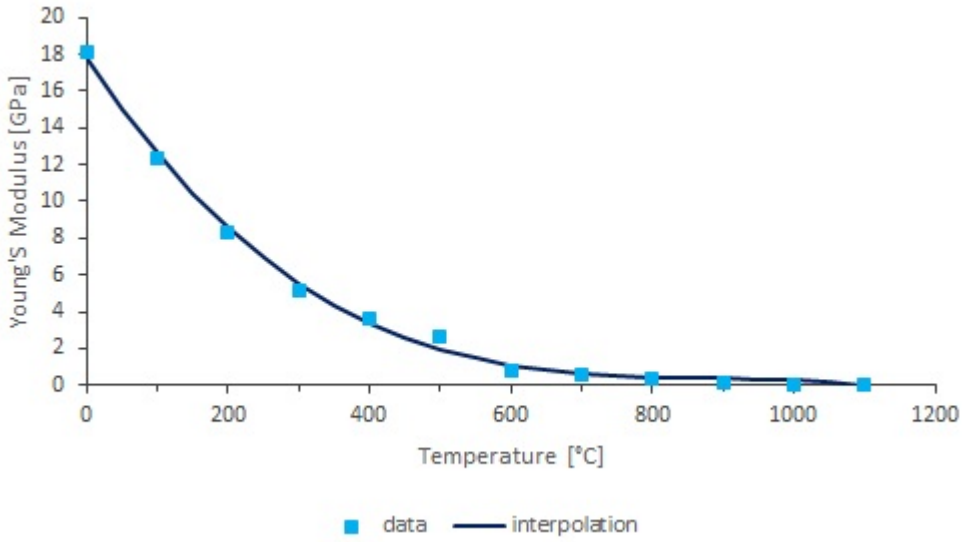

Figure 3.30: *Exponential decay of Young's Modulus E with temperature θ.*

Since the exponential decay shown above is typical for silicate aggregates, the curve can be compared with experimental data which refer to similar types of concrete. For example, Figure (3.31) reports the results of [Marechal, 1970], where different mixes have been tested. If compared to our analytical graph, the curves have similar trends.

The fire induced damage can be considered as reversible or irreversible: in the former case, once the lining has cooled down, its mechanical properties are the *undisturbed* ones. Instead, if the phenomenon is assumed irreversible, the properties describing concrete depend on the maximum temperature that has been reached in the layer, thus at the end of the fire the material has lost most of its strength and stiffness.

Another way to assess the condition of the tunnel after a fire is to consider the residual properties of concrete. The residual properties refer to the experimental data that are found in a fire test after the sample has returned to the environmental temperature. To this aim, the review of [Phan and Carino, 1998] has been used. In Figure (3.32) the reduction of E with respect to the initial value at 20°C is reported, for *unstressed* samples. It may be noticed that the concrete lining of a tunnel would be better represented by a stressed test. However, due to the scarcity of data, the unstressed residual response is taken into account.

In this work, only the case of *Normal Strength Concrete* (NSC) is considered.

These results show that after the sample has cooled down, the material regains a

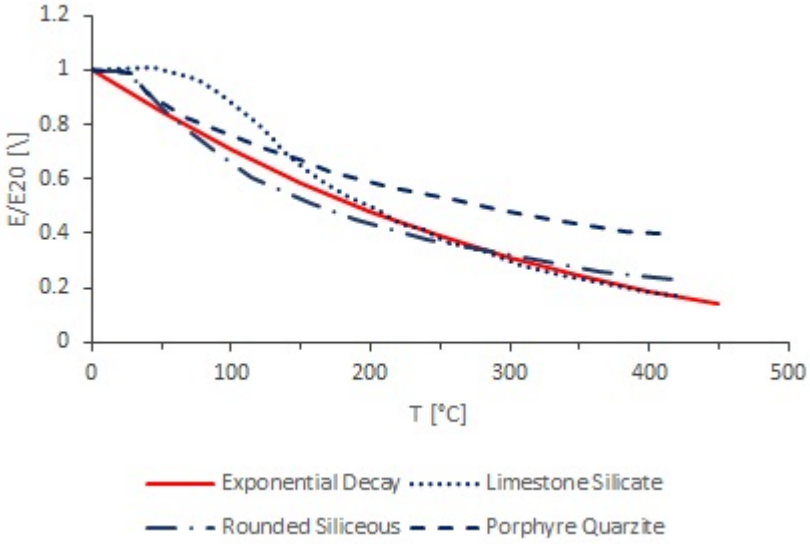

Figure 3.31: *Comparison between the analytical curve for Young's Modulus reduction and experimental results of [Marechal, 1970] for* $\theta < 400\,°C$.

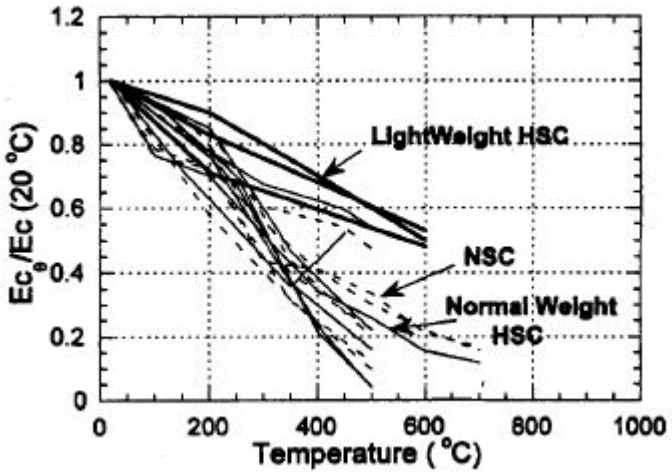

Figure 3.32: *Modulus of Elasticity-Temperature Relationships from Unstressed Residual-Strength Test Results. [Phan and Carino, 1998]*

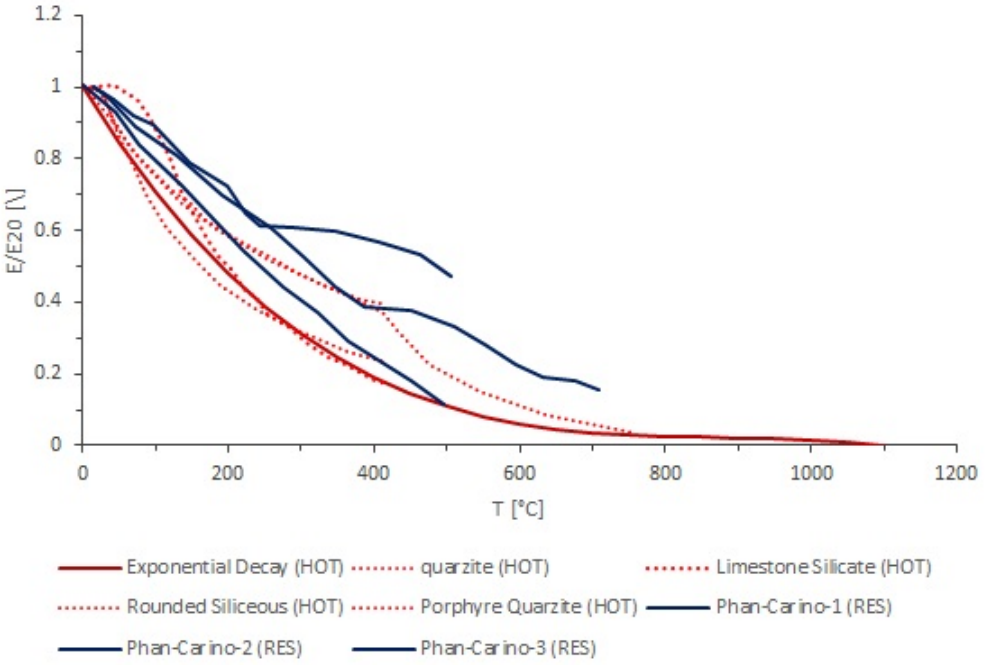

Figure 3.33: *Residual and hot Young's Modulus. Data from [Phan and Carino, 1998]and [Marechal, 1970].*

small part of its initial stiffness. Figure (3.33) reports both the hot ad residual experimental curves. As shown in the graph, the interpolation curve is in agreement with the experimental data, in particular with the lower bound.

3.3.2 Friction angle and cohesion

Concrete may be associated to many combinations of friction angle and cohesion depending on its composition. In [Oztekin et al., 2016] experimental tests on NSC have been conducted, resulting in the determination of cohesion between 5 and 13 MPa, while friction angle ranges between 27° and 34°. In this work, for uniaxial compression strength $f_{ck} = 31\ MPa$, the model has been tested considering the following properties:

- friction angle $\phi = 32°$
- cohesion $c = 8.62$ MPa

When dealing with high temperatures, cohesion and friction angle cannot remain to the values of the initial conditions, since the strength of concrete is influ-

enced by temperature. In this work, they are assumed to proportionally reduce with the strength of concrete.
The same reduction factor is applied to both the coefficients. Failure occurs for the following values:

$f_{c\theta}$ [MPa]	ϕ [°]	c [MPa]
31	32	8.62
30	31.52	8.49
29	30.89	8.32
28	30.27	8.15
27	29.67	7.99
26	29.07	7.83
25	28.20	7.60
20	24.22	6.52
15	19.74	5.32
10	14.49	3.90
5	8.12	2.19

Table 3.2: *Variation of friction angle and cohesion with strength.*

The two parameters proportionally reduce by a multiplying factor F_r lower than 1, which decreases with progressive damage (Figure 3.34).

To have a continuous variation of cohesion and friction angle, an analytical relation with the compression strength should be established, rather than a tabular list of values. The friction angle and cohesion can be calculated as functions of the strength $f_{c\theta}$ at temperature θ using two quadratic functions (Figures 3.35 and 3.36):

$$\phi = -0.0169 \cdot f_{c\theta}^2 + 1.5297 \cdot f_{c\theta} + 0.6312 \tag{3.44}$$

$$c = -0.0046 \cdot f_{c\theta}^2 + 0.4121 \cdot f_{c\theta} + 0.17 \tag{3.45}$$

The choice of applying the same reduction factor to both the parameters is the simplest one and represents a first approach to deal with the problem. However, different assumptions could be made: an example is to first reduce cohesion and to start reducing the friction angle later. In fact, the literature suggests that as soon as concrete is heated, the bounds between cement paste and aggregates tend to break, resulting in a decrease in cohesion [Hager, 2013]. Given the high variability of the mechanical response of concrete to high thermal loads, these parameters should be chosen upon appropriate testing and calibration.

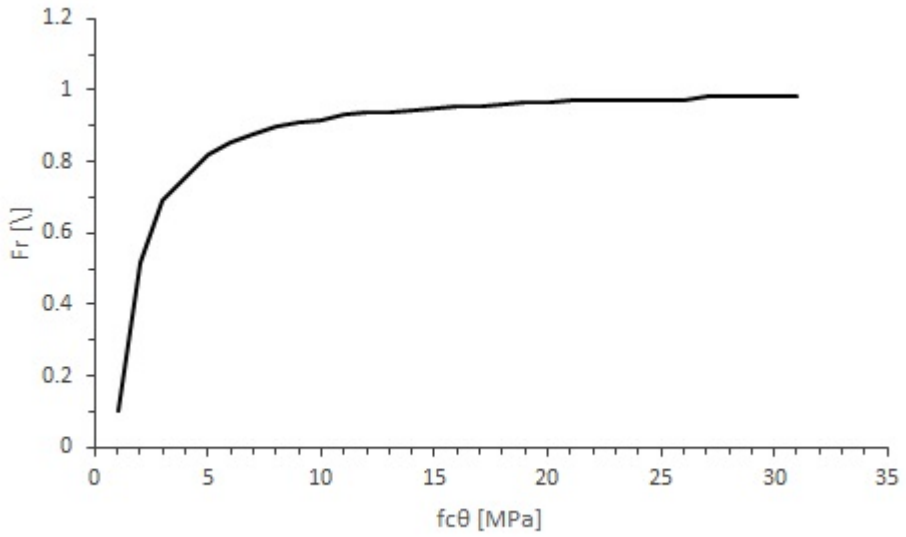

Figure 3.34: *Friction angle and cohesion reduction factor as function of concrete strength* $f_{c\theta}$

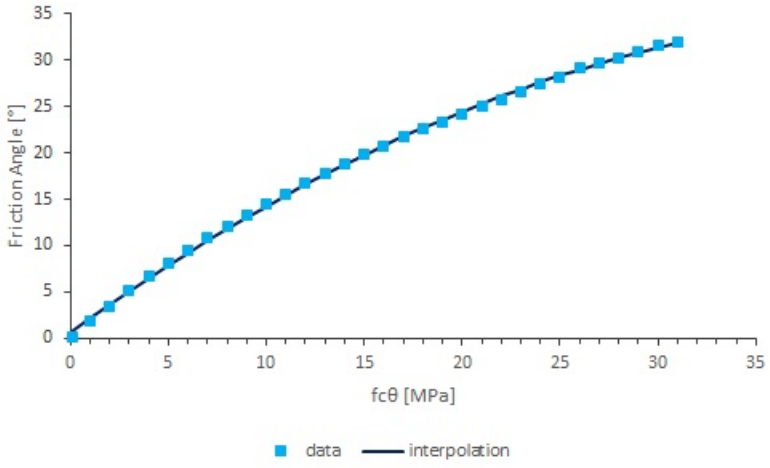

Figure 3.35: *Friction angle* ϕ *as function of compressive strength* $f_{c\theta}$ *at temperature* θ

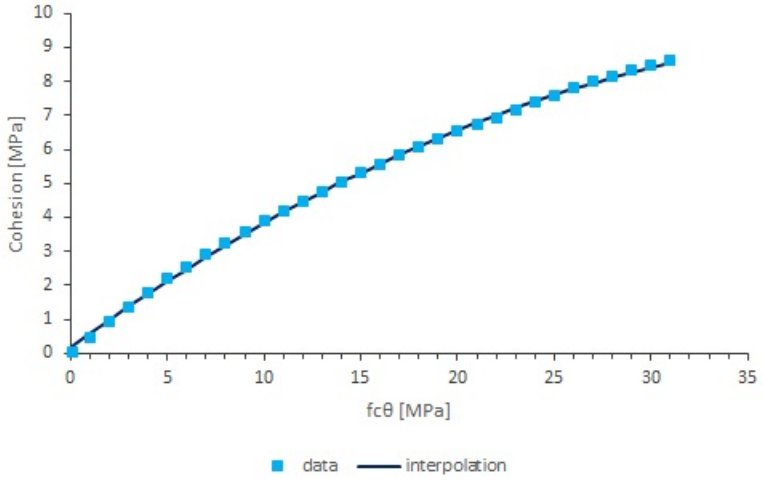

Figure 3.36: *Cohesion c as function of compressive strength $f_{c\theta}$ at temperature θ*

Chapter 4

Results and Discussion

4.1 Heat transfer analysis

The development of fire in a tunnel depends upon many variables, such as its geometry or the presence of a ventilation system. As a consequence, various fire scenarios may be chosen to predict the effects induced by fire on the structure.
The environmental temperature of the tunnel is fixed at $T_0 = 20°C$ for a hundred-meter-deep tunnel. The value of T_0 increases with depth and depends on the length of the tunnel as well.
In this analysis, the tunnel is supposed to be subjected to standard fire ISO834, followed by a cooling phase linear with time (Figure 4.1).

The multi-layer model allows to calculate the fire induced stress state by introducing a temperature field $T(r)$ that in the previous section was represented by analytical curves (quadratic or logarithmic). Otherwise, the temperature field can

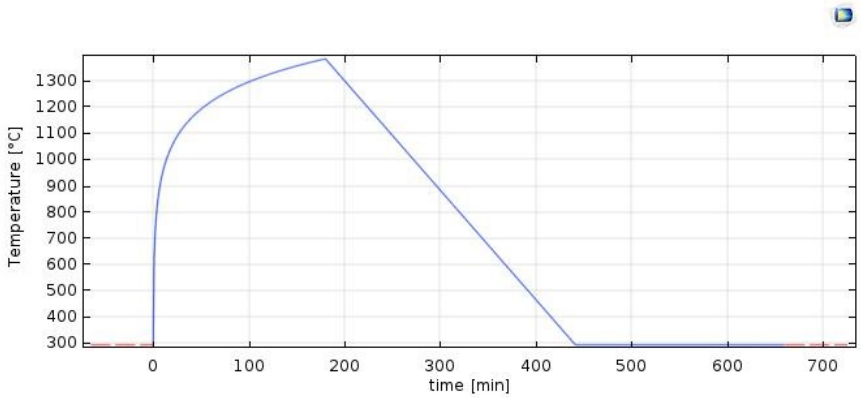

Figure 4.1: *Fire curve imposed as boundary condition at the intrados of the tunnel.*

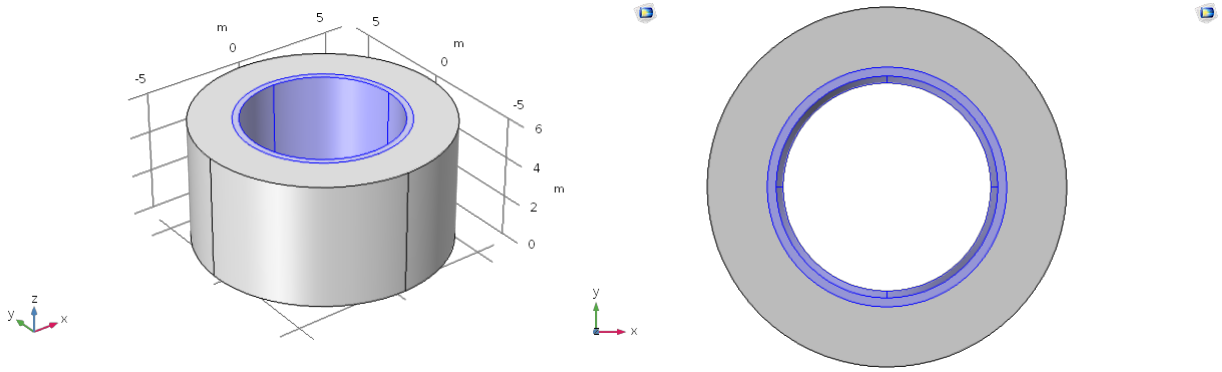

(a) 3-dimensional view *(b) x-y plane*

Figure 4.2: *Rock (gray) and concrete lining (blue) model in COMSOL Multiphysics*

be the solution of a heat transfer analysis.
The heat transfer problem can be easily solved by implementing the Fourier equation of heat conduction in a finite element model or, alternatively, by analytically solving the Fourier equation. In the present work, the software COMSOL Multiphysics has been used to be provided with the temperature curves inside the 30-cm thick concrete lining and in the surrounding rock. The geometry of the problem (Figure 4.2) is composed of two domains: the concrete lining and the rock. To solve the heat transfer problem, the default material properties for soil and concrete of COMSOL are used. In particular, the thermal conductivity plays a fundamental role when dealing with heat transfer problem. The default conductivity of soil λ_s refers to [Mostafa, 1999]:

$$\lambda_s = \begin{cases} 0.0747638 + 1.451056 \cdot 10^{-4} \cdot \theta & \text{if } 293 < \theta[^\circ C] < 475 \\ 139.2152 - 1.028413 \cdot \theta + 0.002851159 \cdot \theta^2 + & \\ -3.513043 \cdot 10^{-6} \cdot \theta^3 + 1.623188 \cdot 10^{-9} \cdot \theta^4 & \text{if } 475 < \theta[^\circ C] < 525 \end{cases} \quad (4.1)$$

Concrete is assigned with λ_c defined by [Morabito, 1989].It is defined between $253 < \theta[^\circ C] < 363$ as:

$$\lambda_c = 26.91105 - 0.2477056 \cdot \theta + 8.606168 \cdot 10^{-4} \cdot \theta^2 + -1.00482 \cdot 10^{-6} \cdot \theta^3 \quad (4.2)$$

The effects of fire on the structure for the first ten hours are shown in the contour plots of Figure (4.3) and plotted in the graph of Figure (4.4). During the first two hours, heat is transferred only in concrete, while the rock remains at T_0. After two hours the rock starts being heated, reaching temperature values up to 370°C.

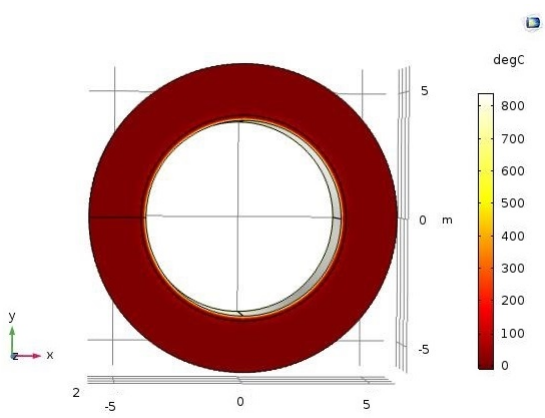

(a) 30 min

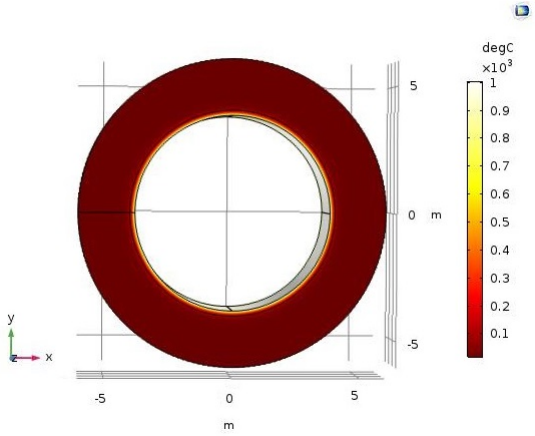

(b) 90 min

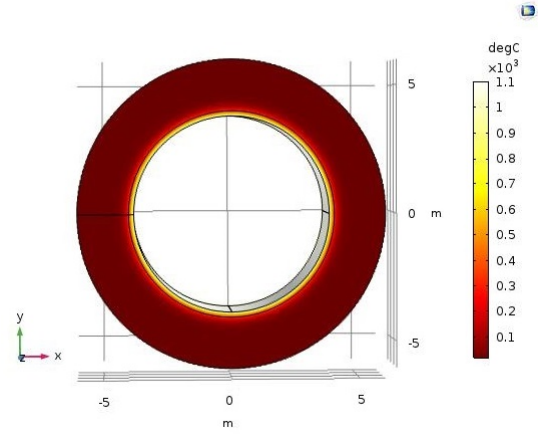

(c) 180 min

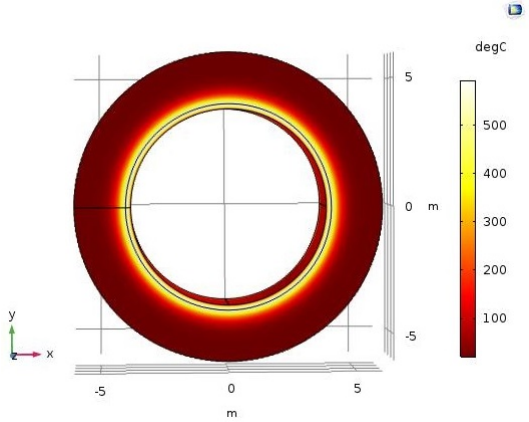

(d) 420 min

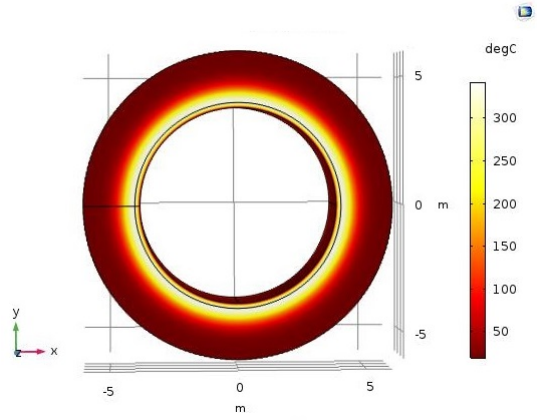

(e) 600 min

Figure 4.3: *Contour plots of the temperature at different time steps from the transient heat transfer analysis.*

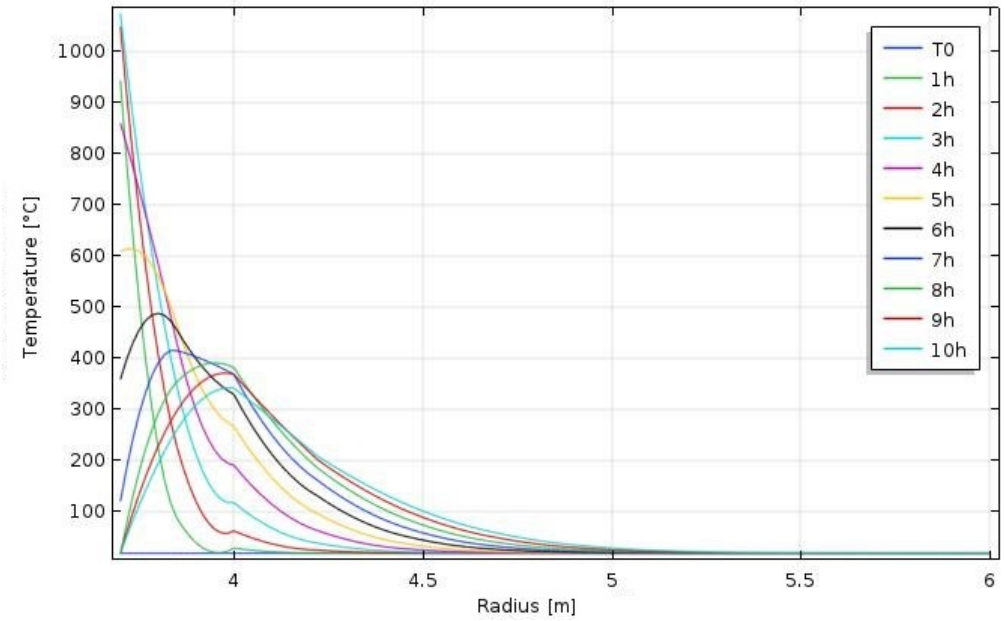

Figure 4.4: *Temperature inside the concrete ring and the rock for different time steps.*

Thus, the peak temperature is shifted with time towards the rock and at the same time the peak value decreases. Looking at the results of the first ten hours, only one meter of rock is subjected to heating, but the trend suggests that heat could be transferred further in the following time steps. In fact, if a thicker rock ring is analysed and a greater time lapse is considered in the analysis, it is possible to have an idea of the time that is needed to completely cool down the tunnel. The results show that the first ten meters of rock are affected by a temperature variation. After about three days, the concrete lining returns to the initial temperature, while the effects of fire tend to completely disappear in the rock after about ten days (Fig. 4.5).

At the interface between rock and lining there is a discontinuity in the temperature gradient, due to the different thermal conductivities of the two materials.
Looking at the temperature variation with time at different positions (Figure 4.6), it is possible to see once again that the concrete has very good insulation properties. In fact, at the intrados (i.e. for $r = 3.7\,m$) the temperature is equal to the imposed boundary condition, while for $r = 3.8\,m$ the delayed peak value is almost half T_{max} at the intrados. On the other hand, the rock has a higher value of thermal conductivity: looking at the first meter of rock, the peak is shifted in time, but it diminishes slowly (Figure 4.7).

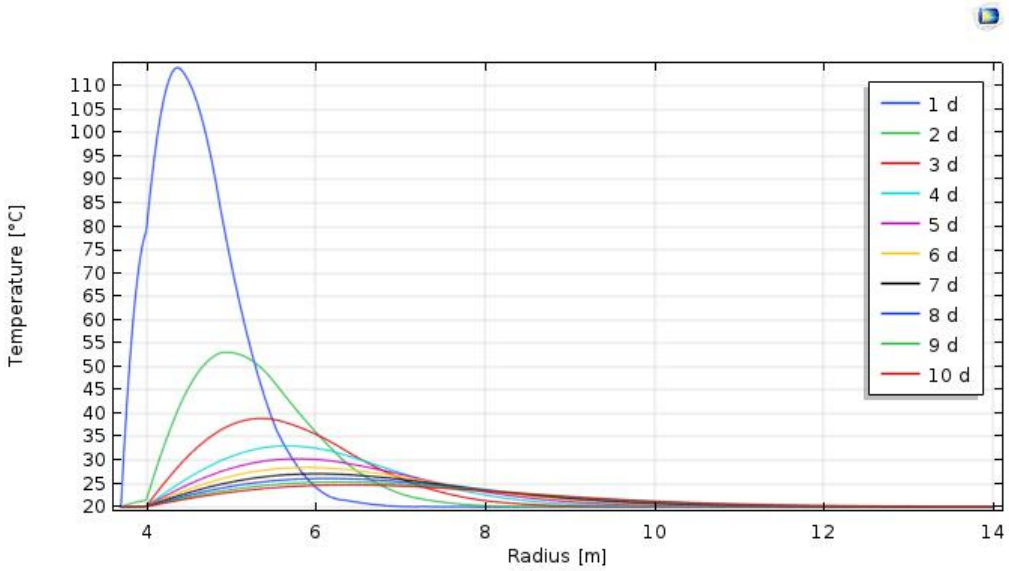

Figure 4.5: *Effects of fire after one to ten days.*

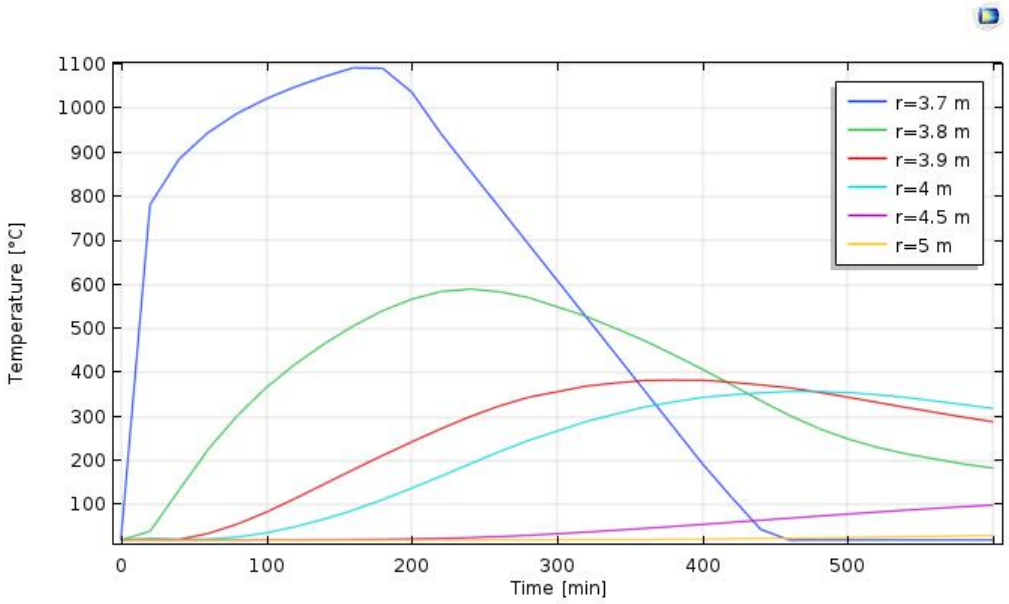

Figure 4.6: *Temperature variation at different reference points in the lining (r=3.7 m - r=4 m) and in the rock (from r=4 m on).*

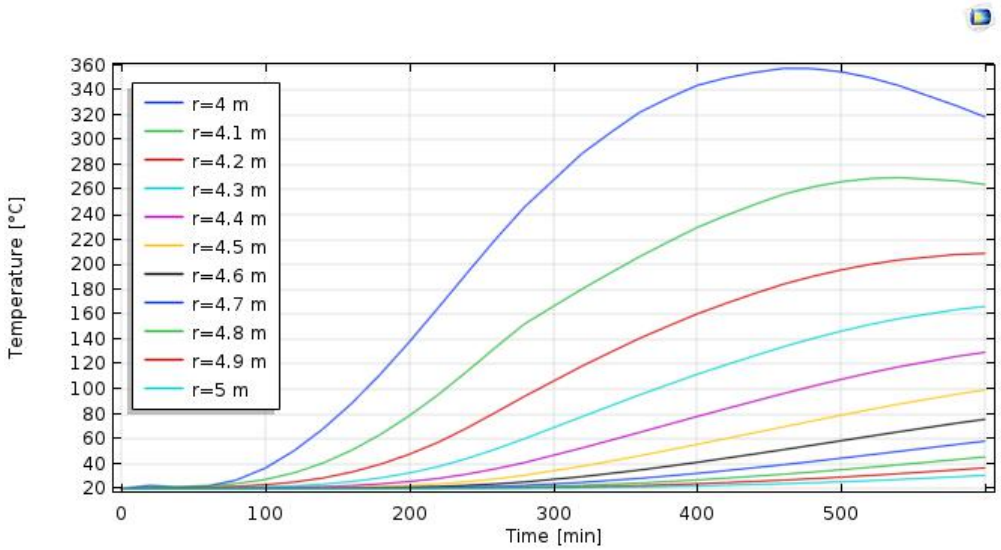

Figure 4.7: *Temperature variation within time inside the rock.*

4.2 Tunnel response under fire

The results of the heat transfer analysis can be used to evaluate the state of stress and radial displacement that are generated by the presence of fire. These first results refer to a purely elastic behaviour, therefore the cooling phase brings the stress-strain state back to the initial condition.
The thermal problem and the mechanical one are coupled by defining the coefficient of thermal expansion α for both materials. In this work, the coefficients have been taken by the literature and are reported in the following table:

domain	name	unit	value
rock	α_r	$\frac{1}{^\circ C}$	10^{-5}
concrete	α_c	$\frac{1}{^\circ C}$	$9.26 \cdot 10^{-6}$

Table 4.1: *Thermal coefficients for rock and concrete*

Based on the multi-layer model, the lining is subdivided into thirty one-centimeter thick layers, where the inner radius is $r_0 = 3.7\,m$ and the external one is $r = 4\,m$. The rock ring is composed of 174 layers of variable dimensions to form a 50-meter-thick ring, from $r = 4\,m$ to $r_n = 54\,m$. The layers which lay close to the interface are one-centimeter thick as well, but as the radius increases, the effects of temper-

ature diminish and thus the external layers reach a thickness of 0.5 meters. Each layer has been assigned with its mechanical and thermal properties and with the average value $\Delta T(t)$ calculated over the layer's width, from the thermal analysis results at time t.
As already seen in the heat transfer results, ten days are needed to make the tunnel completely cool. Since the main mechanical effects on the structure develop during the first ten hours, the stress state is analysed for this time lapse.

Looking at the radial displacement (Figures 4.8 and 4.9) for different time steps, the maximum divergence is reached four hours after the beginning of fire (i.e. during the cooling phase) and at the interface between rock and lining. The radial displacement at this time step is of about 14.45 mm and a similar value is reached five hours after the fire: this is due to the fact that concrete is thermally insulated and it needs several hours to get cooler.
The peak displacement shifts with time: at first, the maximum divergence is reached within the lining, whereas in the following time steps it reaches the rock layers: for example, after 10 hours the peak displacement $u_r = 2.16\,mm$ is reached at about $r = 5.35\,m$, which is 1.35 m far from the rock-lining interface.
The results show that null divergence is never reached and for great radius the radial displacement asymptotically tends to zero: this is due to the choice of an elastic model.
The lining and the first layers of rock are subjected to compressive radial stress, which reaches its peak of about 3.6 MPa inside the concrete lining at T=3 hours (Figure 4.10).
Then, for greater radius, the fire induced radial stress diminishes, resulting in almost null radial stress about 25 meters away from the lining-rock interface. Looking at Figure (4.11), the peak stress is reached within the very first layers of concrete lining, but it shifts towards the rock at the following time steps.
Radial compression grows up to the third hour, but as soon as the fire is ceased, it decreases. Ten hours after the fire, the stress state is completely different with respect to the previous hours: the lining has cooled down, while the peak temperature lays in the rock. This leads to the formation of a region characterised by radial compression near the rock, whereas the most internal part of the lining is subjected to radial tension. This stress gradient could induce the spalling of the intrados of the lining, but to have a better analysis of the state of stress, the circumferential stresses should be considered as well.
As soon as temperatures are very low, such as after 24 hours, the concrete ring is

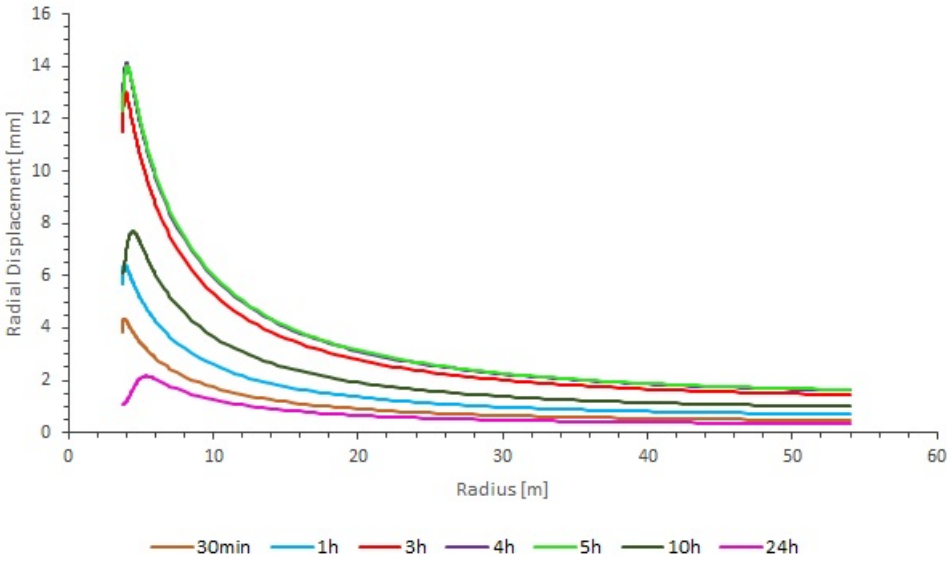

Figure 4.8: *Radial displacement of concrete lining and rock.Positive values mean outward direction.*

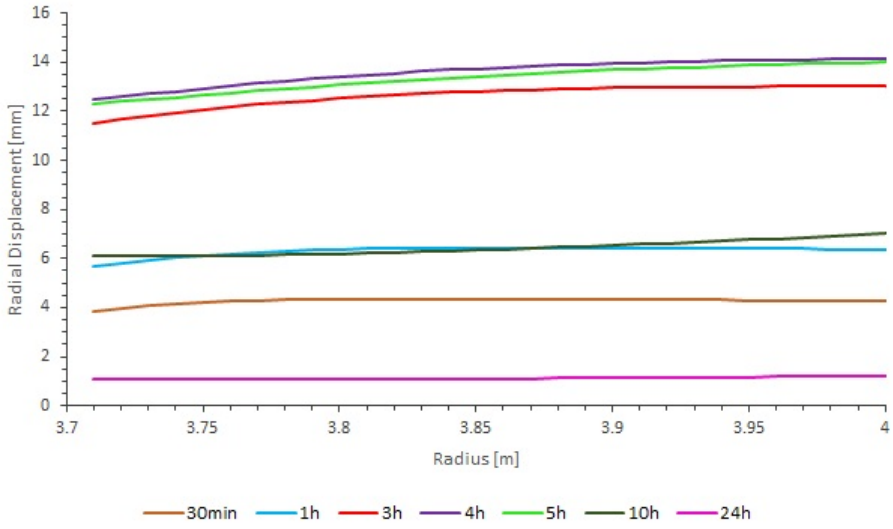

Figure 4.9: *Radial displacement of concrete lining.*

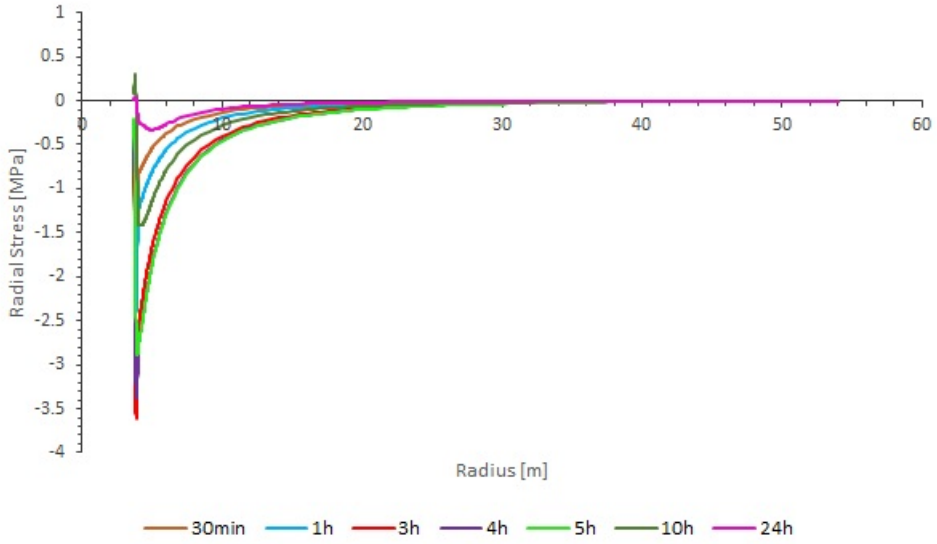

Figure 4.10: *Radial stress in lining and rock.*

not subjected anymore to radial stress.

The hoop stress state (Figures 4.12 and 4.13) involves the concrete lining and the first meters of rock. As already seen in Section 1.2.3, during the first hours the intrados is characterised by very high values of temperature, whereas the external part of the lining is still at its initial condition, T_0. This leads to the formation of compressive hoop stress at the intrados and tensile ones externally.

As soon as all the lining is heated, the stress gradient diminishes (e.g. in 5h curve), while after 10 hours the situation is reversed: the intrados has now completely cooled, while the lining near the rock is still characterised by high temperature: thus, for small radius the lining has tensile stresses, for larger ones it is compressed. As already mentioned, it is important to remark that the stress gradient that forms inside the lining is one of the main causes of spalling. Moreover, by comparing radial stress and hoop stress, it should be noted that they differ of about two orders of magnitude and so the stress deviator is very high. This information is essential because it permits to make some important assumptions: in particular, the deviator should be compared with the triaxial strength of concrete, but since $q = \sigma_\theta - \sigma_r \simeq \sigma_\theta$, it is sufficient to compare the hoop stress with the uniaxial compression strength.

Finally, the axial stress (Figures 4.14 and 4.15) reaches values that could be comparable to those of the circumferential stress (i.e. two orders of magnitude bigger than radial stress). At the beginning, the inner part of the lining is axially com-

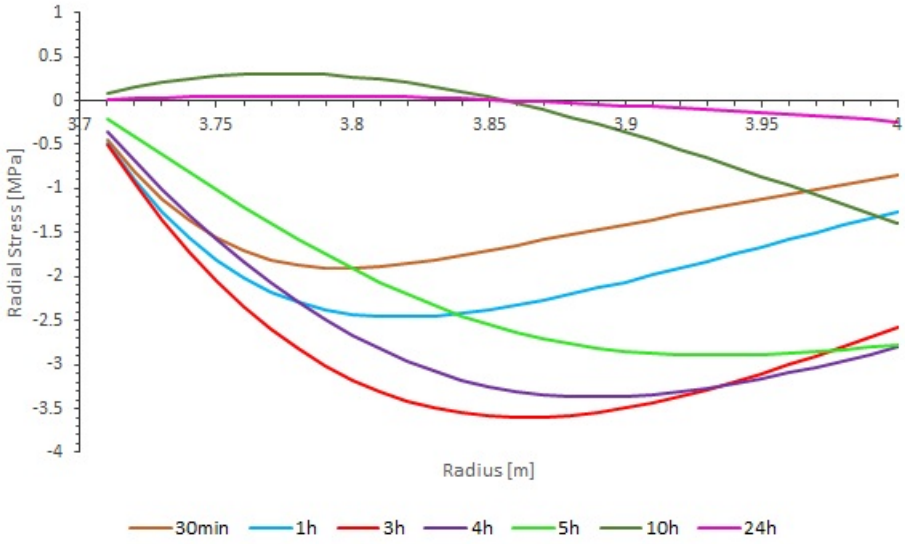

Figure 4.11: *Radial stress state in the lining at different time steps.*

pressed, while the external one is in slight tension. Then, in the cooling phase the stress state tends to go back to the initial condition.
The main reason why the axial stress is so high is that the cylinder is assumed to be constrained at one end, while at the other end there is a very stiff spring which limits the axial expansion of the tunnel. In fact, the axial deformation ε_z is constant in all the layers and it is in the order of 10^{-8}. This limitation of movement causes the rise in stress in this direction.
These results refer to an elastic model, thus the final condition returns to the initial one. However, to be closer to reality, the consequences of such high stresses should be considered: in fact, even if the tunnel cools down, the fire induced stress state could lead to irreversible damage.

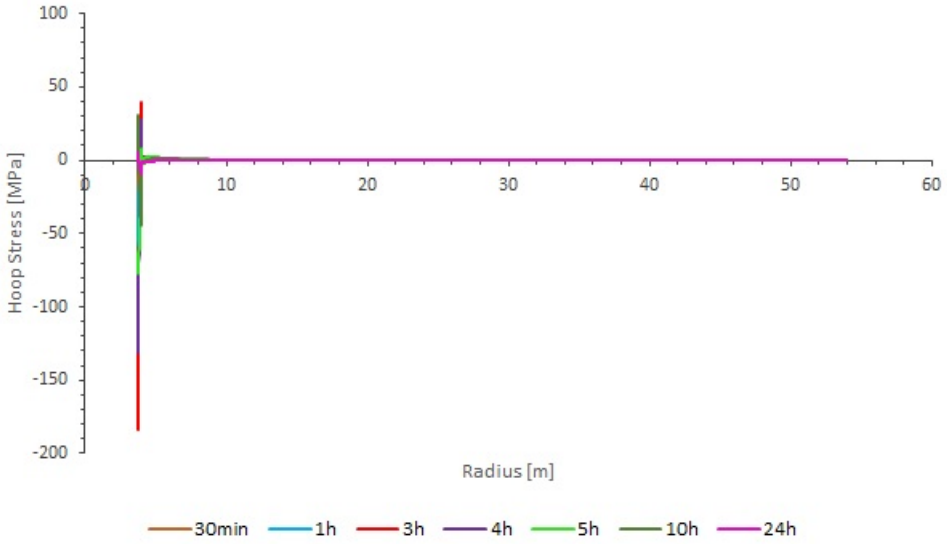

Figure 4.12: *Hoop stresses generated by the variation of temperature induced by fire.*

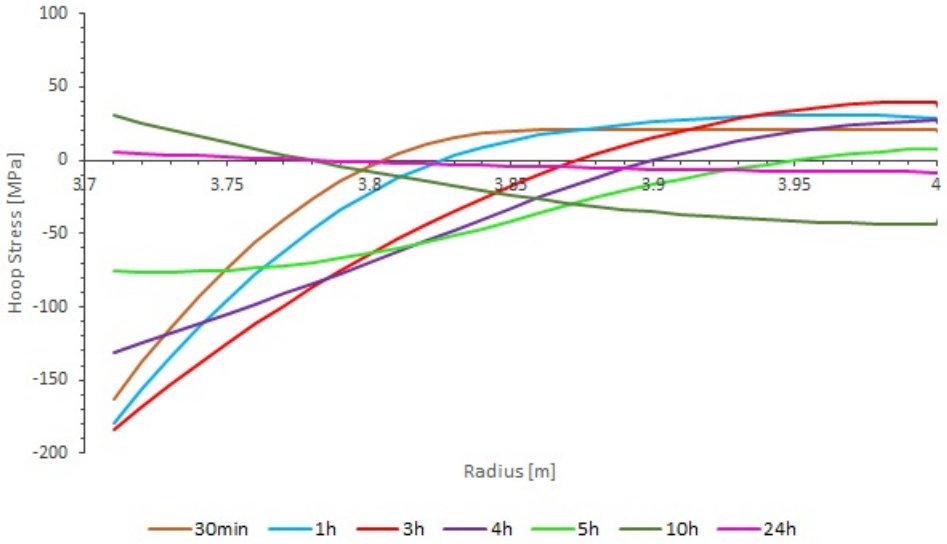

Figure 4.13: *Hoop stresses in the concrete lining.*

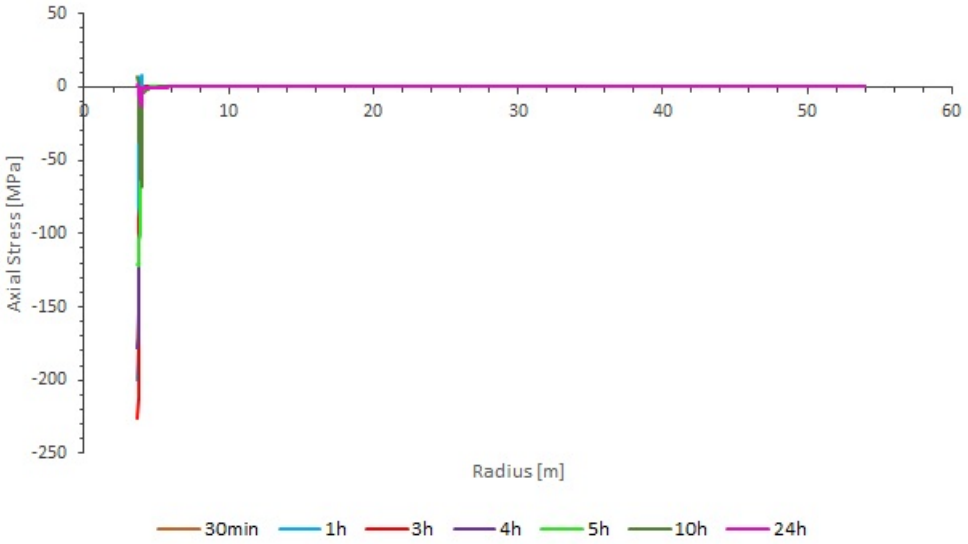

Figure 4.14: *Axial stress in the concrete lining and surrouding rock.*

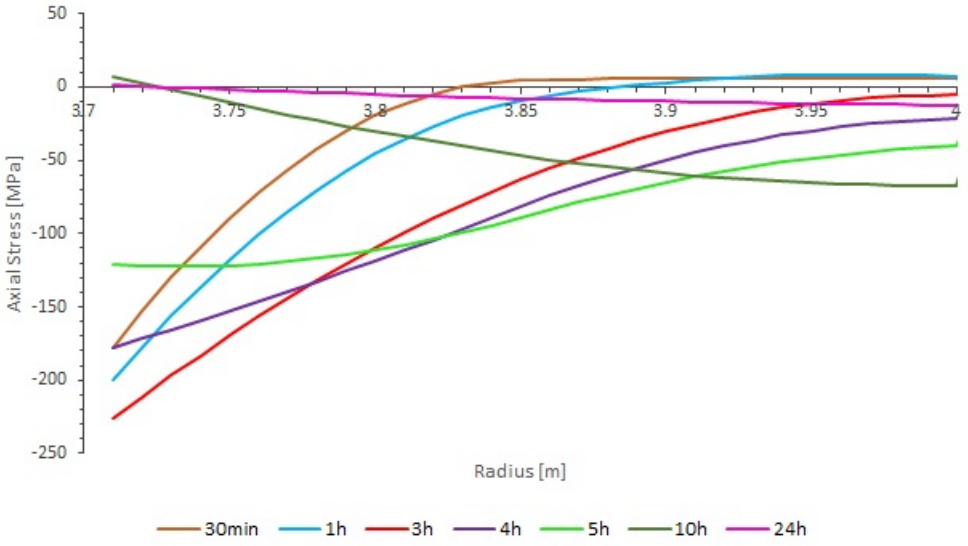

Figure 4.15: *Axial stress in the concrete lining.*

4.3 Fire induced damage

The multi-layer model allows one to calculate the stress state that is generated in the support of a tunnel and in the surrounding rock during and after a fire.
However, when a particular material is subjected to such high temperatures its thermal and mechanical behaviour may substantially change, mainly because of changes in its micro-structure and in the chemical bounds.
In this section the multi-layer model is slightly modified, with the aim of considering the main two fire induced effects on concrete: the material properties degradation and the possibility of having spalling. The numerical code is consequently adapted to permit the user to include one or two of these degradation effects.

4.3.1 Degradation of concrete

In this section the fire-induced damage is introduced by means of concrete degradation. In particular, as already mentioned in subsection 1.2.3 the material loses its strength and stiffness with temperature.
The temperature-dependant strength reduction is described by coefficient $k_{c\theta}$ in Equation (3.39), while the Young's Modulus reduction with θ is reported in Equation (3.43).
The dependence of these two parameters on temperature results in a not homogeneous distribution of stiffness in the concrete ring. As temperature rises, the material loses its strength and becomes more ductile.
Thus, the results that are presented derive from a model that is constituted of thirty layers of concrete, each one characterised by its average temperature, resulting from the purely thermal analysis, and by its temperature-dependent Young's Modulus.

The fire-induced effects can be introduced in two different ways: if the effects on the concrete stiffness are considered reversible, it is sufficient to describe the dependence of the Young's Modulus on temperature, but as soon as the tunnel cools down, the stiffness of the material returns to the initial value. In the other case, the effects of high temperatures are considered irreversible: once the peak temperature is reached, concrete is permanently damaged and its stiffness cannot return to the pre-fire conditions. This assumption is put into practice by assigning

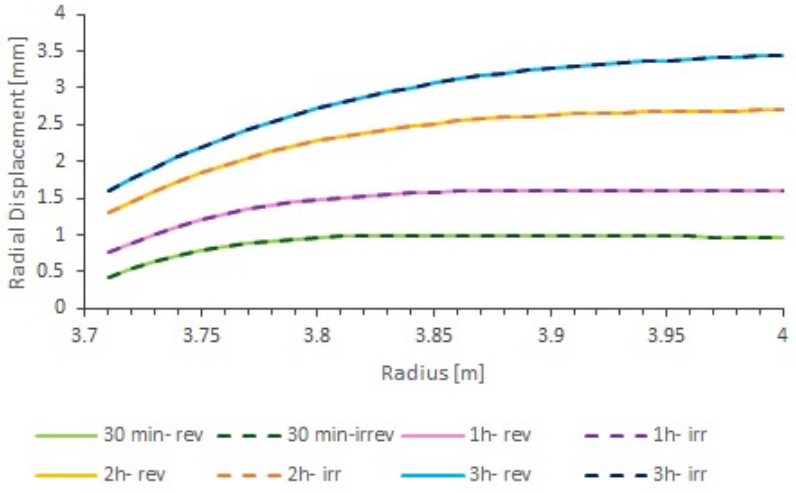

Figure 4.16: *Radial displacement of the concrete lining during the heating phase. The results of the reversible and irreversible models are the same.*

to each layer a stiffness which does not depend on the current temperature, but on the peak temperature that has characterised the layer.
Since the temperature rises during the heating phase, the results of the two different models are the same up to the third hour, while in the cooling phase the results diverge. For instance, the inner layers of concrete depend upon the temperature values at T=3 hours, whereas for greater radius the peak temperature may be the one at four or five hours, since the temperature peak shifts with time. Figure (4.16) shows the radial divergence during the heating phase, while Figure (4.17) shows the stress state in the same period of time.
As already mentioned above, the results given by the models are the same. Besides that, it may be noticed that in this case both the radial displacement and the stress state are far lower than the one obtained neglecting fire induced damage. The peak displacement reaches about 3.5 mm at T=3 hours and the radial, hoop and axial stress diminish of about one order of magnitude. The reduction of stiffness makes the material more ductile, this is why it is characterised by lower values of stress.

During the cooling phase the results of the two models become different. The real state of stress is estimated to lay between two boundary conditions: the reversible case and the irreversible one, if the material is more realistically assumed to behave in an only partially reversible way ([Phan and Carino, 1998], [Rilem Technical Committee, 2004], [Ma et al., 2015]). This is why the results of the two

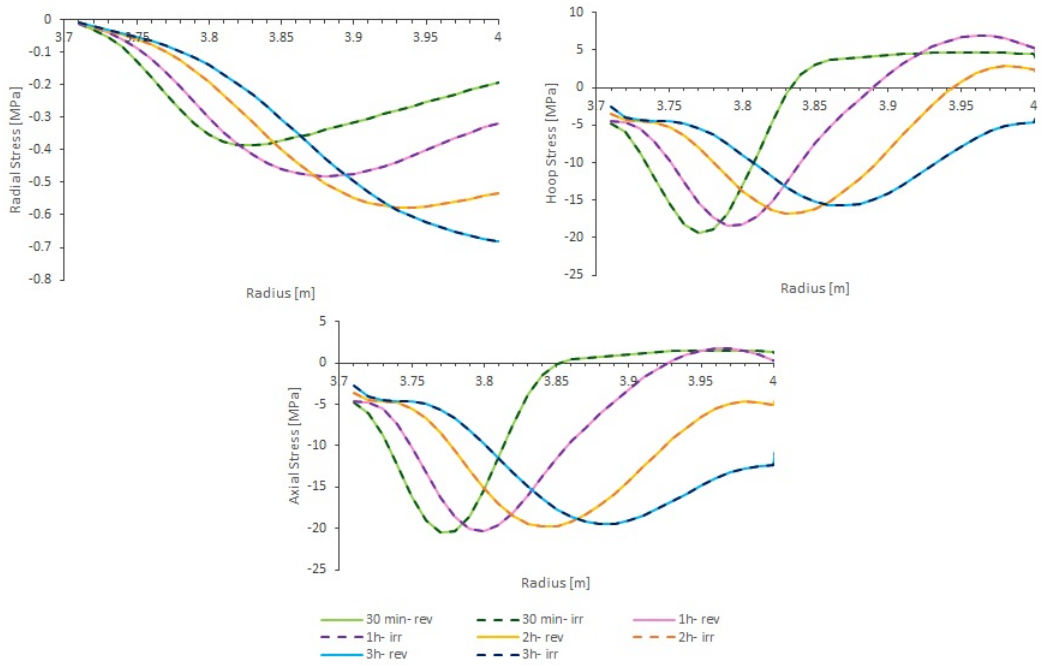

Figure 4.17: *Stress state in the concrete lining during the heating phase in the reversible and irreversible models.*

models are reported in the same graph.
For instance, Figure (4.18) shows the radial displacement 10 hours after the fire. The reversible case represents the worst condition, since the material is supposed to be more rigid with respect to the other case. The stress state (Figure 4.19) is characterised by very different results: on one hand, the reversible model presents a small radial tension at the intrados, balanced by compression getting closer to the rock; the hoop stresses are positive (tension) where the lining is cool, while they are negative (compression) where the temperatures are still high. Finally, the lining is axially compressed, reaching values up to 20 MPa.
On the other hand, the irreversible model is characterised by smaller stress variations: in the three graphs the lining is shown as entirely compressed, thus the stress variations inside the material are more limited.

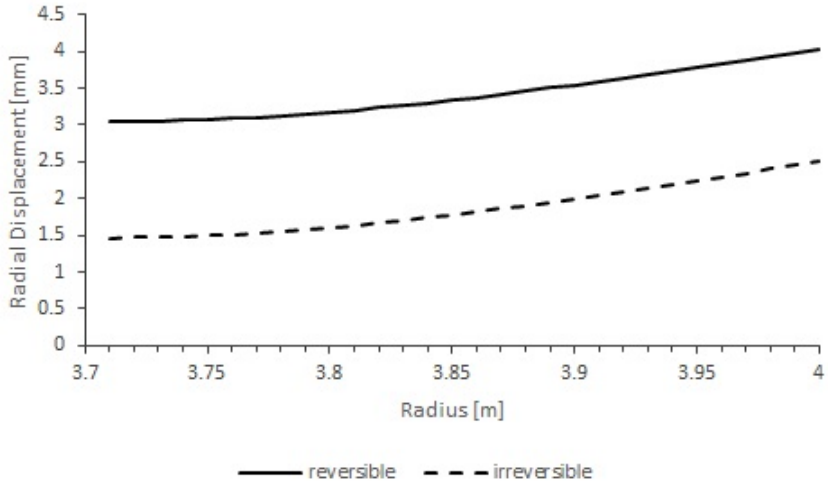

Figure 4.18: *Radial displacement 10 hours after the fire. Comparison between reversible and irreversible case.*

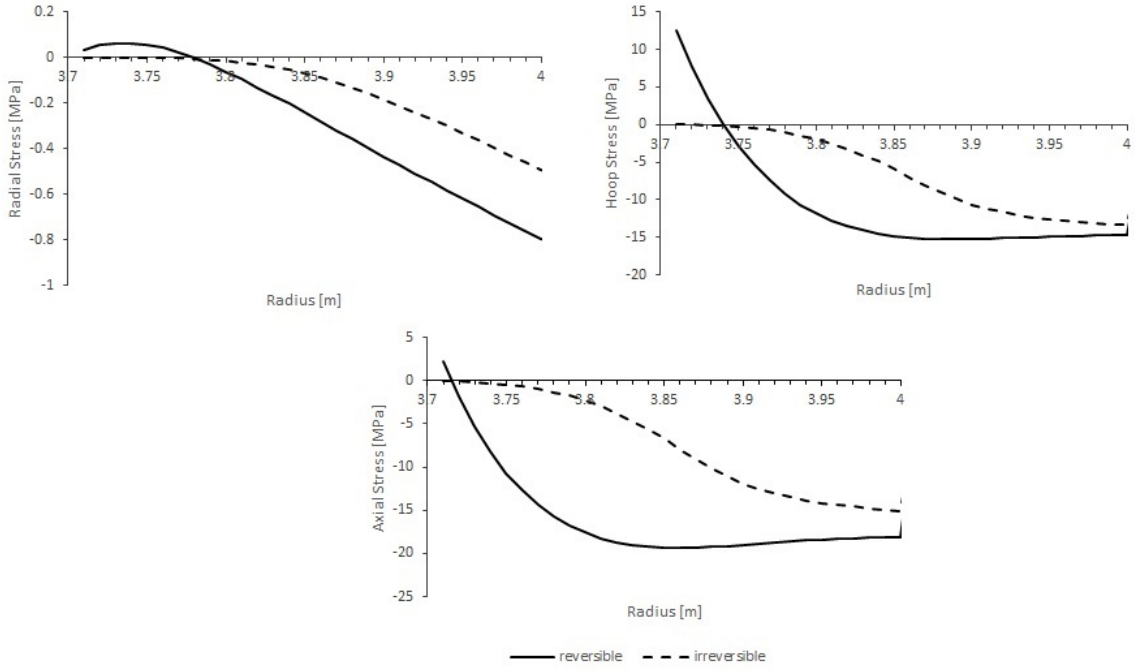

Figure 4.19: *Stress state 10 hours after the fire. Comparison between reversible and irreversible model.*

4.3.2 Spalling

Spalling represents the aspect of greatest concern when dealing with fire in tunnels. As reported in section 1.2.3, it is caused by a combination of factors, thus it is very hard to find a criterion which establishes whether concrete spalls or not.
In this work, spalling is expected to occur as soon as the material reaches failure according to the Mohr-Coulomb criterion. Thus, this phenomenon depends on the stress state that characterises each one-centimeter-thick layer of concrete and it occurs when the stress state reaches a limit condition which makes the concrete layer fail.
The Mohr-Coulomb criterion identifies the limit boundary between the admissible and the not admissible stress states and it is defined as:

$$F(\sigma) = \sigma_r K_p - \sigma_\theta - 2c\sqrt{K_p} = 0 \tag{4.3}$$

where $K_p = \dfrac{1+\sin\phi}{1-\sin\phi}$, σ_r and σ_θ are respectively the minimum and the maximum principle stresses.

Further details about the criterion are reported in subsection 2.1.2.
In absence of confined (triaxial) compression tests, and for a given value of uniaxial compression strength ($\sigma_r = 0$, $\sigma_\theta = f_{ck}$):

$$|f_{ck}| = 2c\sqrt{K_p} \tag{4.4}$$

The first step is to evaluate the stress state in the lining at equilibrium with the rock, in order to define the conditions of concrete before being subjected to fire. This may be done using the multi-layer model: the hollow cylinder is composed of concrete layers only, no temperature variation is imposed, but it is loaded by external pressure given by the rock. The value of p_{ext} may be estimated from the equilibrium point of the Convergence-Confinement Method (section 2.4) and, for our case, it is p=506.85 kPa.
The radial and hoop stresses in the lining are reported in Figures (4.20) and (4.21). Once the stress state of the lining is defined, using the Mohr-Coulomb criterion each layer may be tested in order to know whether its state of stress is admissible and the regime is elastic ($F(\sigma) < 0$). In this case, all layers are elastic.

When dealing with a fire event, each layer is associated with its strength $f_{c\theta}$, which depends on temperature. Then, the friction angle and cohesion can be calculated as function of the current strength, as shown in Paragraph (3.3.2). The

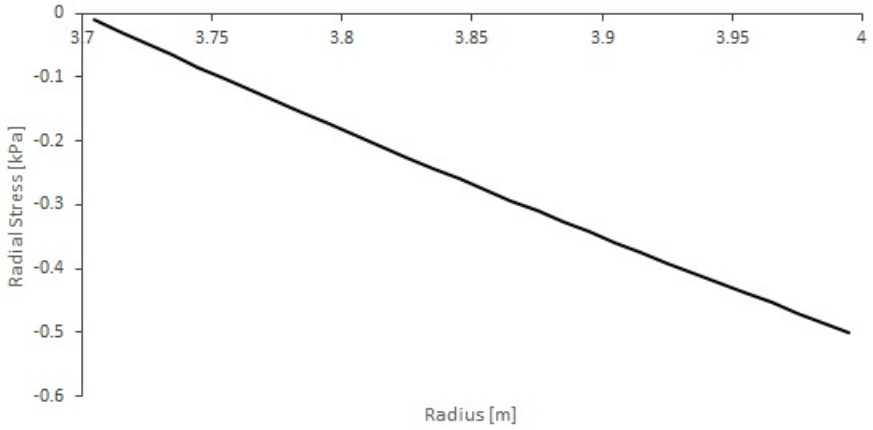

Figure 4.20: *Radial stress in the lining at equilibrium with the surrounding rock after tunnel excavation.*

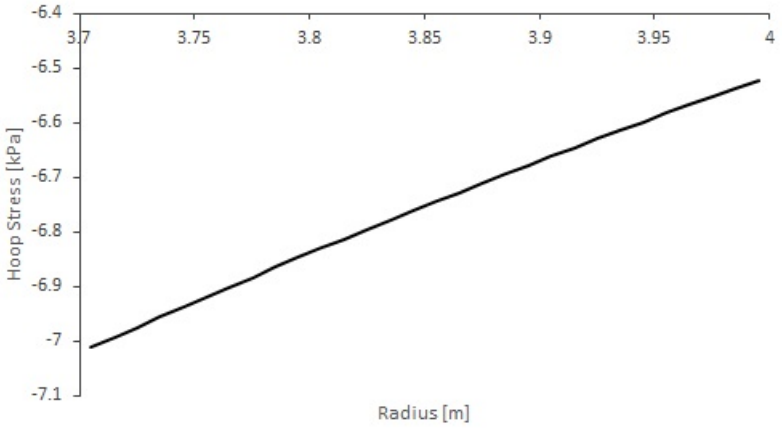

Figure 4.21: *Hoop stress in the lining at equilibrium with the surrounding rock after tunnel excavation.*

stress state induced by fire must be superimposed to the pre-existent state of stress, which represents the equilibrium between rock and lining:

$$\sigma_r = \sigma_{r0} + \Delta\sigma_r \tag{4.5}$$

$$\sigma_\theta = \sigma_{\theta 0} + \Delta\sigma_\theta \tag{4.6}$$

The final state of stress is introduced in Equation (4.3), which establishes whether the stress variation induced by fire eventually leads the material to a not admissible stress condition. The not admissible condition is associated to the failure of the layer.

The phenomenon can be verified in three different cases:

1. in the simple multi-layer model, where concrete degradation with temperature is not considered;
2. in the model with reversible damage, where the reduction of stiffness is recoverable;
3. in the model with irreversible damage, where concrete degradation is not recoverable.

For the sake of simplicity, the following graphs report the possibility of having spalling in the lining by associating to each layer the unit value if spalling occurs, otherwise the null value is reported.

In the first case, failure is expected to occur for a long period of time and to reach a depth of 22 cm. In particular, up to the 6^{th} hour, the layers that are involved in the spalling phenomenon tend to increase, reaching $r = 3.92\,m$ (Figure 4.22). From the 7^{th} hour on (Figure 4.23), the inner layers are no more subjected to failure due to cooling and the consequent stress release, whereas the external part of the intrados (i.e. from $r = 3.76\,m$) is characterised by failure.
These results show that the stress state that develops during and after a fire is such that the material fails. In this case the model indicates the attainment of a critical stress condition, that may load to failure, although not in the form of spalling, that requires a free surface.

The reversible model takes into account the reduction of stiffness and strength with temperature, leading to a lower stress state in all the layers. As soon as the tunnel has cooled down, the Young's Modulus describing concrete is brought back to the initial one, because the damage is assumed reversible.
In this case, spalling is verified up to $r = 3.79\,m$, so only the inner 9 centimeters of concrete spall (Figure 4.24). In particular, the maximum depth is reached three and four hours after the beginning of the fire, while from the 6^{th} hour on, concrete is no more involved in failure. This is due to the fact that the reduction of stiffness makes the material more ductile, thus the stresses are lower than those calculated in the previous model.

Finally, the irreversible model takes into account the concrete degradation with temperature and assumes that its initial properties are not recoverable. In Figure (4.25), spalling reaches 10 centimeters of depth during the 4^{th} hour. In the follow-

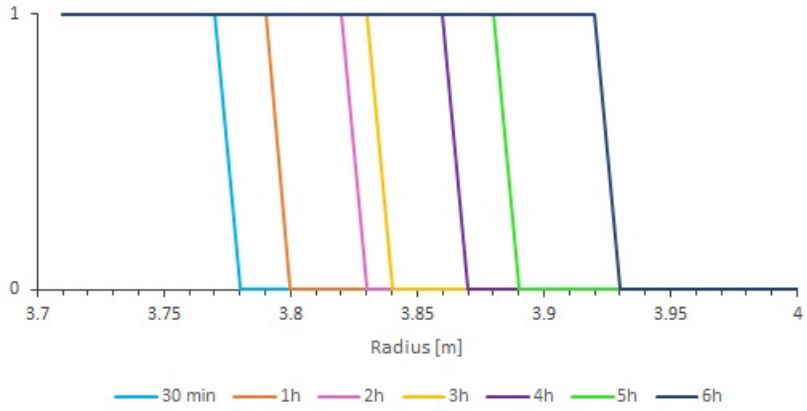

Figure 4.22: *Spalling in the first 6 hours of simulation. The layers up to* $r = 3.92\,m$ *spall.*

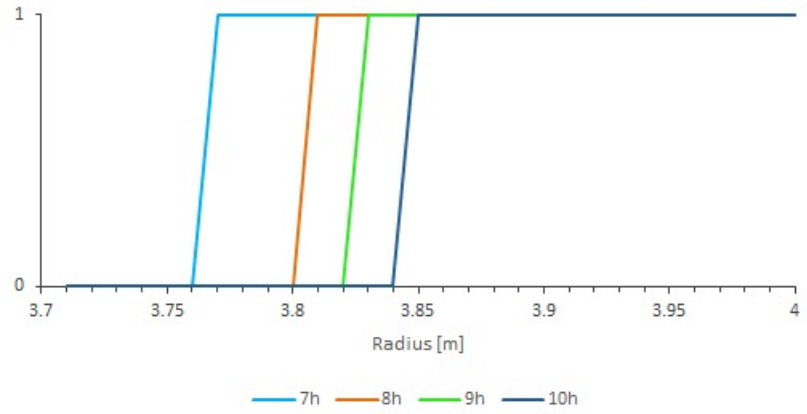

Figure 4.23: *Spalling after the* 6^{th} *hour of simulation. The layers which lay close to the rock fail.*

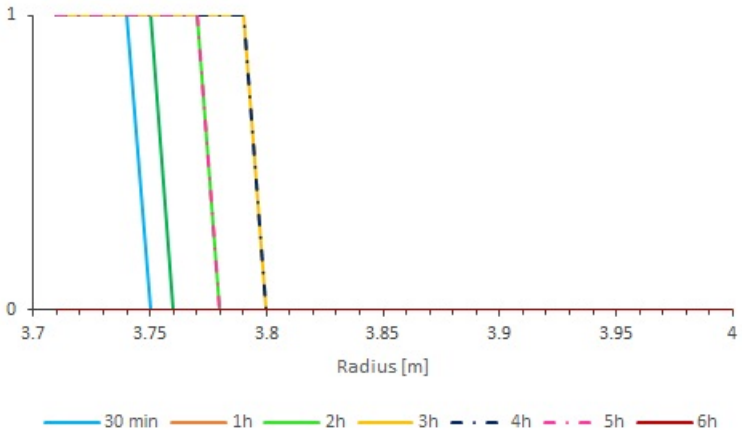

Figure 4.24: *Spalling of the concrete lining according to the reversible model.*

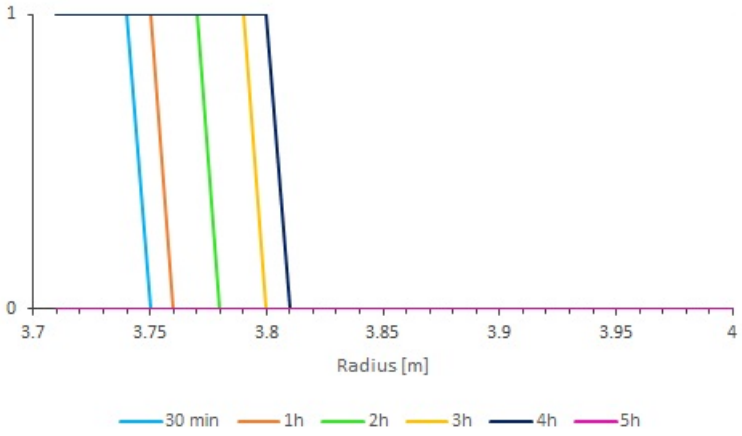

Figure 4.25: *Spalling of the concrete lining according to the irreversible model.*

ing time steps the stress state is such that failure is no more occurring.

Even if they are introduced in a simplified way, these models take into account both the fire induced effects: concrete degradation and spalling.
These results represent a first attempt to build a practical and immediate tool that is able to predict the effects of fire on tunnels. The limits of the approach lie in the assumption that the progressive failure does not change the temperature field and the stress-strain distribution.
In fact, because of spalling the lining becomes progressively thinner. Thus, to have a better comprehension of the phenomenon, the temperature profile should be newly calculated at each time step as soon as spalling is verified. In this way, the temperature profile would change depending on the thermal conductivity of the material and on the depth that is reached by spalling.

Conclusions

The present work has the objective of presenting a new analytical model, that can be easily implemented and whose main advantages are the practicality and the promptness. The model is able to evaluate the stress state that develops in tunnels in two different situations: during their excavation and when subjected to a standard fire.
The effects of rock excavation and support installation are investigated using the Convergence-Confinement Method, which allows to calculate the alteration of the stress state in the rock and to find the final equilibrium condition between the concrete lining and the surrounding rock after the process.
The fire performance of the tunnel is analysed by means of a multi-layer model, where both the concrete ring and surrounding rock are discretized in layers, each one characterised by its own temperature variation, mechanical and thermal parameters. The model is limited to the elastic regime. The lining is expected to diverge up to 14 mm four hours after the beginning of the fire and it is characterised by compression both in the radial and circumferential directions. In particular, the hoop stress reaches its maximum about 200 MPa at the intrados.
Since concrete is subjected to very high temperatures, its mechanical and thermal properties change during the fire event. This is the reason why the fire induced damage is introduced in the model, in terms of concrete degradation and possible spalling.
The first effect is considered by using a temperature-dependent stiffness, that comes from laboratory tests results on hot concrete samples, taken from the literature. Since concrete is a composite material, it is very difficult to assess its general behaviour: thus, the concrete damage is assumed reversible in one model and irreversible in another, constituting two boundaries of possible results. In both cases, the lining is subjected to a lower stress state, due to the increase in its ductility. The radial displacement decreases as well.
Spalling is introduced as soon as the stress state in the lining satisfies the Mohr-

Coulomb failure criterion: the results show that the first centimeters of the intrados are affected by this phenomenon.
As already mentioned, the model assumes that the behaviours of the concrete lining and the rock are elastic, this may be a simplification, even though damage is introduced.
For a more accurate simulation, the load history undergone by the lining should be repeated in the laboratory on concrete samples: it is firstly compressed by the rock, then it is rapidly heated by fire and finally it cools down under sustained stress. Performing ad hoc tests in the laboratory would provide a more precise idea of the temperature effects on the stiffness of the material and, consequently, of its behaviour.
To get these results, some assumptions have been made: concrete is considered homogeneous, and the presence of reinforcement is neglected. To be more precise, the effects of temperature on the interaction between steel reinforcement bars, cement paste and aggregates should be taken into account. In particular, spalling is expected not to overcome the depth of the reinforcement bars.
Moreover, the Mohr-Coulomb criterion is based on friction angle and cohesion, which characterise the material at normal conditions. In this case, being concrete subjected to very high temperatures, the parameters are assumed to decrease proportionally with temperature. A further step would consist in introducing experimental-based data on the dependence of these coefficients on temperature.
The results of this work refer to a Normal Strength Concrete, composed of silicate aggregates. Since concrete is a mixture of different components, it could behave in many different ways, making it very difficult to assess its general behaviour.
To conclude, this model is extremely simple, immediate and suited for preliminary assessment of the tunnel behaviour in case of fire, in this case representing a good alternative to numerical simulations, which may last several hours. On the other hand, the practicality of the present model is guaranteed at the cost of making some simplifying assumptions.
In particular, the approach used to study the possibility of having spalling in the model represents a first attempt to be improved. Further analyses on the progression and development in time of the phenomenon are required, especially by updating the temperature field in the lining.

Appendix A

Equilibrium equation in cylindrical coordinates

Axisymmetric problems are usually solved using cylindrical coordinates. The infinitesimal volume has a particular geometry which is shown in Figure (A.1).
The equilibrium equations are obtained by imposing the equilibrium of the stresses components in each direction at the material point, which can be subjected both to volume forces and to stress.

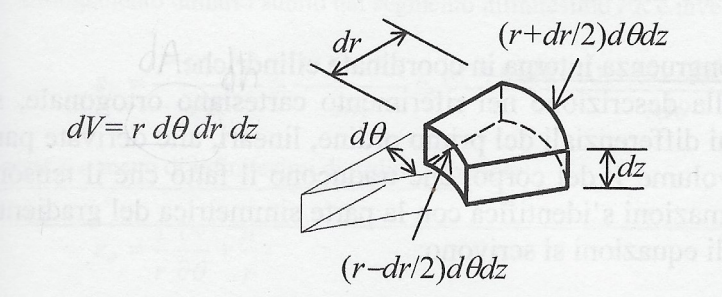

Figure A.1: *Representative volume element in cylindrical coordinates [Corigliano and Taliercio, 2005]*

The equilibrium in the radial direction is:

$$
\begin{aligned}
&-\sigma_r\big(r-\frac{dr}{2}\big)d\theta dz+\big(\sigma_r+\frac{\partial\sigma_r}{\partial r}dr\big)\big(r+\frac{dr}{2}\big)d\theta dz+\\
&\quad-\tau_{\theta r}drdz+\big(\tau_{\theta r}+\frac{\partial\tau_{\theta r}}{\partial\theta}dr\big)drdz-\sigma_\theta\frac{d\theta}{2}drdz-\big(\sigma_\theta+\frac{\partial\sigma_\theta}{\partial\theta}d\theta\big)drdz\frac{d\theta}{2}+\\
&\qquad-\tau_{zr}rd\theta dr+\big(\tau_{zr}+\frac{\partial\tau_{zr}}{\partial z}dz\big)rd\theta dr+F_rrd\theta drdz=0 \quad \text{(A.1)}
\end{aligned}
$$

The equilibrium equation in circumferential direction θ is:

$$\begin{aligned}-\sigma_\theta dr dz + \big(\sigma_\theta + \frac{\partial \sigma_\theta}{\partial \theta} d\theta\big) dr dz - \tau_{z\theta} r d\theta dr + \big(\tau_{z\theta} + \frac{\partial \tau_{z\theta}}{\partial z} dz\big) r d\theta dr + \\ - \tau_{r\theta}\big(r - \frac{dr}{2}\big) d\theta dz + \big(\tau_{r\theta} + \frac{\partial \tau_{r\theta}}{\partial r} dr\big)\big(r + \frac{dr}{2}\big) d\theta dz + \\ + \tau_{\theta r} \frac{d\theta}{2} dr dz + \big(\tau_{r\theta} + \frac{\partial \tau_{\theta r}}{\partial \theta} d\theta\big) \frac{d\theta}{2} dr dz + F_\theta r d\theta dr dz = 0 \quad \text{(A.2)}\end{aligned}$$

And in the axial direction:

$$\begin{aligned}-\sigma_z r d\theta dr + \big(\sigma_z + \frac{\partial \sigma_z}{\partial z} dz\big) r d\theta dr - \tau_{\theta z} dr dz + \big(\tau_{\theta z} + \frac{\partial \tau_{\theta z}}{\partial \theta} d\theta\big) dr dz + \\ - \tau_{rz}\big(r - \frac{dr}{2}\big) d\theta dz + \big(\tau_{rz} + \frac{\partial \tau_{rz}}{\partial r} dr\big)\big(r + \frac{dr}{2}\big) d\theta dz + F_z r d\theta dz dr = 0 \quad \text{(A.3)}\end{aligned}$$

By simplifying these equations it is possible to obtain the final equilibrium equations in cylindrical coordinates:

$$\begin{cases} \dfrac{\partial \sigma_r}{\partial r} + \dfrac{1}{r}\dfrac{\partial \tau_{\theta r}}{\partial \theta} + \dfrac{\partial \tau_{zr}}{\partial z} + \dfrac{\sigma_r - \sigma_\theta}{r} + F_r = 0 \\ \dfrac{\partial \tau_{r\theta}}{\partial r} + \dfrac{1}{r}\dfrac{\partial \sigma_\theta}{\partial \theta} + \dfrac{\partial \tau_{z\theta}}{\partial z} + \dfrac{2\tau_{r\theta}}{r} + F_\theta = 0 \\ \dfrac{\partial \tau_{rz}}{\partial r} + \dfrac{1}{r}\dfrac{\partial \tau_{\theta z}}{\partial \theta} + \dfrac{\partial \sigma_z}{\partial z} + \dfrac{\tau_{rz}}{r} + F_z = 0 \end{cases} \quad \text{(A.4)}$$

These equations can be further simplified by making some assumptions. First, if the problem has an axisymmetric geometry and there are no loads acting on the circumferential direction all the cross sections of the cylinder have the same state of stress. As a consequence, there is no dependence on coordinate θ: all the terms that are derived in θ are null and the tangential stresses $\tau_{z\theta}$ and $\tau_{r\theta}$ are equally null.
Secondly, if the problem is in plane strain conditions, there will be no axial deformations and this results in τ_{zr} and $\tau_{z\theta}$ equal to zero. Finally, if there are no Body Forces the last term of each equation becomes null. If all these hypothesis hold true, the only components of the stress tensor that are not null are σ_r, σ_θ and σ_z, as function of the radial coordinate r. In this case, equation (A.4) becomes:

$$\frac{\partial \sigma_r}{\partial r} + \frac{\sigma_r - \sigma_\theta}{r} = 0 \quad \text{(A.5)}$$

Appendix B

State of stress in elastic field

When dealing with an elastic medium subjected to a volume force or pressure, the stress state can be calculated by imposing equilibrium, compatibility and Hooke equations. Hooke equations refer to linear elastic homogeneous media and express the relation between stresses and strains:

$$\begin{cases} \varepsilon_r = \dfrac{\sigma_r}{E} - \dfrac{\nu}{E}(\sigma_\theta + \sigma_z) \\ \varepsilon_\theta = \dfrac{\sigma_\theta}{E} - \dfrac{\nu}{E}(\sigma_r + \sigma_z) \\ \varepsilon_z = \dfrac{\sigma_z}{E} - \dfrac{\nu}{E}(\sigma_\theta + \sigma_r) \end{cases} \tag{B.1}$$

Compatibility between strains and displacement is imposed using the following relation:

$$\frac{\epsilon_r - \epsilon_\theta}{r} = \frac{\partial \epsilon_\theta}{\partial r} \tag{B.2}$$

Finally, equilibrium is imposed:

$$\frac{\partial \sigma_r}{\partial r} + \frac{\sigma_r - \sigma_\theta}{r} = 0 \tag{B.3}$$

It is possible to demonstrate that in an elastic medium $\sigma_r + \sigma_\theta = constant$ through the following simple calculations. By introducing Hooke relations (B.1) in the compatibility (Eq. B.2), we obtain:

$$\frac{1}{r}\frac{1+\nu}{E}\left[\Big(\sigma_r(1-\nu)-\nu\sigma_\theta\Big)-\Big(\sigma_\theta(1-\nu)-\nu\sigma_r\Big)\right] = \frac{1+\nu}{E}\frac{\partial}{\partial r}\Big[(1-\nu)\sigma_\theta-\nu\sigma_r\Big] \tag{B.4}$$

which becomes:

$$\frac{\sigma_r - \sigma_\theta}{r} = (1-\nu)\frac{\partial \sigma_\theta}{\partial r} - \nu\frac{\partial \sigma_r}{\partial r} \tag{B.5}$$

By introducing the equilibrium equation (B.3):

$$-\frac{\partial \sigma_r}{\partial r} = (1-\nu)\frac{\partial \sigma_\theta}{\partial r} - \nu\frac{\partial \sigma_r}{\partial r} \tag{B.6}$$

The equation finally becomes:

$$\frac{\partial}{\partial r}(\sigma_\theta + \sigma_r) = 0 \tag{B.7}$$

It is thus demonstrated that the sum of radial and tangential stresses is constant.

Appendix C

Convergence-Confinement Method for soil

For sake of simplicity, when dealing with soil and rock it is often convenient to use associated flow rules, where the plastic potential coincides with the plasticity function. In this case, if Mohr-Coulomb plasticity function is adopted, the dilatancy angle ψ coincides with the friction angle ϕ.
However, the real experimentally observed soil dilatancy is overestimated when the friction angle is assumed, therefore a non-associated flow rule would be preferred. The radial convergence expression using non-associated flow rule can be found in [Carranza-Torres and Fairhurst, 2000] and is the following:

$$u_{pl} = a\frac{1+\nu}{E}\Bigg[(1-2\nu)(F-p_0) + (k_p - \nu k_p - \nu)(p-F) + \\ + (1-\nu)(1-k_p^2)\frac{(p-F)}{(k_p+k_p')}\left(1-\left(\frac{r_{pl}}{a}\right)^{k_p+k_p'}\right)\Bigg] \quad \text{(C.1)}$$

where:

$$F = \frac{2c\sqrt{k_p}}{k_p - 1} \quad \text{(C.2)}$$

and:

$$k_p' = \frac{1+\sin\psi}{1-\sin\psi} \quad \text{(C.3)}$$

Considering the case study in Paragraph 2.4 and by introducing the dilatancy angle $\psi = 15°$, the GRC changes with respect to the curve for associated flow rule. In fact, reducing the dilatancy from $\psi = \phi = 30°$ (associated case) to $\psi = 15°$

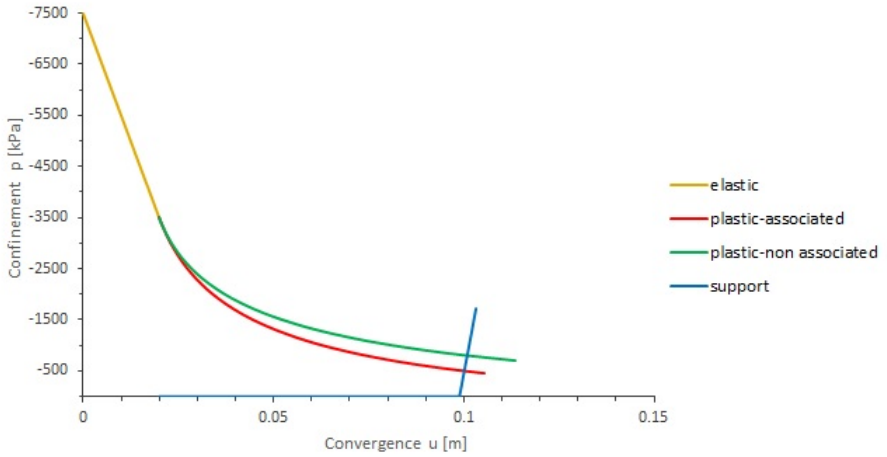

Figure C.1: *Convergence-Confinement Method for dilatant (associated flow rule) and non-dilatant (non-associated flow rule).*

(non-associated case) leads to a higher radial convergence towards the centre of the tunnel (Figure C.1). This is due to the fact that a dilatant material expands while moving, thus generating additional compressive stresses that limit the inward movement.

References

American Concrete Institute ACI. *Fire endurance of concrete elements.* ACI 2003 manual of concrete practice, ACI216R-89, Farmington Hills, Mich., 2001.

L.R. Alejano, A. Rodriguez-Dono, E. Alonso, and G. Fdez.-Manín. Ground reaction curves for tunnels excavated in different quality rock masses showing several types of post-failure behaviour. *Tunnelling and Underground Space Technology*, (24):689–705, 2009.

R. Aliberti and G. Miglietta. *Sul comportamento strutturale di rivestimenti in gallerie profonde soggetti ad incendio.* 2014.

F. Amberg. For a correct interpretation of ground reaction curves. *Lombardi Engineering Ltd.*, 2011.

P. Bamonte, P.G. Gambarova, and A. Nafarieh. High-temperature behaviour of structural and non-structural shotcretes. *Cement and Concrete Composites*, 73: 42–53, 2016.

K. Bekish. Numerical Simulations of Pressure effects in Passive Houses. *Ghent University*, 2018.

A. Caner, S. Zlatanic, and N. Munfah. Structural Fire Performance of Concrete and Shotcrete Tunnel Liners. *Structural Engineering*, 131(12), 2005.

C. Carranza-Torres and C. Fairhurst. Application of the Convergence-Confinement Method of Tunnel Design to Rock Masses That Satisfy the Hoek-Brown Failure Criterion. *Tunnelling and Underground Space Technology*, 15(2):187–213, 2000.

C. Carranza-Torres, B. Rysdahl, and M. Kasim. On the elastica nalysis of a circular lined tunnel considering the delayed installation of the support. *International Journal of Rock Mechanics and Mining Sciences*, (61):57–85, 2013.

A. Corigliano and A. Taliercio. *Meccanica Computazionale. Soluzione del problema elastico lineare.* Società Editrice Esculapio, 2005.

L. Corradi Dell'Acqua. *Meccanica delle strutture.* McGraw-Hill Education, 2010.

Eurocode2. *Design of Concrete Structures Part 1-2: General rules - Structural Fire Design.* 2005.

I Hager. Behaviour of cement concrete at high temperature. *Bulletin of the Polish Academy of Sciences. Technical Sciences*, 61(1), 2013.

E. Hoek. *Practical Rock Engineering.* 2000.

H. Ingason. Design fire curves for tunnels. *Fire Safety Journal*, 44:259–265, 2009.

R. Kallada Janardhan and S. Hostikka. Experiments and Numerical Simulations of Pressure Effects in Apartment Fires. *Fire Technology*, 53:1353–1377, 2017.

G.A. Khoury. Effect of fire on concrete and concrete structures. *Progress in Structural Engineering and Materials*, 2(4):429–447, 2000.

D. Kolymbas. *Tunnelling and Tunnel Mechanics. A Rational Approach to Tunnelling.* 2008.

K. Larsson. *Fires in Tunnels and their effect on Rock.* 2006.

F. LoMonte, P. Bamonte, and C. Beltrami. Reinforced Concrete Tunnels exposed to Fire: effects of Geometry and Fire Curve. 2019.

Q. Ma, R. Guo, Z. Zhao, Z. Lin, and K. He. Mechanical properties of concrete at high temperature—A review. *Construction and Building Materials*, 93:371–383, 2015.

J.C. Marechal. *Variations in the modulus of elasticity and Poisson's ratio with temperature.* ACI-Int. Seminar on CNR, Berlin, 1970.

R. Jansson McNamee. *Fire Spalling of Concrete: Theoretical and Experimental Studies.* 2013.

P. Morabito. Measurement of the thermal properties of different concretes. *High Temperatures. High Pressures*, 21(1):51–59, 1989.

M.S. Mostafa. . *High Temperatures. High Pressures*, 31:543, 1999.

502 NFPA. *Standard for road tunnels, bridges, and other limited access highways.* National Fire Protection Association, 2008.

P.P. Oreste. Analysis of structural interaction in tunnels using the convergence-confinement approach. *Tunnelling and Underground Space Technology*, 18(4): 347–363, 2003a. doi: https://doi.org/10.1016/S0886-7798(03)00004-X.

P.P. Oreste. A Procedure for Determining the Reaction Curve of Shotcrete Lining Considering Transient Conditions. *Rock Mechanics and Rock Engineering*, 36 (3):209–236, 2003b.

E Oztekin, S. Pul, and M Husem. Experimental determination of Drucker-Prager yield criterion parameters for normal and high strength concretes under triaxial compression. *Construction and building materials*, (112):725–732, 2016.

L. T. Phan and N. J. Carino. Review of mechanical properties of HSC at elevated temperatures. *Journal of materials in civil engineering*, 10(1):58–65, 1998.

Piarc. World Road, Association Mondiale de la Route. 2014.

World Road Association PIARC. *Fire and smoke control in road tunnels*. 05.05B-1999, 1999.

C. Pichler, R. Lackner, and H.A. Mang. Safety Assessment of Concrete Tunnel Linings under Fire Load. *Structural Engineering*, 132(6), 2005.

Promat-Tunnel. Types of fire exposure. URL `https://www.promat-tunnel.com/en/advices/fire-protection/fire%20curves`.

HTC Rilem Technical Committee. *Mechanical Concrete Properties at High Temperatures Modelling and Application. State of Art Report*. RILEM Publications SARL, 2004.

K. Savov, R. Lackner, and H.A. Mang. Stability assessment of shallow tunnels subjected to fire load. *Fire Safety Journal*, 40:745–763, 2005.

K. Vedeld and H.A. Sollund. *Explicit analytical solutions for heated, pressurized two-layer cylinders*. University of Oslo, 2013.

K. Vedeld and H.A. Sollund. Stresses in heated pressurized multi-layer cylinders in generalized plane strain conditions. *Pressure Vessels and Piping*, 120-121:27–35, 2014.

S. Wallis. Fire damage rebuild of Mont Blanc road link. *TunnelTalk*, 2001.